Non-reflecting Boundary Conditions for the Numerical Solution of Wave Propagation Problems in Unbounded Domains

Inauguraldissertation

zur
Erlangung der Würde eines Doktors der Philosophie
vorgelegt der
Philosophisch-Naturwissenschaftlichen Fakultät
der Universität Basel

von

Christoph Kirsch

aus Bäretswil (ZH)

Zürich, 2005

Genehmigt von der Philosophisch-Naturwissenschaftlichen Fakultät
auf Antrag von

Prof. Dr. M. J. Grote
Prof. Dr. P. Joly (INRIA Rocquencourt)

Basel, den 8. Februar 2005

Prof. Dr. Hans-Jakob Wirz
Dekan

Contents

Chapter 1

Introduction

1.1 Acoustic waves in fluids

We consider a domain Ω in q-dimensional space, filled with a physical medium. To describe the dynamics of the medium, we let $\rho(\boldsymbol{x}, t)$ denote the mass density and $\boldsymbol{v}(\boldsymbol{x}, t)$ the velocity of the medium at the point $\boldsymbol{x} \in \mathbb{R}^q$, and at the time $t \in \mathbb{R}$. From the *conservation of mass* in an isolated system, we obtain the continuity equation

$$\frac{\partial \rho}{\partial t} + \operatorname{div}(\rho \boldsymbol{v}) = 0. \tag{1.1}$$

The *conservation of momentum* yields the equation of motion

$$\rho \frac{\partial \boldsymbol{v}}{\partial t} + \rho \left(\boldsymbol{v} \cdot \nabla\right) \boldsymbol{v} = \boldsymbol{f} + \operatorname{div}_2 \underline{\boldsymbol{T}}. \tag{1.2}$$

Here $\boldsymbol{f}$ denotes a *volume force density,* which describes exterior forces that influence the entire medium, for example gravity of electromagnetic forces. The stress tensor $\underline{\boldsymbol{T}}$ describes *contact forces* inside the medium. It is determined by the properties of the material, namely the mass density ρ, the velocity field $\boldsymbol{v}$ and also the temperature. We assume *adiabatic change of condition,* i. e. no heat exchange. Therefore the temperature is constant. If the medium is an ideal (dry) fluid, in liquid or gaseous condition, the stress tensor is given by $\underline{\boldsymbol{T}} = -p\underline{\boldsymbol{I}}$, where the pressure p is determined by the mass density ρ via a thermodynamic constitutive equation, $p = p(\rho)$. In this case, $\operatorname{div}_2 \underline{\boldsymbol{T}} = -\nabla p$, and the equation of motion (1.2) becomes *Euler's equation for inviscid fluids (1755):*

$$\rho \frac{\partial \boldsymbol{v}}{\partial t} + \rho \left(\boldsymbol{v} \cdot \nabla\right) \boldsymbol{v} = \boldsymbol{f} - \nabla p. \tag{1.3}$$

The continuity equation (1.1) and Euler's equation (1.3) describe the change of state of the ideal fluid over time. As we will consider small changes only, we

linearize the equations (1.1), (1.3) around a hydrostatic equilibrium $(\rho_0, \mathbf{0})$, $\rho_0 > 0$ constant. We obtain the following linearized equations for the perturbation $(\tilde{\rho}, \tilde{\boldsymbol{v}})$:

$$\frac{\partial \tilde{\rho}}{\partial t} + \rho_0 \mathrm{div} \tilde{\boldsymbol{v}} = 0, \qquad \rho_0 \frac{\partial \tilde{\boldsymbol{v}}}{\partial t} + p'(\rho_0) \nabla \tilde{\rho} = \boldsymbol{f}. \tag{1.4}$$

We take an additional time derivative in (1.4), which yields the *decoupled* second-order equations

$$\frac{\partial^2 \tilde{\rho}}{\partial t^2} - p'(\rho_0) \Delta \tilde{\rho} = -\mathrm{div} \boldsymbol{f}, \qquad \frac{\partial^2 \tilde{\boldsymbol{v}}}{\partial t^2} - p'(\rho_0) \nabla (\mathrm{div} \tilde{\boldsymbol{v}}) = \frac{1}{\rho_0} \frac{\partial \boldsymbol{f}}{\partial t}. \tag{1.5}$$

The equations in (1.5) indicate that the perturbation of the mass density, $\tilde{\rho}$, as well as the perturbation of the pressure, $\tilde{p} = p'(\rho_0)\tilde{\rho}$, satisfy the *scalar wave equation* with wave speed $\sqrt{p'(\rho_0)}$. If the perturbation of the velocity field, $\tilde{\boldsymbol{v}}$, is rotation-free, then because of the operator identity $\mathrm{rot}\,\mathrm{rot} \equiv \nabla \mathrm{div} - \Delta$, each component of $\tilde{\boldsymbol{v}}$ also satisfies the scalar wave equation with wave speed $\sqrt{p'(\rho_0)}$.

1.2 Numerical methods for wave propagation in unbounded domains

In practical wave propagation problems, unbounded domains occur frequently, for example in radar or sonar applications, and also in geophysics. The domain where waves propagate is unbounded in these applications, or at least very large compared to the size of the interesting region. A numerical method for the simulation of waves in an unbounded domain must not involve the discretization of the entire domain, which is prohibitively expensive. Instead, such a numerical method should rely on a bounded domain with a size that is comparable to the size of the interesting region. The unbounded domain outside this region has to be accounted for by an accurate mathematical model, which can be combined with the numerical method in the interior at little additional cost.

We consider an unbounded, connected domain $\Omega_\infty = \mathbb{R}^q \setminus K$, $K \subset \mathbb{R}^q$ compact. We study the propagation of acoustic waves in Ω_∞ in the time interval $I = (0, T)$, $T > 0$. Therefore, we are interested in the solution $U = U(\boldsymbol{x}, t)$ of the scalar wave equation

$$\frac{\partial^2 U}{\partial t^2} - \mathrm{div}(\underline{\boldsymbol{A}} \nabla U) = F \quad \text{in } \Omega_\infty \times I, \tag{1.6}$$

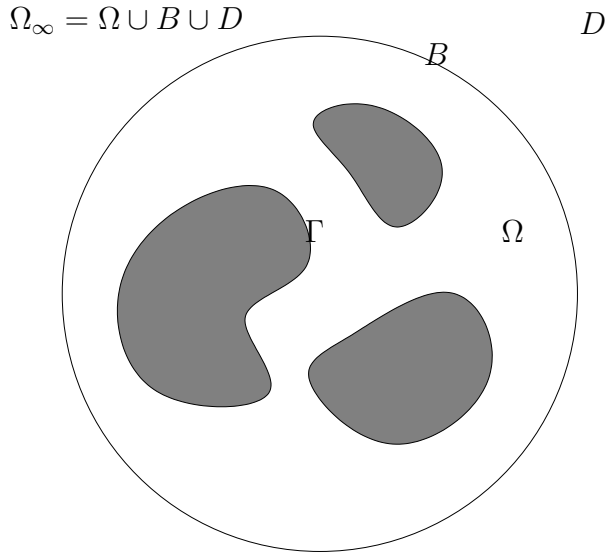

Figure 1.1: The unbounded domain Ω_∞ decomposed in a bounded computational domain Ω and an unbounded exterior region D, with an artificial boundary B in between.

together with appropriate initial conditions in $\Omega_\infty \times \{0\}$ and boundary conditions on $\Gamma \times I$, where $\Gamma = \partial K$. In (1.6), the function $\underline{\boldsymbol{A}} = \underline{\boldsymbol{A}}(\boldsymbol{x}, t)$ describes the inhomogeneity and anisotropy in the material under consideration, whereas the right-hand side $F = F(\boldsymbol{x}, t, U, \nabla U)$ describes the nonlinearity of the medium and also the sources which are present in Ω_∞.

In the time-harmonic case, or more generally when the Laplace transformed solution is considered, we are interested in the solution $u = u(\boldsymbol{x})$ of the scalar Helmholtz equation

$$\operatorname{div}(\underline{\boldsymbol{a}} \nabla u) + (is)^2 u = f \quad \text{in } \Omega_\infty, \tag{1.7}$$

together with appropriate boundary conditions on Γ. For time-harmonic solutions, $is =: \omega > 0$ is the angular frequency, whereas in general, $is \in \mathbb{C} \setminus \{0\}$, $\arg(is) \in [0, \pi)$, is a complex number.

For wave propagation in unbounded domains, it is usually assumed that the material is homogeneous, isotropic and linear outside some compact domain, and that no exterior sources are present. It is also assumed that the medium is at rest for times $t \leq 0$. The unbounded domain Ω_∞ is then decomposed in an open bounded domain Ω and an open unbounded domain D, with boundaries $\partial D =: B$, $\partial\Omega = \Gamma \cup B$, such that $\Omega_\infty = \Omega \cup B \cup D$ is a disjoint union of sets – see Fig. 1.1. In D, by assumption $\underline{\boldsymbol{A}} \equiv \underline{\boldsymbol{a}} \equiv c^2 \underline{\boldsymbol{I}}$, with

$c > 0$ constant. Then the solution U of the time-dependent problem satisfies

$$\frac{1}{c^2}\frac{\partial^2 U}{\partial t^2} - \Delta U = 0 \quad \text{in } D \times I, \tag{1.8}$$

and the Laplace transformed solution u satisfies

$$\Delta u + k^2 u = 0 \quad \text{in } D, \tag{1.9}$$

with $k := is/c$, which in the case $k > 0$ (time-harmonic) is called the wave number. For the uniqueness of a solution to (1.9), the Rellich-Sommerfeld condition is additionally required [69, 73]:

$$\lim_{R\to\infty} \int_{S_R} \left| \frac{\partial u}{\partial r} - iku \right|^2 ds = 0, \tag{1.10}$$

where S_R denotes the sphere with radius $R > 0$, centered at the origin.

Exterior Dirichlet and Neumann problems are strongly well posed. The most important fact for our considerations is the unique determination of the solution to the time-dependent problem (1.8) by traces of U, $\partial_n U$ or $\partial_t U$ on $B \times I$ [56], and of the solution to the stationary problem (1.9), (1.10) by traces of u or $\partial_n u$ on B [84].

There are many methods for the numerical solution of wave propagation problems in unbounded domains, see the monograph [26] for an overview. Among the most widely used methods we find the following four, which we will briefly discuss in the following subsections:

- methods based on boundary integral equations
- infinite elements
- non-reflecting boundary conditions
- absorbing layers

1.2.1 Methods based on boundary integral equations

These methods are originally used in the case $\Omega = \emptyset$, $B = \Gamma$, $D = \Omega_\infty$, i. e. when the medium is homogeneous, isotropic and linear everywhere in Ω_∞. They are based on the numerical solution of boundary integral equations (BIE) on B which involve the free-space fundamental solution of (1.8) or (1.9). Such boundary integral equations arise in scattering and potential theory [82], and there are several possible formulations.

As an example, we consider the stationary exterior Neumann problem, which is given by (1.9), (1.10) and the boundary condition

$$\frac{\partial u}{\partial n} = g \quad \text{on } B. \tag{1.11}$$

In the indirect single-layer potential formulation, the solution u is written as an integral involving a *single layer distribution* w on B,

$$u = Sw \quad \text{in } D, \tag{1.12}$$

where S is a linear integral operator with the free-space fundamental solution u^* of (1.9), (1.10) as its kernel. From an expression for the normal derivative of Sw and with the Neumann condition (1.11), a Fredholm integral equation of the second kind for the unknown density w is obtained:

$$w + Kw = g \quad \text{on } B. \tag{1.13}$$

Here K is a linear integral operator with the normal derivative of u^* as its kernel. If (1.13) has a unique solution w, then the solution u to the exterior Neumann problem (1.9), (1.10), (1.11) is given by (1.12). There are other possible formulations that can be used instead of (1.12), such as direct and double-layer potential formulations. Each formulation gives rise to a different boundary integral equation. See [55] for an overview of boundary integral equations for the three-dimensional Helmholtz equation. For Helmholtz problems, it may happen that the integral equation (1.13) does *not* have a unique solution. This is the case when the wave number k in (1.9) is an eigenvalue of the associated problem, which is the interior Dirichlet problem in our example. The difficulty becomes more serious for large values of k, because the eigenvalues of the associated interior problem become more and more dense as k increases. A remedy is to solve a modified boundary integral equation which has a unique solution, such as the combined field integral equation (CFIE) [15].

A popular method for the numerical solution of integral equations of the type (1.13) is the boundary element method (BEM). The boundary B is discretized, and the unknown density w is expanded into shape functions, which have local support on the elements. The unknown expansion coefficients w_i are then given by the solution of the linear system

$$\underline{\boldsymbol{C}}\boldsymbol{w} = \boldsymbol{f}, \tag{1.14}$$

where the entries of the matrix $\underline{\boldsymbol{C}}$ are computed by applying the linear operator $I + K$ to the shape functions, cf. (1.13), and the entries on the right-hand

side $\boldsymbol{f}$ are the nodal values of the function g in (1.11). Because K is a non-local operator, the matrix $\underline{\boldsymbol{C}}$ will be full, and it turns out that it is also non-symmetric for the standard BEM. However, there are methods, such as the Galerkin BEM, that yield symmetric linear equation systems. In the non-symmetric case, (1.14) is solved iteratively with the generalized minimal residual (GMRES) method [70]. The matrix-vector products that have to be computed during each iteration can be accelerated with the help of the fast multipole method (FMM) [32], which enables the rapid evaluation of potentials such as those arising in the entries of the matrix $\underline{\boldsymbol{C}}$. See [26], Chapter 2, and the references therein for more information on the boundary element method for time-harmonic problems.

In the time-dependent case, boundary integral equation formulations involve retarded potentials, which arise from the free-space fundamental solution of (1.8). These integral operators are non-local in space and in time. With a similar procedure as described before in the time-harmonic case it is possible to solve time-dependent boundary integral equations numerically in an efficient way. Instead of the FMM, its time-dependent counterpart, a plane wave time domain (PWTD) algorithm [22] can be used for the rapid evaluation of the retarded potentials.

The biggest advantages of methods based on integral equations over methods based on the discretization of a volume are that

- the spatial dimension of the domain to be discretized is reduced by one, and that
- the boundary condition at infinity is satisfied exactly.

The main drawbacks of these methods are that

- a fundamental solution is required, that
- the integral kernels are singular, and that
- the system matrix is full.

We note that the boundary element method can be combined with methods based on volume discretization, such as the finite element method. These coupled FE/BE methods ([26], Section 2.7) are useful when the elimination of Ω_∞ by an integral equation on Γ is not possible, for example when no fundamental solution can be found. This is the case when the medium is inhomogeneous or nonlinear, i. e. if there are variable coefficients or a nonlinear right-hand side in the partial differential equation (1.8) or (1.9). If the inhomogeneity or nonlinearity is local, it can be enclosed in a computational

volume $\Omega \neq \emptyset$, where the problem is solved by the finite element method, for instance. The unbounded domain D is then eliminated by a boundary integral equation on B, which is solved together with the problem in Ω.

1.2.2 Infinite element methods

These methods came up when it was realized that boundary element methods may be expensive for complicated boundaries and large scale computations ([14], Section 1), which is due to the dense structure of the matrix in the BE system (1.14). The idea is to surround the scatterer with a bounded volume Ω with an exterior separable boundary B. The remaining unbounded domain D is then discretized by infinite elements with shape functions that satisfy the Rellich-Sommerfeld condition (1.10) approximately.

The infinite element method (IEM) starts with a variational formulation of the problem in the unbounded domain. In the time-harmonic case, the variational formulation of (1.9), (1.10), (1.11) is given by

> Find $u \in H^1_w(\Omega_\infty)$ such that
>
> $$(\nabla u, \nabla v)_{\Omega_\infty} - k^2 (u, v)_{\Omega_\infty} = \langle g, v \rangle_\Gamma \qquad (1.15)$$
>
> for all $v \in H^1_{w^*}(\Omega_\infty)$.

Here $H^1_w(\Omega_\infty) := \{u : \Omega_\infty \to \mathbb{C} \,|\, \|u\|_{1,w} < \infty\}$ denotes a weighted Sobolev space with the norm induced by the weighted inner product

$$(u, v)_{1,w} := \int_{\Omega_\infty} w \left(\nabla u \cdot \nabla \overline{v} + u \overline{v}\right) d\boldsymbol{x} + \int_{\Omega_\infty} \left(\frac{\partial u}{\partial r} - iku\right) \overline{\left(\frac{\partial v}{\partial r} - ikv\right)} \, d\boldsymbol{x}. \qquad (1.16)$$

The weights are given by $w(\boldsymbol{x}) := |\boldsymbol{x}|^{-(q-1)}$ and $w^*(\boldsymbol{x}) := |\boldsymbol{x}|^{q-1}$ for a problem in q space dimensions. The inner products used in (1.15) are given by

$$(u, v)_\Omega := \int_\Omega u \overline{v} \, d\boldsymbol{x}, \quad \langle u, v \rangle_\Gamma := \int_\Gamma u \overline{v} \, ds. \qquad (1.17)$$

The variational problem (1.15) is solved numerically with a coupled FE/IE method. For that purpose, a smooth artificial boundary is introduced, which splits the unbounded domain Ω_∞ into a bounded domain Ω and an unbounded domain D. The bounded domain Ω is triangulated and a standard *hp*-FE subspace $S^p_h(\Omega) \subset H^1(\Omega)$ is defined. This induces a finite element partition and a finite element subspace $S^p_h(B)$ on the artificial boundary.

The unbounded domain D is partitioned into infinite cones based on the elements in B. The finite-dimensional hp-IE subspaces $S_{h,w}^{p,N}(D) \subset H_w^1(D)$ and $S_{h,w^*}^{p,N}(D) \subset H_{w^*}^1(D)$ are chosen such that for each function v in these spaces, $v|_B \in S_h^p(B)$ is valid. Then the discrete version of (1.15) is given by

Find $u_h^N \in V_{h,N}^p$ such that

$$(\nabla u_h^N, \nabla v)_{\Omega_\infty} - k^2 (u_h^N, v)_{\Omega_\infty} = \langle g, v \rangle_\Gamma \qquad (1.18)$$

for all $v \in V_{h,N}^{p,*}$,

where the finite-dimensional trial and test spaces are defined by

$$V_{h,N}^p := \{v \in H_w^1(\Omega_\infty) \,|\, v|_\Omega \in S_h^p(\Omega),\ v|_D \in S_{h,w}^{p,N}(D)\}, \qquad (1.19)$$

$$V_{h,N}^{p,*} := \{v \in H_{w^*}^1(\Omega_\infty) \,|\, v|_\Omega \in S_h^p(\Omega),\ v|_D \in S_{h,w^*}^{p,N}(D)\}. \qquad (1.20)$$

Choosing basis functions in $V_{h,N}^p$ and $V_{h,N}^{p,*}$ finally yields from (1.18) a system of linear equations for the unknown coefficients of u_h^N with respect to that basis. The basis functions can be chosen such that the coupling in the element integrals is local, which leads to a sparse stiffness matrix. The IE shape functions proposed in [14] are products of angular and radial shape functions, where the angular part consists of conventional $(q-1)$-dimensional interpolation polynomials, which provide continuity over the faces of adjacent elements. The radial part is given by a truncated multipole expansion of radiating solutions to the Helmholtz equation, like those described in Section 1.3. Still, for the computation of the entries in the stiffness matrix, integrals over unbounded domains have to be evaluated. See [26], Section 6.7, and the references therein for various infinite elements. [25] provides a summary of IE formulations for exterior Helmholtz problems and also explains the numerical implementation of coupled FE/IE methods. [20] provides the convergence analysis for these methods. [71] compares the performance of infinite element methods with several (low-order) absorbing boundary conditions.

1.2.3 Non-reflecting boundary conditions

These can also be seen as conditions on the artificial boundary B that match the unknown solution in Ω with the solution of the exterior problems (1.8) or (1.9), (1.10) in D. Because of the unique determination of the solution to these problems by the trace $u|_B$, there exists a well-defined mapping $M : u|_B \mapsto (\partial_n u)|_B$. This is called the *Dirichlet-to-Neumann (DtN)* map, because it maps the *Dirichlet data* $u|_B$ to the *Neumann data* $(\partial_n u)|_B$. The condition

$$\frac{\partial u}{\partial n} = Mu \quad \text{on } B, \qquad (1.21)$$

is an exact *non-reflecting boundary condition* (NRBC), by construction. With the Laplace transformation $\mathcal{L}$ [83], we also obtain an exact non-reflecting boundary condition for the time-dependent problem:

$$\frac{\partial U}{\partial n} = \mathcal{L}^{-1}\left(M\mathcal{L}U\right) \quad \text{on } B \times I. \tag{1.22}$$

Note that in general the condition (1.21) is non-local in space and that (1.22) is additionally non-local in time. The spatial non-locality is acceptable if some fast numerical transformation can be used. The non-locality in time, however, implies that the computational cost and storage both grow with time, a property that renders such a boundary condition useless for long-time simulations.

One possibility to obtain an explicit expression for the DtN map M is by means of the free-space fundamental solution of (1.8) or (1.9). The non-reflecting boundary condition then takes the form of a boundary integral equation. This approach has been followed in [74] for the time-dependent case. It is based on the formulation in [78], which was implemented in [29]. Because of the retarded potentials involved, the temporal non-locality is restricted to a *fixed amount of data from the past.* This amount is proportional to the diameter of the computational domain. If the boundary integral equation is solved with the boundary element method and combined with a finite element method in the interior, a combined FE/BE method, as described before, is obtained. An advantage of the method is its flexibility regarding the shape of the artificial boundary. However, for artificial boundaries with simple shapes, such as spheres or spheroids, boundary conditions that allow a more efficient implementation can be derived.

For time-harmonic problems in separable coordinates, Mu can be written in the form $\mathcal{H}^{-1}(\hat{E}_\ell(\mathcal{H}u)_\ell)$ with the spatial harmonic transform $\mathcal{H}$, which in 2D polar coordinates, for instance, is the standard Fourier transformation. For coordinate systems in which the Laplace operator separates, the DtN map for each harmonic coefficient $(\mathcal{H}u)_\ell$ is thus a multiplication by a constant $\hat{E}_\ell$, which depends on the size of the computational domain and on the wave number k. $\hat{E}_\ell$ is sometimes called the *kernel* of the non-reflecting boundary condition. It usually involves special functions, such as Hankel functions for spherical coordinates. See [42], Section 2.1, for a derivation of the NRB kernel in various separable coordinate systems. Explicit expressions for Mu have been derived for acoustic waves in 2D and 3D with circular and spherical boundaries in [54]. The DtN map for elastic waves in 2D with a circular boundary has been derived in [30].

For practical purposes, the harmonic series in the DtN map has to be truncated at some finite index N. The truncated DtN condition is exact for

waves consisting of the first N harmonic modes. To ensure well-posedness of the problem in Ω with the truncated DtN condition imposed on B, a difficulty which has been pointed out in [45], the *modified DtN (MDtN)* condition was derived. If the truncated DtN operator is denoted by M^N, the MDtN condition takes the form

$$\left(\frac{\partial}{\partial n} - ik\right) u = (M - ik)^N u \quad \text{on } B, \tag{1.23}$$

an expression approaching (1.21) as $N \to \infty$. The MDtN condition is exact for waves consisting of the first N harmonic modes, and the problem in Ω with (1.23) is well-posed. The MDtN condition was first derived for acoustic waves in 2D and 3D with elliptic and spheroidal coordinates in [36] and then for elastic waves in 2D with a circular boundary in [47]. In [24], the MDtN condition was derived for elastic waves in 3D with a spherical artificial boundary. See also [26, 27] for more information on the DtN method. The DtN and MDtN condition are non-local in space, because harmonic transforms have to be computed, which involve boundary integrals. In a numerical scheme, this leads to a system of linear equations where the matrix consists of a full block, with a size proportional to the square of the number of grid points on the boundary. Therefore the computation of matrix-vector products during an iterative scheme for the solution of the linear equation system may become expensive, especially in 3D. The efficient implementation of the DtN and MDtN condition for the Helmholtz equation has been treated in [66]. There were also attempts to localize the DtN map, which yields approximate boundary conditions. Such a boundary condition can be of arbitrarily high order, though [31].

In the time-dependent case, (1.22) takes the form

$$\frac{\partial U}{\partial n} = \mathcal{H}^{-1}\left(E_\ell * (\mathcal{H}\mathcal{L}U)_\ell\right) \quad \text{on } B \times I, \tag{1.24}$$

where the kernel satisfies $\mathcal{L}E_\ell = \hat{E}_\ell$. Here, $*$ denotes convolution in time. If the kernel $\hat{E}_\ell$ is known for a time-harmonic problem, the exact non-reflecting boundary condition for the corresponding time-dependent problem is given by the Volterra integral equation (1.24). Fast convolution algorithms have been developed especially for the solution of such equations [57]. Despite the non-locality of (1.24) in space and time, the work with fast convolution is acceptable, and storage only grows logarithmically with time. We note that for an artificial boundary of general shape, a computationally cheaper *exact* NRBC may not be found.

It turns out that in spherical coordinates and in odd space dimensions, the kernel $\hat{E}_\ell$ is a rational function of the wave number k. Therefore the

convolutions $E_\ell * (\mathcal{HL}U)_\ell$ can be written as solutions of ordinary differential equations in time, which yields a *temporally local, exact* NRBC. In [72, 36, 37], this boundary condition has been derived for the wave equation in 3D. The number of ordinary differential equations to be solved together with the problem in the interior can be drastically reduced by using rational approximation of the kernel $\hat{E}_\ell$ with carefully selected poles. In doing so, the NRBC becomes approximate. However, about 20 ordinary differential equations are sufficient to approximate the boundary condition for nearly 1000 Fourier modes, the approximation error still being below 10^{-8} [3]. The localization in space is possible as well. For that purpose, the kernel $\hat{E}_\ell$, as a function of the wave number, is approximated by a finite continued fraction. Then the convolutions $E_\ell * (\mathcal{HL}U)_\ell$ can be evaluated recursively with partial differential equations on $B \times I$, which yields a *temporally and spatially local, approximate* NRBC, the order of which can be chosen arbitrarily high by raising the number of terms in the continued fraction expansion. The condition derived in [43] is such a local condition, and it can also be used in even space dimensions. A condition derived earlier in [9] is also an approximate local condition, but it involves derivatives of the same order as its accuracy, and is therefore only used as a low-order local NRBC. It is based on a sequence of specially chosen differential operators, which eliminate more and more terms in a progressive wave expansion of the solution to the wave equation. For cartesian coordinates, which are suited for planar artificial boundaries, the non-reflecting boundary kernel is not a-priori a rational function. It can be approximated by a rational function or by continued fractions to yield local approximate boundary conditions. The first of these are derived in [21], where Padé approximations have been used. Due to the high order of the derivatives involved, this is only used as a low-order NRBC. There are several local approximate boundary conditions of arbitrarily high order. See [28] for a review on high-order local conditions. We refer to [79] as a comprehensive review on non-reflecting boundary conditions.

1.2.4 Absorbing layers

An alternative to non-reflecting boundary conditions are absorbing layers. The computational domain Ω is surrounded by a layer Ω_ℓ with an interior boundary B_i and an exterior boundary B_e. The idea is to modify the partial differential equation (1.8) or (1.9) in Ω_ℓ, in such a way that waves leaving the computational Ω are damped on their way through the layer. Even if outgoing waves are reflected at the exterior layer boundary B_e, the amplitude of spurious reflections travelling back into Ω can be made arbitrarily small, if the layer parameters are chosen appropriately. One essential difficulty in

the development of absorbing layers was to find a layer that does not reflect outgoing waves from Ω at the interior boundary B_i. These would actually be undamped, spurious reflections that spoil the numerical solution throughout Ω. A layer which lets waves pass into Ω_ℓ without any reflection on B_i is called a *perfectly matched* layer (PML). Such a layer was first discovered for the time-dependent Maxwell's equations [12], with a rectangular box as the computational domain. This is a shape for which non-reflecting boundary conditions do not exist yet. PMLs can also be derived in spherical and cylindrical coordinates [80, 16]. Still, there is one important restriction: the domain enclosed by the interior layer boundary B_i must be convex. This is clear because waves leaving Ω cannot reenter, by construction of the PML.

Arbitrary PML formulations may not be well-posed. For example, the first PML formulation was only weakly well-posed. See [68] for well-posed formulations of PML for Maxwell's equation in various coordinates. Even if the PML formulation is well-posed, it may admit solutions that grow exponentially in time. This is the case when the PML formulation is unstable. In [10] a necessary condition for the stability of the PML model for a general hyperbolic system is presented.

1.3 Non-reflecting boundary conditions with spherical artificial boundaries

Separation of variables and spherical harmonics In spherical coordinates we write $\boldsymbol{x} = (r, \boldsymbol{\xi})$, $r > 0$, $\boldsymbol{\xi} \in S^{q-1}$, where S^{q-1} denotes the unit sphere in q-dimensional space. The Laplace operator then separates into a radial and an angular part,

$$\Delta = \frac{\partial^2}{\partial r^2} + \frac{q-1}{r}\frac{\partial}{\partial r} + \frac{1}{r^2}\Delta_S, \tag{1.25}$$

where Δ_S denotes the Laplace-Beltrami operator on S^{q-1}. The eigenfunctions of Δ_S are the *spherical harmonics,* denoted by S_n, $n \geq 0$. There are $N(q,n) = O(n^{q-2})$, $n \to \infty$, linearly independent spherical harmonics of degree n in q space dimensions. They can be constructed recursively from the spherical harmonics in lower dimensions, beginning with the standard Fourier basis $e^{\pm in\phi}$ in $2D$ [64]. After normalization, the q-dimensional spherical harmonics form a complete orthonormal system of functions in the Hilbert space $L^2(S^{q-1})$ with the usual L^2 inner product

$$(f, g) := \int_{S^{q-1}} f\overline{g}\, ds. \tag{1.26}$$

Each spherical harmonic S_n satisfies $\Delta_S S_n = -n(n+q-2)S_n$.

Fourier coefficients and Hankel functions If u is a solution to the exterior Helmholtz problem (1.9), (1.10), the Fourier coefficient $u_n(r) := (u(r,\cdot), S_n)$ with respect to any spherical harmonic of degree $n \geq 0$ satisfies the ordinary differential equation

$$\frac{d^2u_n}{dr^2} + \frac{q-1}{r}\frac{du_n}{dr} + \left(k^2 - \frac{n(n+q-2)}{r^2}\right)u_n = 0, \tag{1.27}$$

$$\lim_{r\to\infty} r^{\frac{q-1}{2}}\left(\frac{d}{dr} - ik\right)u_n = 0. \tag{1.28}$$

With the transformation $u_n(r) = z^{-\alpha}v_n(z)$, $z := kr$, $\alpha := (q-2)/2$, the function v_n becomes a radiating solution of Bessel's differential equation. Therefore

$$u_n(r) = a_n \frac{H_\nu^{(1)}(kr)}{r^\alpha}, \quad \nu := n + \alpha. \tag{1.29}$$

In (1.29), $H_\nu^{(1)}$ denotes the Hankel function of the first kind with order ν, which is a holomorphic function with an isolated singularity at the origin.

Dirichlet-to-Neumann map For a spherical artificial boundary $B = S_R$, with radius $R > 0$, the solution for $r > R$ is determined by its values at $r = R$:

$$u_n(r) = \left(\frac{R}{r}\right)^\alpha \frac{H_\nu^{(1)}(kr)}{H_\nu^{(1)}(kR)} u_n(R), \quad r \geq R. \tag{1.30}$$

We denote by $(\mathcal{H}u)_n := u_n(R)$, $n \geq 0$, the coefficients of the harmonic transform of u on B. Then the DtN map is given by

$$Mu = \frac{1}{R}\mathcal{H}^{-1}\left(\hat{E}_n(kR)\,(\mathcal{H}u)_n\right), \tag{1.31}$$

where coefficients of the DtN kernel are given by

$$\hat{E}_n(z) = z\left(\frac{H_\nu^{(1)\prime}(z)}{H_\nu^{(1)}(z)} - \frac{\alpha}{z}\right) = z\frac{d}{dz}\log\left(z^{-\alpha}H_\nu^{(1)}(z)\right), \quad n \geq 0. \tag{1.32}$$

The DtN condition (1.21) with the kernel (1.32) was formulated by Keller and Givoli in 1989 [54].

Time-harmonic case: multipole expansion For the localization of the DtN condition, and also for the time-dependent case, the Laurent series expansion of the Hankel function is useful. For the Fourier coefficients, we then obtain

$$u_n(r) = \frac{e^{ikr}}{r^{\alpha+1/2}} \sum_{j=0}^{\infty} \frac{\hat{f}_n^j}{r^j}, \tag{1.33}$$

where the coefficients $\hat{f}_n^j \in \mathbb{C}$ satisfy the recurrence relation

$$ik\hat{f}_n^j = \frac{1}{2j}\left(j(j-1) - \left(\nu - \frac{1}{2}\right)\left(\nu + \frac{1}{2}\right)\right)\hat{f}_n^{j-1}, \quad j \geq 1. \tag{1.34}$$

The multiplication with S_n and the summation over all spherical harmonics yields a multipole expansion for solutions to the Helmholtz equation (1.9), which was given by Wilcox in the 3D case [84]:

$$u(r, \boldsymbol{\xi}) = \frac{e^{ikr}}{r^{\alpha+1/2}} \sum_{j=0}^{\infty} \frac{\hat{f}^j(\boldsymbol{\xi})}{r^j}, \tag{1.35}$$

where the functions $\hat{f}^j : S^{q-1} \to \mathbb{C}$ satisfy the partial differential equations

$$ik\hat{f}^j = \frac{1}{2j}\left(j(j-1) + \Delta_S - \left(\alpha - \frac{1}{2}\right)\left(\alpha + \frac{1}{2}\right)\right)\hat{f}^{j-1}, \tag{1.36}$$

for $j \geq 1$. Here it was used that $\Delta_S S_n = -(\nu - \alpha)(\nu + \alpha)S_n$. We emphasize the following two distinct features of solutions to the Helmholtz equation (1.9):

- the expansion into a power series in $1/r$ (1.33), (1.35)
- recurrence relations for the coefficients (1.34), (1.36)

These two features have been exploited separately or in common in the derivation of non-reflecting boundary conditions. We also note that in odd space dimensions $q = 1, 3, \ldots$, i. e. $\alpha + 1/2 \in \mathbb{N}_0$, the series in (1.33) reduces to a *finite* sum, because the right-hand side of the recursion (1.34) vanishes for $j = \nu + 1/2$ in that case.

Time-harmonic case: non-reflecting boundary conditions The differentiation of (1.33) yields

$$\left(\frac{d}{dr} - ik\right)\left(r^{\alpha+\frac{1}{2}} u_n\right)(r) = -\frac{e^{ikr}}{r} \sum_{j=1}^{\infty} j\frac{\hat{f}_n^j}{r^j}, \quad r \geq R. \tag{1.37}$$

With the definition of

$$\hat{\psi}_n^j := \frac{e^{ikR}\hat{f}_n^j}{R^j}, \quad j \geq 0, \tag{1.38}$$

together with (1.33) and (1.34) we obtain

$$\left(\frac{d}{dr} - ik\right)\left(r^{\alpha+\frac{1}{2}}u_n\right)\Big|_{r=R} = -\frac{1}{R}\sum_{j=1}^{\infty} j\hat{\psi}_n^j, \tag{1.39}$$

with

$$ik\hat{\psi}_n^j = \frac{1}{R}\frac{1}{2j}\left(j(j-1) - \left(\nu - \frac{1}{2}\right)\left(\nu + \frac{1}{2}\right)\right)\hat{\psi}_n^{j-1}, \quad j \geq 1, \tag{1.40}$$

$$\sum_{j=0}^{\infty}\hat{\psi}_n^j = R^{\alpha+\frac{1}{2}}\, u_n|_{r=R}\,. \tag{1.41}$$

In odd space dimensions, the series in (1.39), (1.41) reduce to finite sums, which means that (1.40), (1.41) will form a finite system of linear equations for the unknown coefficients $\hat{\psi}_n^j$ on the right-hand side of the boundary condition (1.39). The application of the inverse harmonic transform yields a global, exact non-reflecting boundary condition.

The successive application of special differential operators, given by

$$\hat{B}_0 := I, \quad \hat{B}_{m+1} := \left(\frac{\partial}{\partial r} - ik + \frac{2m}{r}\right)\hat{B}_m,\ m \geq 0, \tag{1.42}$$

to the multipole expansion (1.35) eliminates more and more terms in the series, such that $\hat{B}_\ell(r^{\alpha+1/2}u) = O(r^{-2\ell})$, $r \to \infty$, for any $\ell \geq 0$:

$$\hat{B}_\ell\left(r^{\alpha+\frac{1}{2}}u\right)(r,\boldsymbol{\xi}) = (-1)^\ell \frac{e^{ikr}}{r^\ell}\sum_{j=\ell}^{\infty}\frac{j!}{(j-\ell)!}\frac{\hat{f}^j(\boldsymbol{\xi})}{r^j}, \quad \ell \geq 0. \tag{1.43}$$

The functions $\hat{w}^\ell := \hat{B}_\ell(r^{\alpha+\frac{1}{2}}u)$, $\ell \geq 0$, therefore have the properties

$$\hat{w}^0 = r^{\alpha+\frac{1}{2}}u, \quad \left(\frac{\partial}{\partial r} - ik + \frac{2\ell}{r}\right)\hat{w}^\ell = \hat{w}^{\ell+1}, \quad \hat{w}^\ell = O(r^{-2\ell}),\ r \to \infty. \tag{1.44}$$

With (1.36) it is possible to derive a recurrence relation for the functions $\hat{w}^\ell = \hat{w}^\ell(r,\boldsymbol{\xi})$, which involves only angular partial derivatives, namely

$$\left(-ik + \frac{\ell}{r}\right)\hat{w}^\ell = \frac{1}{2r^2}\left(\ell(\ell-1) + \Delta_S - \left(\alpha - \frac{1}{2}\right)\left(\alpha + \frac{1}{2}\right)\right)\hat{w}^{\ell-1} + \frac{1}{2}\hat{w}^{\ell+1}, \tag{1.45}$$

for $\ell \geq 1$. Setting $\hat{w}^{p+1} := 0$ for a $p \geq 0$ yields a local, approximate non-reflecting boundary condition of order $2p+2$.

Time-dependent case: progressive wave expansion The Laplace transform with parameter $s \in \mathbb{C}$ conveys the wave equation (1.8) to the Helmholtz equation (1.9) with wave number $k = is/c$, where c denotes the wave speed. The inverse Laplace transform thus transfers a solution $u(r, \boldsymbol{\xi})$ of the Helmholtz equation (1.9) to a solution $U(r, \boldsymbol{\xi}, t)$ of the wave equation (1.8). From (1.33), we obtain for the Fourier coefficient $U_n(r,t) := (U(r,\cdot,t), S_n)$ with respect to any spherical harmonic of degree $n \geq 0$ the expansion

$$U_n(r,t) = \frac{1}{r^{\alpha+\frac{1}{2}}} \sum_{j=0}^{\infty} \frac{f_n^j(t-r/c)}{r^j}, \tag{1.46}$$

where the functions f_n^j satisfy the ordinary differential equations

$$\frac{1}{c}\frac{df_n^j}{dt} = -\frac{1}{2j}\left(j(j-1) - \left(\nu - \frac{1}{2}\right)\left(\nu + \frac{1}{2}\right)\right) f_n^{j-1}, \quad j \geq 1. \tag{1.47}$$

The multipole expansion (1.35) yields the *progressive wave expansion,* after applying the inverse Laplace transform:

$$U(r, \boldsymbol{\xi}, t) = \frac{1}{r^{\alpha+\frac{1}{2}}} \sum_{j=0}^{\infty} \frac{f^j(\boldsymbol{\xi}, t-r/c)}{r^j}, \tag{1.48}$$

with the following recursion for the coefficient functions f^j:

$$\frac{1}{c}\frac{\partial f^j}{\partial t} = -\frac{1}{2j}\left(j(j-1) + \Delta_S - \left(\alpha - \frac{1}{2}\right)\left(\alpha + \frac{1}{2}\right)\right) \hat{f}^{j-1}, \quad j \geq 1. \tag{1.49}$$

Initial conditions for f_n^j or f^j are obtained by the initial conditions on U.

Time-dependent case: non-reflecting boundary conditions The first non-reflecting boundary condition for the time-dependent problem (1.8) with a spherical artificial boundary of radius $R > 0$ is probably the one proposed by Bayliss and Turkel in 1980 [9]. It takes the form

$$B_\ell(r^{\alpha+\frac{1}{2}}U) = 0 \quad \text{on } B \times I, \tag{1.50}$$

for an $\ell \geq 0$, where the differential operators B_m, $m \geq 0$, are defined by

$$B_0 := I, \quad B_{m+1} := \left(\frac{1}{c}\frac{\partial}{\partial t} + \frac{\partial}{\partial r} + \frac{2m}{r}\right) B_m, \; m \geq 0. \tag{1.51}$$

The condition (1.50) is local in space and time, and it is an approximate condition of order 2ℓ. It involves both temporal and spatial derivatives of

order ℓ, though. which renders the combination of (1.50) with a numerical scheme complicated for large ℓ. This NRBC is therefore used only as a low-order condition.

Another non-reflecting boundary condition is obtained by taking the inverse Laplace transform of (1.39)–(1.41). For the n-th Fourier coefficient, it reads

$$\left(\frac{1}{c}\frac{\partial}{\partial t}+\frac{\partial}{\partial r}\right)\left(r^{\alpha+\frac{1}{2}}U_n\right)\Big|_{r=R}=-\frac{1}{R}\sum_{j=1}^{\infty}j\psi_n^j, \tag{1.52}$$

with

$$\frac{d\psi_n^j}{dt} = \frac{1}{R}\frac{1}{2j}\left(j(j-1)-\left(\nu-\frac{1}{2}\right)\left(\nu+\frac{1}{2}\right)\right)\psi_n^{j-1}, \quad j\geq 1, \tag{1.53}$$

$$\sum_{j=0}^{\infty}\psi_n^j = r^{\alpha+\frac{1}{2}}\,U_n|_{r=R}\,. \tag{1.54}$$

In odd space dimensions, the series reduce to finite sums, and (1.53), (1.54) form a finite system of ordinary differential equations for the functions ψ_n^j used in (1.52). For 3D problems, this non-reflecting boundary condition has been proposed in 1993 by Sofronov [72] and independently by Grote and Keller, in 1995 [36, 37]. It is an exact condition, local in time and global in space. It involves only low-order derivatives in space and time, and an auxiliary system of ordinary differential equations has to be solved. A spatial harmonic transform and also its inverse have to be computed in each time-step for (1.54) and (1.52).

Another non-reflecting boundary condition can be derived from (1.44), (1.45). It was proposed by Hagstrom and Hariharan in 1998 for problems in 2D and 3D [43] and is of the form

$$\left(\frac{1}{c}\frac{\partial}{\partial t}+\frac{\partial}{\partial r}\right)\left(r^{\alpha+\frac{1}{2}}U\right)=w^1 \quad \text{on } B\times I, \tag{1.55}$$

with

$$\left(\frac{1}{c}\frac{\partial}{\partial t}+\frac{\ell}{r}\right)w^\ell=\frac{1}{2r^2}\left(\ell(\ell-1)+\Delta_S-\left(\alpha-\frac{1}{2}\right)\left(\alpha+\frac{1}{2}\right)\right)w^{\ell-1}+\frac{1}{2}w^{\ell+1}, \tag{1.56}$$

for $\ell\geq 0$, and

$$w^0=r^{\alpha+\frac{1}{2}}U, \qquad w^{p+1}=0, \tag{1.57}$$

for a $p\geq 0$. The Hagstrom-Hariharan condition is actually a modification of the Bayliss-Turkel condition. It is an approximate condition of order $2p+2$, local in space and in time. It involves only low-order derivatives, and an

auxiliary system of partial differential equations on the artificial boundary has to be solved. There are no harmonic transformations or special functions involved in this NRBC. It can be applied in any space dimension.

1.4 Methods for multiple scattering problems

By *multiple* scattering problem we denote a wave propagation problem, where the scatterer consists of several components, i. e. is not connected as a set. In a multiple scattering problem, waves are reflected back and forth between the different scatterer components. The truncation of such a problem with an artificial boundary that is a single sphere, for example, may lead to a very large computational domain and there is possibly a lot of space discretized where the problem is extremely simple. Our idea is to truncate the unbounded domain with an artificial boundary that is the *union of several well-separated spheres.* Each of the spheres may contain one of the scatterer components, for example.

The important new feature of a multiple scattering problem compared to a single scattering problem is that waves are not purely outgoing from a domain component anymore, but there are waves from one domain component *entering* all the other domain components. This feature prevents us from the use of an absorbing layer on each domain component, because such a layer does not allow waves entering the domain it encloses. It is also not plausible that infinite elements can be constructed that allow for general configurations of domain components.

The numerical methods available in the multiple scattering case are the methods based on integral equations and the non-reflecting boundary conditions. The methods based on integral equations have been successfully used for the solution of problems with very complicated scatterers. We refer to the introduction of Chapter 2 and to the references therein for more information. However, these methods need the knowledge of a fundamental solution, which can probably not be found if the problem is inhomogeneous or nonlinear.

There is no previous work, to our knowledge, where it is attempted to use non-reflecting boundary conditions for the solution of a multiple scattering problem. Because non-reflecting boundary conditions arise from the matching of an interior, numerical solution with an exterior, exact solution, the development of NRBCs for multiple scattering problems is possible, though. Such non-reflecting boundary conditions are the topic of this thesis. The following two chapters are shortly outlined in the next paragraphs.

The crucial tool for the derivation of NRBCs for multiple scattering prob-

lems is the decomposition of the solution to the exterior problem (1.8) or (1.9) into multiple purely outgoing waves, $u = \sum_j u_j$, where each u_j is associated to exactly one of the domain components. This decomposition is unique if the solution to the multiple scattering problem is unique, which follows from the uniqueness of solutions to each of the auxiliary problems. In our proofs, we have restricted to artificial boundaries that are unions of spheres. The proofs have been done in Chapter 2 for the time-harmonic case and in Chapter 3 for the time-dependent case.

Once having the decomposition at hand, the purely outgoing waves are propagated from the boundary B_j of one domain component to the boundaries B_ℓ of all the other domain components, $\ell \neq j$. This is done with propagation operators, which are described in the following chapters. We also introduce operators that transfer the traces $u_j|_{B_j}$ to the traces of the normal derivatives $(\partial_n u_j)|_{B_\ell}$, $\ell \neq j$. These transfer operators are like Dirichlet-to-Neumann maps, but between different boundary components. Because of the unique decomposition $u = \sum u_j$ in the exterior region D, the non-reflecting boundary condition for u is written as a linear combination of propagation and transfer operators applied to the traces $u_j|_{B_j}$. This new boundary condition reduces to the well-known DtN condition and the Grote-Keller condition, respectively, in the single scattering case. Therefore, these non-reflecting boundary conditions are generalizations of the single scattering conditions to the multiple scattering case.

We then prove exactness of the non-reflecting boundary condition, which means that the solution in the bounded domain Ω, with the non-reflecting boundary condition imposed on B, is equal to the restriction of the solution in the unbounded domain Ω_∞ to Ω. Therefore, these boundary conditions correctly propagate waves between all scatterer components, and no spurious reflections occur on the artificial boundary components.

In each chapter, we also give numerical examples that show both the accuracy of the non-reflecting boundary condition for multiple scattering problems and the possibly drastic reduction of the size of the computational domain compared to the previously known boundary conditions for the single scattering case.

Acknowledgements

This thesis was written at the Mathematics Department of the University of Basel, Switzerland. My sincere thanks go to Prof. Marcus J. Grote for his excellent support during my doctoral studies. He always had time for motivating discussions, and to give useful advice.

I would also like to thank Prof. Patrick Joly from INRIA Rocquencourt, France, for his interest in my work, and for his willingness to act as a co-referee for my thesis.

Special thanks go to my parents, for their constant, loving support during my education.

Chapter 2

The time-harmonic case

The contents of this chapter appeared in J. Comput. Phys. [41].

Abstract A Dirichlet-to-Neumann (DtN) condition is derived for the numerical solution of time-harmonic multiple scattering problems, where the scatterer consists of several disjoint components. It is obtained by combining contributions from multiple purely outgoing wave fields. The DtN condition yields an exact non-reflecting boundary condition for the situation, where the computational domain and its exterior artificial boundary consist of several disjoint components. Because each sub-scatterer can be enclosed by a separate artificial boundary, the computational effort is greatly reduced and becomes independent of the relative distances between the different subdomains. The DtN condition naturally fits into a variational formulation of the boundary value problem for use with the finite element method. Moreover, it immediately yields as a by-product an exact formula for the far-field pattern of the scattered field. Numerical examples show that the DtN condition for multiple scattering is as accurate as the well-known DtN condition for single scattering problems (Keller and Givoli (1989, J. Comput. Phys., 82, 172), Givoli (1992, Elsevier, Amsterdam)), while being more efficient due to the reduced size of the computational domain.

2.1 Introduction

For the numerical solution of scattering problems in infinite domains, a well-known approach is to enclose all obstacles, inhomogeneities and nonlinearities with an artificial boundary B. A boundary condition is then imposed on B, which leads to a numerically solvable boundary value problem in a finite domain Ω. The boundary condition should be chosen such that the solution

of the problem in Ω coincides with the restriction to Ω of the solution in the original unbounded region.

If the scatterer consists of several obstacles, which are well separated from each other, the use of a single artificial boundary to enclose the entire scattering region, becomes too expensive. Instead it is preferable to enclose every sub-scatterer by a separate artificial boundary B_j. Then we seek an exact boundary condition on $B = \bigcup B_j$, where each B_j surrounds a single computational sub-domain Ω_j. This boundary condition must not only let outgoing waves leave Ω_j without spurious reflection from B_j, but also propagate the outgoing wave from Ω_j to all other sub-domains Ω_ℓ, which it may reenter subsequently. To derive such an exact boundary condition, an analytic expression for the solution everywhere in the exterior region is needed. Neither absorbing boundary conditions [21, 8], nor perfectly matched layers [12, 80, 48] provide us with such a representation. Instead we shall seek a Dirichlet-to-Neumann (DtN) boundary condition, which is based on a Fourier series representation of the solution in the exterior region.

Exact DtN conditions have been derived for various equations and geometries, but always in the situation of a single computational domain, where the scattered field is purely outgoing outside Ω [54, 26, 35, 27, 24]. In a situation of multiple disjoint computational domains, however, waves are not purely outgoing outside the computational domain $\Omega = \bigcup \Omega_j$, as they may bounce back and forth between domains. We shall show how to overcome this difficulty and derive an exact DtN condition for multiple scattering. The derivation presented below for the Helmholtz equation in two space dimensions readily extends to multiple scattering problems in other geometries and also to different equations. Because this exact boundary condition allows the size of the computational sub-domains, Ω_j, to be chosen independently of the relative distances between them, the computational domain, Ω, can be chosen much smaller than that resulting from the use of a single, large computational domain.

There is an extended literature on the solution of multiple scattering problems – see Martin [60] for an introduction and overview. Due to the difficulties mentioned above, numerical methods used for multiple scattering so far have mainly been based on integral representations [59, 62], while in the single scattering case many alternative methods, such as absorbing boundary conditions, perfectly matched layers, or the DtN approach are known. To our knowledge this work constitutes the first attempt to generalize the well-known DtN approach to multiple scattering.

Some of the analytical techniques we shall use, have been known in the "classical" scattering literature for quite some time. For instance, in 1913 Záviška [85] considered multiple scattering from an array of parallel circular

cylinders. He derived an infinite linear system for the unknown Fourier coefficients of the scattered field, which involve Fourier expansions of the purely outgoing wave fields about individual cylindrical obstacles. This method can be generalized to cylinders with non-circular cross-sections [67]. Another class of methods is based on single and double layer potentials, which involve integration with the Green's function over the artificial boundary. From this representation, systems of integral equations can be derived for multiple scattering problems – see Twersky [81] and Burke and Twersky [13] for an extensive overview of previous work until 1964, and [60] for more recent references.

In Section 2, we derive the DtN and modified DtN map for two scatterers. We show that the solution to the boundary value problem in Ω, with the DtN condition imposed on B, coincides with the restriction to Ω of the solution in the unbounded region Ω_∞. The formulation is generalized to an arbitrary number of scatterers in Section 3. In Section 4, we state a variational formulation of the artificial boundary value problem for use with the finite element method. An explicit formula for the far-field pattern of the solution, based on the decomposition of the scattered field into multiple purely outgoing wave fields, is derived in Section 5. Finally, in Section 6, we consider a finite difference implementation of the multiple-DtN method and demonstrate its accuracy and convergence. We also compare the multiple-DtN approach to the well-known (single-)DtN method and show that both the numerical solutions and the far-field patterns, obtained by these two different methods, coincide.

2.2 Two scatterers

We consider acoustic wave scattering from two bounded disjoint scatterers in unbounded two-dimensional space. Each scatterer may contain one or several obstacles, inhomogeneities, and nonlinearity. We let Γ denote the piecewise smooth boundary of all obstacles and impose on Γ a Dirichlet-type boundary condition, for simplicity. In Ω_∞, the region outside Γ, the scattered field $u = u(r, \theta)$ then solves the exterior boundary value problem

$$\Delta u + k^2 u = f \quad \text{in } \Omega_\infty \subset \mathbb{R}^2, \tag{2.1}$$

$$u = g \quad \text{on } \Gamma, \tag{2.2}$$

$$\lim_{r\to\infty} \sqrt{r} \left(\frac{\partial}{\partial r} - ik \right) u = 0. \tag{2.3}$$

The wave number k and the source term f may vary in space, while f may be nonlinear. The Sommerfeld radiation condition (2.3) ensures that the

scattered field corresponds to a purely outgoing wave at infinity.

Next, we assume that both scatterers are *well separated*, that is we assume that we can surround them by two non-intersecting circles B_1, B_2 centered at c_1, c_2 with radii R_1, R_2, respectively. In the unbounded region D, outside the two circles, we assume that the wave number $k > 0$ is constant, and that f vanishes. In D the scattered field u thus satisfies

$$\Delta u + k^2 u = 0 \quad \text{in } D, \quad k > 0 \text{ constant}, \tag{2.4}$$

$$\lim_{r\to\infty} \sqrt{r} \left(\frac{\partial}{\partial r} - ik \right) u = 0. \tag{2.5}$$

We wish to compute the scattered field, u, in the computational domain $\Omega = \Omega_\infty \setminus D$, which consists of the two disjoint components Ω_1 and Ω_2. A typical configuration with two obstacles is shown in Fig. 2.1. Here the computational domain Ω is internally bounded by $\Gamma = \Gamma_1 \cup \Gamma_2$, and externally by $B = \partial D$, which consists of the two circles B_1 and B_2.

To solve the scattering problem (2.1)–(2.3) inside Ω, a boundary condition is needed at the exterior artificial boundary B. This boundary condition must ensure that the solution in Ω, with that boundary condition imposed on B, coincides with the restriction of the solution in the original unbounded region Ω_∞.

2.2.1 Derivation of the DtN map

On B we shall now derive a DtN map, which establishes an exact relation between the values of u and its normal derivative. In contrast to the case of a single circular artificial boundary, as considered for example by Givoli [26] and Grote and Keller [35], we cannot simply expand u outside B in a Fourier series. First, there is no separable coordinate system outside B for the Helmholtz equation [5] and second, u is not purely outgoing in D. Indeed, part of the scattered field leaving Ω_1 will reenter Ω_2, and vice-versa. Hence the boundary condition we seek on B must not only let outgoing waves leave Ω_1 without spurious reflection from B_1, but also propagate the outgoing wave field from Ω_1 to Ω_2, and vice-versa, without any spurious reflection.

We begin the derivation of an exact non-reflecting boundary condition on $B = B_1 \cup B_2$ by introducing a local polar coordinate system (r_j, θ_j) outside each circle B_j, centered at c_j (see Fig. 2.1). Next, we denote by D_1 the unbounded domain outside B_1 with $r_1 > R_1$, and by D_2 the unbounded domain outside B_2 with $r_2 > R_2$. We now decompose the scattered field u in D into two purely outgoing wave fields u_1 and u_2, which solve the following

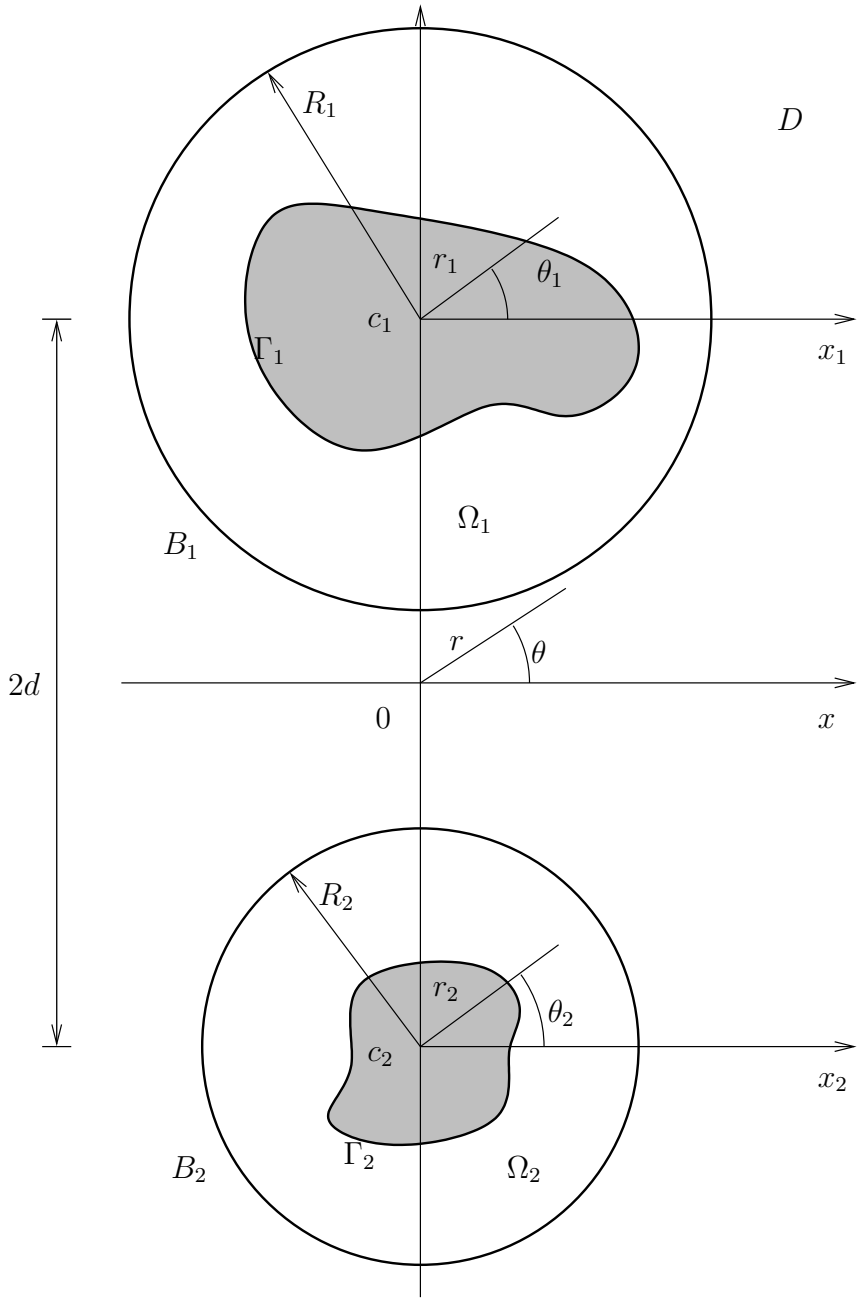

Figure 2.1: A typical configuration with two obstacles bounded by Γ_1 and Γ_2 is shown. The computational domain $\Omega = \Omega_1 \cup \Omega_2$ is externally bounded by the artificial boundary $B = B_1 \cup B_2$. In each domain component Ω_j, we use a local polar coordinate system (r_j, θ_j), while (r, θ) denotes the global polar coordinate system centered at the origin.

problems:

$$\Delta u_1 + k^2 u_1 = 0 \quad \text{in } D_1, \tag{2.6}$$

$$\lim_{r\to\infty} \sqrt{r}\left(\frac{\partial}{\partial r} - ik\right) u_1 = 0, \tag{2.7}$$

and

$$\Delta u_2 + k^2 u_2 = 0 \quad \text{in } D_2, \tag{2.8}$$

$$\lim_{r\to\infty} \sqrt{r}\left(\frac{\partial}{\partial r} - ik\right) u_2 = 0. \tag{2.9}$$

Each wave field is influenced only by a single scatterer and completely oblivious to the other. Therefore, u_1 and u_2 are entirely determined by their values on B_1 or B_2, respectively; they are given in local polar coordinates (r_1, θ_1), (r_2, θ_2) by

$$u_j(r_j, \theta_j) = \frac{1}{\pi}{\sum_{n=0}^{\infty}}' \frac{H_n^{(1)}(kr_j)}{H_n^{(1)}(kR_j)} \int_0^{2\pi} u_j(R_j, \theta') \cos n(\theta_j - \theta')\, d\theta', \quad r_j \geq R_j, \tag{2.10}$$

for $j = 1, 2$. Here the prime after the sum indicates that the term for $n = 0$ is multiplied by $1/2$, while $H_n^{(1)}$ denotes the n-th order Hankel function of the first kind. We now couple u_1 and u_2 with u by matching $u_1 + u_2$ with u on $B = B_1 \cup B_2$:

$$u_1 + u_2 = u \quad \text{on } B. \tag{2.11}$$

Both u and $u_1 + u_2$ solve the homogeneous Helmholtz equation (2.4) in $D = D_1 \cap D_2$, together with the Sommerfeld radiation condition (2.5) at infinity. Since u and $u_1 + u_2$ coincide on B, they coincide everywhere in the exterior region D. We summarize this result in the following proposition. Moreover, before proceeding with the derivation of the DtN map, we shall also prove that such a decomposition always exists and is unique.

Proposition 1. *Let u be the unique solution to the exterior Dirichlet problem (2.1)–(2.3) and assume that u satisfies (2.4), (2.5) in the exterior region, D. Then*

$$u \equiv u_1 + u_2, \quad \text{in } B \cup D, \tag{2.12}$$

where u_1 and u_2 are solutions to the problems (2.6), (2.7) and (2.8), (2.9), respectively, together with the matching condition (2.11). The decomposition of u into the two purely outgoing wave fields u_1 and u_2 is unique.

Proof. By the argument above, we have already shown that if $u = u_1 + u_2$ on B, and u_1 and u_2 solve (2.6)–(2.9), then $u \equiv u_1 + u_2$ everywhere in D. We shall now show that u_1 and u_2 exist and, in fact, are unique.
Existence: In the exterior domain D we use the Kirchhoff-Helmholtz formula [18] to write

$$u(x) = \int_B \left\{ u(y) \frac{\partial \Phi(x,y)}{\partial n(y)} - \frac{\partial u}{\partial n}(y) \Phi(x,y) \right\} ds(y), \quad x \in D. \tag{2.13}$$

Here Φ is the fundamental solution of the Helmholtz equation in two space dimensions,

$$\Phi(x,y) = \frac{i}{4} H_0^{(1)}(k|x-y|), \quad x \neq y, \tag{2.14}$$

while n denotes the outward normal from Ω on the artificial boundary B. Let

$$u_j(x) := \int_{B_j} \left\{ u(y) \frac{\partial \Phi(x,y)}{\partial n(y)} - \frac{\partial u}{\partial n}(y) \Phi(x,y) \right\} ds(y), \quad x \in D_j, \tag{2.15}$$

for $j = 1, 2$. Then, a straightforward calculation shows that u_1 satisfies (2.6), (2.7) whereas u_2 satisfies (2.8), (2.9). Clearly, $u(x) = u_1(x) + u_2(x)$, $\forall x \in D = D_1 \cap D_2$. The expressions (2.13) and (2.15) can be continuously extended up to the artificial boundaries B and B_1, B_2, respectively ([17], Theorem 2.13). Thus, u_1 and u_2 also satisfy the matching condition (2.11).
Uniqueness: Following a suggestion of S. Tordeux (INRIA, private communication, July 2003), we let $u \equiv v_1 + v_2$ be another decomposition in $B \cup D$, where v_1 and v_2 solve (2.6), (2.7) and (2.8), (2.9), respectively. We shall now show that $v_1 \equiv u_1$ and that $v_2 \equiv u_2$ throughout D. To do so, we let $w_1 := u_1 - v_1$ and $w_2 := u_2 - v_2$. Hence, w_1 and w_2 satisfy (2.6), (2.7) and (2.8), (2.9), respectively. Because w_2 is regular throughout D_2, it is also regular, and therefore bounded, everywhere inside B_1, including the local origin, c_1. Thus, in the vicinity of B_1, w_1 and w_2 can be written in the local polar coordinates, (r_1, θ_1), as

$$w_1(r_1,\theta_1) = \sum_{n\in\mathbb{Z}} a_n H_n^{(1)}(kr_1) e^{in\theta_1}, \tag{2.16}$$

$$w_2(r_1,\theta_1) = \sum_{n\in\mathbb{Z}} b_n J_n(kr_1) e^{in\theta_1}, \tag{2.17}$$

for $r_1 \in I := [R_1, R_1 + \varepsilon]$, with $\varepsilon = |c_2 - c_1| - (R_1 + R_2) > 0$, because the scatterers are assumed to be well separated. From the uniqueness of u we obtain $w_1 + w_2 = u_1 + u_2 - (v_1 + v_2) \equiv 0$ in $B \cup D$. Therefore

$$a_n H_n^{(1)}(kr_1) + b_n J_n(kr_1) = 0, \quad \forall\, n \in \mathbb{Z},\ r_1 \in I. \tag{2.18}$$

Since $H_n^{(1)}$ and J_n are two linearly independent solutions of Bessel's differential equation, we conclude that $a_n = b_n = 0$ for all $n \in \mathbb{Z}$. Thus, $v_1 \equiv u_1$ and $v_2 \equiv u_2$ in $B \cup D$. □

As a consequence of the proposition, we can now explicitly determine a DtN map for u by differentiating u with respect to the outward normal n on B_1 and B_2 as follows:

$$\begin{aligned} \partial_n u &= M[u_1] + T[u_2] \quad \text{on } B_1, && (2.19)\\ \partial_n u &= M[u_2] + T[u_1] \quad \text{on } B_2, && (2.20)\\ u_1 + P[u_2] &= u \quad \text{on } B_1, && (2.21)\\ P[u_1] + u_2 &= u \quad \text{on } B_2. && (2.22) \end{aligned}$$

Here the operator M corresponds to the *standard single-DtN operator*

$$M[u_j](\theta_j) := \frac{1}{\pi}{\sum_{n=0}^{\infty}}' \frac{kH_n^{(1)\prime}(kR_j)}{H_n^{(1)}(kR_j)} \int_0^{2\pi} u_j(R_j,\theta') \cos n(\theta_j - \theta')\, d\theta', \qquad (2.23)$$

$j = 1, 2$. The *transfer operator* T and *propagation operator* P are given by

$$\begin{aligned} T[u_1](\theta_2) &:= \frac{\partial u_1}{\partial r_2}(R_2,\theta_2), \quad T[u_2](\theta_1) := \frac{\partial u_2}{\partial r_1}(R_1,\theta_1), && (2.24)\\ P[u_1](\theta_2) &:= u_1(R_2,\theta_2), \quad P[u_2](\theta_1) := u_2(R_1,\theta_1). && (2.25) \end{aligned}$$

The expressions on the right-hand sides of (2.19), (2.20) and on the left-hand sides of (2.21), (2.22) can be evaluated explicitly by using the definitions (2.23)–(2.25) and the (exact) Fourier representation (2.10), valid in each local coordinate system. These calculations involve some technical but straightforward coordinate transformations. For instance, in the particular situation shown in Fig. 2.1, $T[u_2]$ and $P[u_2]$ are explicitly given (in local polar (r_1, θ_1)-coordinates) on B_1 for $\theta_1 \in [0, 2\pi)$ by

$T[u_2](\theta_1) =$

$$\begin{aligned} &\frac{1}{r_2}\Bigg[(R_1 + 2d\sin\theta_1)\, \frac{1}{\pi}{\sum_{n=0}^{\infty}}' \frac{kH_n^{(1)\prime}(kr_2)}{H_n^{(1)}(kR_2)} \int_0^{2\pi} u_2(R_2,\theta') \cos n(\theta_2 - \theta')\, d\theta' + \\ &+ \frac{1}{r_2} 2d\cos\theta_1 \frac{1}{\pi}{\sum_{n=0}^{\infty}}' \frac{nH_n^{(1)}(kr_2)}{H_n^{(1)}(kR_2)} \int_0^{2\pi} u_2(R_2,\theta') \sin n(\theta_2 - \theta')\, d\theta' \Bigg], \qquad (2.26) \end{aligned}$$

$$P[u_2](\theta_1) = \frac{1}{\pi}{\sum_{n=0}^{\infty}}' \frac{H_n^{(1)}(kr_2)}{H_n^{(1)}(kR_2)} \int_0^{2\pi} u_2(R_2,\theta') \cos n(\theta_2 - \theta')\, d\theta', \qquad (2.27)$$

where

$$r_2 = \sqrt{R_1^2 + 4dR_1 \sin\theta_1 + 4d^2}, \tag{2.28}$$

$$\sin\theta_2 = \frac{1}{r_2}\left(R_1 \sin\theta_1 + 2d\right), \tag{2.29}$$

$$\cos\theta_2 = \frac{1}{r_2} R_1 \cos\theta_1. \tag{2.30}$$

The expressions for $T[u_1]$ and $P[u_1]$ on B_2 are similar to (2.26)–(2.30), with r_2 replaced by r_1, θ_2 by θ_1, etc.

The matching condition (2.21), (2.22) cannot be inverted explicitly, and u_1 and u_2 thereby eliminated from the DtN condition (2.19)–(2.22). Instead, we shall compute the values of u_1 on B_1 and u_2 on B_2, in addition to the values of u. These auxiliary values are also useful during post-processing, as they yield explicit expressions both for u everywhere outside Ω and for its far-field pattern – see Section 2.5.

With the DtN condition given by (2.19)–(2.22), we now state the boundary value problem for u inside the computational domain $\Omega = \Omega_1 \cup \Omega_2$:

$$\Delta u + k^2 u = f \quad \text{in } \Omega \tag{2.31}$$

$$u = g \quad \text{on } \Gamma \tag{2.32}$$

$$\partial_n u = M[u_1] + T[u_2], \quad \text{on } B_1 \tag{2.33}$$

$$\partial_n u = M[u_2] + T[u_1], \quad \text{on } B_2 \tag{2.34}$$

$$u_1 + P[u_2] = u \quad \text{on } B_1 \tag{2.35}$$

$$P[u_1] + u_2 = u \quad \text{on } B_2 \tag{2.36}$$

We now show that this boundary value problem has a unique solution, which coincides with the solution to the original problem (2.1)–(2.3).

Theorem 1. *Let u be the unique solution to the exterior Dirichlet problem (2.1)–(2.3) and assume that u satisfies (2.4), (2.5) in the exterior region, D. Then the double scattering boundary value problem (2.31)–(2.36) has a unique solution in Ω, which coincides with the restriction of u to Ω.*

Proof. Existence: We shall show that $u|_\Omega$ is a solution to (2.31)–(2.36). Since u satisfies (2.1), (2.2) it trivially satisfies (2.31), (2.32). To show that $u|_\Omega$ satisfies the DtN condition (2.33)–(2.36) on B, we consider in $B \cup D$ the unique decomposition $u \equiv u_1 + u_2$, provided by Proposition 1. Since $u_1 + u_2$ satisfies the DtN boundary condition (2.33)–(2.36) on B, by construction, so does the restriction of u to Ω. Therefore, $u|_\Omega$ is a solution to the boundary value problem (2.31)–(2.36).

Uniqueness: We extend the argument of Harari and Hughes [45] for a single scatterer to the case of two scatterers. Let v, together with $v_1|_{B_1}$ and $v_2|_{B_2}$, denote another solution of (2.31)–(2.36). We shall show that $v \equiv u|_\Omega$. First, we denote by

$$\overline{v_j}(r_j,\theta_j) := \frac{1}{\pi}{\sum_{n=0}^{\infty}}' \frac{H_n^{(1)}(kr_j)}{H_n^{(1)}(kR_j)} \int_0^{2\pi} v_j(R_j,\theta')\cos n(\theta_j-\theta')\,d\theta', \tag{2.37}$$

the two purely outgoing wave fields, defined for $r_j \geq R_j$, $j = 1, 2$. Next, we construct an extension

$$\overline{v} := \begin{cases} v, & \text{in } \Omega \\ \overline{v_1}+\overline{v_2}, & \text{in } B \cup D \end{cases} \tag{2.38}$$

of v into the exterior region D. We shall now show that $w := u - \overline{v}$ vanishes in Ω. To begin, we remark that w and its normal derivative are continuous everywhere in Ω_∞, while w satisfies $\Delta w + k^2 w = 0$ in Ω and $w = 0$ on Γ. By using integration by parts we now find that

$$\int_\Omega |\nabla w|^2 - k^2|w|^2\,dx = \int_B w\frac{\partial\overline{w}}{\partial n}\,ds, \tag{2.39}$$

from which we infer that

$$\int_B w\frac{\partial\overline{w}}{\partial n} - \overline{w}\frac{\partial w}{\partial n}\,ds = 0. \tag{2.40}$$

Let B_r denote the sphere of radius $r > 0$ centered at the origin. Again we use integration by parts, (2.40) and the fact that w is a solution of (2.4) to obtain

$$\begin{aligned} 0 &= \int_B w\frac{\partial\overline{w}}{\partial n} - \overline{w}\frac{\partial w}{\partial n}\,ds = \int_D w\Delta\overline{w} - \overline{w}\Delta w\,dx - \lim_{r\to\infty}\int_{B_r} w\frac{\partial\overline{w}}{\partial r} - \overline{w}\frac{\partial w}{\partial r}\,ds \\ &= -\lim_{r\to\infty}\int_{B_r} w\frac{\partial\overline{w}}{\partial r} - \overline{w}\frac{\partial w}{\partial r}\,ds. \end{aligned} \tag{2.41}$$

From the radiation condition (2.5) and (2.41) we now infer that

$$\begin{aligned} 0 &= \lim_{r\to\infty} \int\limits_{B_r} \left| \sqrt{r} \left(\frac{\partial}{\partial r} - ik \right) w \right|^2 ds \\ &= \lim_{r\to\infty} r \int\limits_{B_r} \left| \frac{\partial w}{\partial r} \right|^2 + k^2 |w|^2 - ik \left(w \frac{\partial \overline{w}}{\partial r} - \overline{w} \frac{\partial w}{\partial r} \right) ds \\ &= \lim_{r\to\infty} r \int\limits_{B_r} \left| \frac{\partial w}{\partial r} \right|^2 + k^2 |w|^2 \, ds. \end{aligned} \tag{2.42}$$

Since $k^2 > 0$ we conclude that

$$\lim_{r\to\infty} \int\limits_{B_r} |w|^2 \, ds = 0. \tag{2.43}$$

Equation (2.43) then implies that $w \equiv 0$ in D, by Rellich's theorem ([18], Lemma 2.11). By continuity, we also have $w = 0$ on B. Finally we apply Proposition 1 to w, which yields the unique decomposition $w \equiv w_1 + w_2$ with $w_1 \equiv 0$ and $w_2 \equiv 0$ in $B \cup D$. Because of the DtN condition (2.33)–(2.36) we conclude that $\partial_n w = 0$ on B. Since the problem

$$\Delta w + k^2 w = 0 \quad \text{in } \Omega \tag{2.44}$$
$$w = 0 \quad \text{on } \Gamma \tag{2.45}$$
$$w = 0 \quad \text{on } B \tag{2.46}$$
$$\partial_n w = 0 \quad \text{on } B \tag{2.47}$$

has only the trivial solution (which is verified directly by expanding the solution of (2.44) in a Fourier series and by using the linear independence of the Hankel functions), $w \equiv 0$ in Ω or $v \equiv u|_\Omega$. □

2.2.2 The modified DtN map

In practice the infinite sums which occur in the operators M, T, and P in the DtN condition (2.33)–(2.36) have to be truncated at some finite $N \geq 0$. The corresponding truncated operators are denoted by M^N, T^N, and P^N. Even in the situation of a single scatterer, truncation can destroy the uniqueness of the solution in Ω with the truncated DtN condition imposed at B. For single scattering, Harari and Hughes showed that uniqueness is preserved if N is chosen large enough [45]. Alternatively, the modified DtN (MDtN) map

introduced in [35] can be used to overcome this difficulty. Its generalization to the case of two scatterers is straightforward:

$$\begin{aligned} \partial_n u &= iku + (M - ik)^N[u_1] + (T - ikP)^N[u_2] \quad \text{on } B_1 && (2.48)\\ \partial_n u &= iku + (M - ik)^N[u_2] + (T - ikP)^N[u_1] \quad \text{on } B_2 && (2.49)\\ u_1 + P^N[u_2] &= u \quad \text{on } B_1 && (2.50)\\ P^N[u_1] + u_2 &= u \quad \text{on } B_2 && (2.51) \end{aligned}$$

Numerical results with the MDtN map applied to multiple scattering are shown in Section 6.1. They corroborate the expected improvement in accuracy and stability, well-known in the single scatterer case.

2.3 Multiple scattering problems

The derivation of the DtN map presented above for two scatterers is easily generalized to the case of several scatterers. We consider a situation with J scatterers, and surround each scatterer by a circle B_j of radius R_j. Again we denote by $B = \bigcup_{j=1}^{J} B_j$ the entire artificial boundary and by D_j the unbounded region outside the j-th circle. Hence the computational domain $\Omega = \bigcup_{j=1}^{J} \Omega_j$, where Ω_j denotes the finite computational region inside B_j, whereas $D = \bigcap_{j=1}^{J} D_j$ denotes the unbounded exterior region.

In D, we now split the scattered field into J purely outgoing wave fields $u_1, \ldots, u_J$, which solve the problems

$$\Delta u_j + k^2 u_j = 0 \quad \text{in } D_j, \tag{2.52}$$

$$\lim_{r\to\infty} \sqrt{r}\left(\frac{\partial}{\partial r} - ik\right) u_j = 0, \tag{2.53}$$

for $j = 1, \ldots, J$. Thus u_j is entirely determined by its values on B_j; it is given in local polar coordinates (r_j, θ_j) by (2.10). The matching condition is now given by

$$\sum_{j=1}^{J} u_j = u \quad \text{on } B. \tag{2.54}$$

In analogy to Proposition 1 we can show that

$$u \equiv \sum_{j=1}^{J} u_j \quad \text{in } B \cup D \tag{2.55}$$

and that this decomposition is unique. Therefore, we immediately find the DtN map for a multiple scattering problem with J scatterers:

$$\partial_n u = M[u_j] + \sum_{\substack{\ell=1 \\ \ell \neq j}}^{J} T[u_\ell] \quad \text{on } B_j, \tag{2.56}$$

$$u_j + \sum_{\substack{\ell=1 \\ \ell \neq j}}^{J} P[u_\ell] = u \quad \text{on } B_j, \quad j = 1, \ldots, J. \tag{2.57}$$

Here M, T and P operate on the purely outgoing wave fields u_j as follows:

$$M : u_j|_{B_j} \mapsto \left.\frac{\partial u_j}{\partial r_j}\right|_{B_j}, \; T : u_\ell|_{B_\ell} \mapsto \left.\frac{\partial u_\ell}{\partial r_j}\right|_{B_j}, \; P : u_\ell|_{B_\ell} \mapsto u_\ell|_{B_j}. \tag{2.58}$$

We note that *no additional analytical derivations* due to coordinate transformations, etc. are needed once the situation of two scatterers has been resolved. Hence, the standard DtN operator M is given by (2.23), while the operators T and P are again given by (2.26)–(2.30), with '1' replaced by 'j' and '2' by 'ℓ', or vice-versa.

In practice the infinite series in the operators M, T and P need to be truncated at some finite value N_j, which can be different for each sub-domain Ω_j. We denote the corresponding truncated operators by M^{N_j}, T^{N_j}, and P^{N_j}, $j = 1, \ldots, J$. For simplicity of notation we shall assume that all boundary operators are truncated at the same value $N_j = N$, $j = 1, \ldots, J$.

We now extend the modified DtN map (2.48)–(2.51) to the situation of J scatterers:

$$\partial_n u = iku + (M - ik)^N[u_j] + \sum_{\substack{\ell=1 \\ \ell \neq j}}^{J} (T - ikP)^N[u_\ell] \quad \text{on } B_j, \tag{2.59}$$

$$u_j + \sum_{\substack{\ell=1 \\ \ell \neq j}}^{J} P^N[u_\ell] = u \quad \text{on } B_j, \tag{2.60}$$

where $N \geq 0$ is the truncation index.

For $J = 1$, the expressions in (2.56), (2.57) and (2.59), (2.60) reduce to the well-known DtN and modified DtN conditions for single scattering problems [54, 35]. For $J = 2$, they correspond to the conditions derived previously in Section 2.2.

To further simplify the notation, we define the (symbolic) vectors

$$\begin{aligned} \partial_n u|_B &= (\partial_{r_1} u|_{B_1}, \partial_{r_2} u|_{B_2}, \ldots, \partial_{r_J} u|_{B_J})^\top && (2.61)\\ u|_B &= (u|_{B_1}, u|_{B_2}, \ldots, u|_{B_J})^\top && (2.62)\\ u_{\text{out}}|_B &= (u_1|_{B_1}, u_2|_{B_2}, \ldots, u_J|_{B_J})^\top && (2.63) \end{aligned}$$

and the operator matrices

$$\begin{aligned} \boldsymbol{T} &= \left\{T_\ell^j\right\}_{j,\ell=1}^J, \quad T_\ell^j : u_\ell|_{B_\ell} \mapsto \partial_{r_j} u_\ell|_{B_j} && (2.64)\\ \boldsymbol{P} &= \left\{P_\ell^j\right\}_{j,\ell=1}^J, \quad P_\ell^j : u_\ell|_{B_\ell} \mapsto u_\ell|_{B_j} && (2.65) \end{aligned}$$

With these notations we rewrite the DtN map (2.56), (2.57) in matrix-vector notation as

$$\begin{aligned} \partial_n u &= \boldsymbol{T} u_{\text{out}} \quad \text{on } B, && (2.66)\\ \boldsymbol{P} u_{\text{out}} &= u \quad \text{on } B, && (2.67) \end{aligned}$$

and the modified DtN (MDtN) map (2.59), (2.60) as

$$\begin{aligned} \partial_n u &= iku + (\boldsymbol{T} - ik\boldsymbol{P})^N u_{\text{out}} \quad \text{on } B, && (2.68)\\ \boldsymbol{P}^N u_{\text{out}} &= u \quad \text{on } B. && (2.69) \end{aligned}$$

Remark: The derivation of the DtN (or MDtN) condition for multiple acoustic scattering can easily be generalized to different equations (Maxwell's equations [65], linear elasticity [24], etc), to other geometries (ellipsoidal [35], wave-guide [46]), or to three space dimensions. In fact, our approach can be extended to all multiple scattering problems, for which a DtN map is already known for single scattering.

2.4 Variational formulation

In the previous section we have derived the DtN boundary condition (2.66), (2.67) for multiple scattering problems. We shall now show how to combine it with two different numerical schemes used in the interior. In this section, we present a variational formulation of a multiple scattering boundary value problem, which is needed for the numerical solution with any finite element scheme. In Section 6, we shall show how to combine the multiple-DtN boundary condition with a finite difference scheme. Numerical solutions obtained with the finite difference scheme are then compared with a finite element solution using the DtN method in a single larger domain.

We shall now show how to combine the multiple scattering DtN condition (2.66), (2.67) with the finite element method in Ω. The computational domain Ω is bounded in part by B, the union of J disjoint circles, and in part by some interior piecewise smooth boundary, Γ. For simplicity we consider a Dirichlet-type condition on Γ, and assume that the acoustic medium inside Ω is also homogeneous and isotropic. Hence the boundary value problem in Ω is:

$$\begin{aligned} -\Delta u - k^2 u &= f \quad \text{in } \Omega && (2.70)\\ u &= g \quad \text{on } \Gamma && (2.71)\\ \partial_n u &= \boldsymbol{T} u_{\text{out}} \quad \text{on } B && (2.72)\\ \boldsymbol{P} u_{\text{out}} &= u \quad \text{on } B && (2.73) \end{aligned}$$

Next, we introduce the function spaces

$$\begin{aligned} V &= \{v \in H^1(\Omega) \,|\, v|_\Gamma \equiv g\}, && (2.74)\\ V_0 &= \{v \in H^1(\Omega) \,|\, v|_\Gamma \equiv 0\}. && (2.75) \end{aligned}$$

To derive a variational formulation of (2.70)–(2.73) we multiply (2.70) by a test function $v \in V_0$ and integrate over Ω. Then we use integration by parts, together with (2.71)–(2.73), which yields the following variational formulation for (2.70)–(2.73):

Find $u \in V$ such that

$$\begin{aligned} (\nabla u, \nabla v)_\Omega - (k^2 u, v)_\Omega - (\boldsymbol{T} u_{\text{out}}, v)_B &= (f, v)_\Omega, && (2.76)\\ (\boldsymbol{P} u_{\text{out}}, v)_B &= (u, v)_B, && (2.77) \end{aligned}$$

for all $v \in V_0$.

Here, $(\cdot,\cdot)_\Omega$ and $(\cdot,\cdot)_B$ denote the standard L^2-inner products on Ω and B, respectively.

For the finite element discretization of (2.76), (2.77) we choose a triangulation $\mathcal{T}_h$ of $\overline{\Omega}$, with mesh size $h > 0$ and nodes $\mathcal{N}(\mathcal{T}_h) = \mathcal{N}_\Omega \cup \mathcal{N}_\Gamma \cup \mathcal{N}_B$. Then we choose a subspace $V_N \subset V$ of finite dimension $N = |\mathcal{N}(\mathcal{T}_h)| = N_\Omega + N_\Gamma + N_B$, and nodal basis functions

$$\{\Phi_i\}_{i=1}^N \subset V_N, \quad \Phi_i(x_j) = \delta_{ij}, \quad x_j \in \mathcal{N}(\mathcal{T}_h). \tag{2.78}$$

We denote by u_Ω^h the values of the finite element solution on $\mathcal{N}_\Omega$, by u_B^h its values on $\mathcal{N}_B$ and by u_{out}^h the values of u_{out} – see (2.63) – on $\mathcal{N}_B$, which yields from (2.76), (2.77) the following linear system of equations:

$$\left(\begin{array}{cc|c} \multicolumn{2}{c|}{\boldsymbol{K}} & \begin{matrix}\boldsymbol{0}\\ -\boldsymbol{T}\end{matrix} \\ \hline \boldsymbol{0} & -\boldsymbol{I} & \boldsymbol{P} \end{array}\right) \left(\begin{array}{c} u_\Omega^h \\ u_B^h \\ \hline u_{\text{out}}^h \end{array}\right) = \left(\begin{array}{c} f \\ \hline 0 \end{array}\right). \tag{2.79}$$

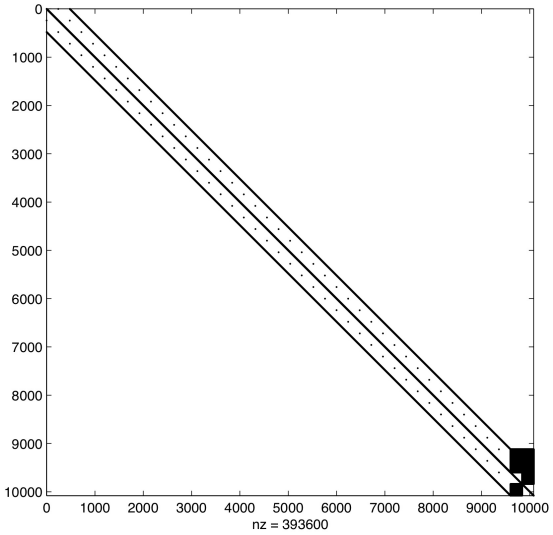

Figure 2.2: The sparsity pattern of the finite difference matrix for a two scatterer problem. There are 21 layers of 240 grid points in each domain Ω_1 and Ω_2. Hence the total number of unknowns is $2 \times (21 \times 240)$ for u plus 2×240 for $u_1|_{B_1}$ and $u_2|_{B_2}$.

Here $\boldsymbol{I}$ denotes the $N_B \times N_B$ identity matrix, while the other entries are given by

$$
\begin{aligned}
K_{ij} &= (\nabla\Phi_j, \nabla\Phi_i)_\Omega - (k^2\Phi_j, \Phi_i)_\Omega, \quad i,j : x_i, x_j \in \mathcal{N}_\Omega \cup \mathcal{N}_B, && (2.80)\\
T_{ij} &= (\boldsymbol{T}\Phi_j, \Phi_i)_B, \quad i,j : x_i, x_j \in \mathcal{N}_B, && (2.81)\\
P_{ij} &= (\boldsymbol{P}\Phi_j, \Phi_i)_B, \quad i,j : x_i, x_j \in \mathcal{N}_B, && (2.82)\\
f_i &= (f, \Phi_i)_\Omega - \sum_{j : x_j \in \mathcal{N}_\Gamma} g(x_j) K_{ij}, \quad i : x_i \in \mathcal{N}_\Omega \cup \mathcal{N}_B. && (2.83)
\end{aligned}
$$

Because the nodal basis functions $\{\Phi_j\}_{j=1}^N$ are local, $\boldsymbol{K}$ is a sparse real $((N_\Omega + N_B) \times (N_\Omega + N_B))$-matrix. The $(N_B \times N_B)$-matrices $\boldsymbol{T}$ and $\boldsymbol{P}$, however, have complex valued entries and are full, because the DtN condition couples all unknowns on B. Clearly the structure of $\boldsymbol{K}$, $\boldsymbol{T}$, and $\boldsymbol{P}$ will depend both on the number of sub-scatterers and on the finite element discretization used. For instance, for two sub-domains each with an equidistant polar mesh with standard continuous $\mathcal{Q}_1$ finite elements, the sparsity pattern of the resulting linear system will essentially look like that shown in Fig. 2.2, with eight instead of four off-diagonal entries per row in $\boldsymbol{K}$. Additional information on finite element analysis for acoustic scattering can be found in [52].

2.5 Far-field evaluation

Once the scattered field u has been computed inside Ω, it is usually of interest to evaluate u also outside Ω during a post-processing step, either at selected locations ("receivers") or in a broader region. If integral representations that involve integration over B with the Green's function, such as (2.13), are used, the evaluation of u outside Ω becomes rather cumbersome and expensive. However, if the multiple-DtN approach is used, the evaluation of u at some location x in D, the region outside Ω, is inexpensive and straightforward. Indeed, since the purely outgoing wave fields u_1 and u_2 are known on B_1 and B_2, respectively, they are known everywhere outside Ω via the Fourier representation (2.10). In fact, we can rewrite (2.10) as

$$u_j(r_j,\theta_j) = \frac{1}{\pi}{\sum_{n=0}^{\infty}}' H_n^{(1)}(kr_j)\cos(n\theta_j)\frac{1}{H_n^{(1)}(kR_j)}\int_0^{2\pi} u_j(R_j,\theta')\cos(n\theta')\,d\theta' +$$

$$+\frac{1}{\pi}{\sum_{n=0}^{\infty}}' H_n^{(1)}(kr_j)\sin(n\theta_j)\frac{1}{H_n^{(1)}(kR_j)}\int_0^{2\pi} u_j(R_j,\theta')\sin(n\theta')\,d\theta', \qquad (2.84)$$

where the two integrals correspond to the cosine and sine Fourier coefficients of $u_j|_{B_j}$, $j=1,2$. Thus, to compute $u(x)=u_1(x)+u_2(x)$ at some $x\in D$, it suffices to compute the Fourier coefficients of u_j on B_j, $j=1,2$, yet only once. Then u_1 and u_2, and thereby $u=u_1+u_2$, can be evaluated anywhere by summing a few terms in the Fourier representation (2.84) of u_1 and u_2.

Yet another quantity which is often of interest is the far-field pattern of the scattered field u. The asymptotic behavior of any solution u to the exterior Dirichlet problem (2.1)–(2.3) is

$$u(r,\theta) \sim \frac{e^{ikr}}{\sqrt{kr}} f(\theta), \quad r\to\infty. \qquad (2.85)$$

The function f is called the far-field pattern of the solution. The value $f(\theta)$ is the far-field response from the scatterer in a direction θ for a given incident wave. We shall now show how to directly compute f from the values of $u_1|_{B_1}$ and $u_2|_{B_2}$.

Let $c_j=(c_j^x,c_j^y)$ denote the center of B_j. The local coordinates (r_j,θ_j), relative to c_j, of a point $(r,\theta)\in D$ given in (global) polar coordinates are

$$r_j = \sqrt{(r\cos\theta-c_j^x)^2+(r\sin\theta-c_j^y)^2}, \qquad (2.86)$$

$$\cos\theta_j = \frac{1}{r_j}(r\cos\theta-c_j^x), \quad \sin\theta_j=\frac{1}{r_j}(r\sin\theta-c_j^y). \qquad (2.87)$$

By combining the contributions from the various purely outgoing wave fields $u_j|_{B_j}$, $j = 1, \ldots, J$, we can then derive an explicit formula for the far-field pattern of u, given by (2.88) below. We summarize this result as a theorem.

Theorem 2. *The far-field pattern f defined in (2.85) of the solution u to the exterior Dirichlet problem (2.1)–(2.3) is entirely determined by the values of the purely outgoing wave fields u_j, $j = 1, \ldots, J$, on the components B_j of the artificial boundary B, which appear in the DtN condition (2.56), (2.57). It is given by*

$$f(\theta) = \frac{1-i}{\pi\sqrt{\pi}} \sum_{j=1}^{J} e^{-ik(c_j^x \cos\theta + c_j^y \sin\theta)} {\sum_{n=0}^{\infty}}' \frac{(-i)^n}{H_n^{(1)}(kR_j)} \int_0^{2\pi} u_j(R_j, \theta') \cos n(\theta - \theta')\, d\theta'. \tag{2.88}$$

Proof. We examine the asymptotic behavior of the Fourier representation (2.10) of each purely outgoing wave field u_j, $j = 1, \ldots, J$, for $r \to \infty$. By Taylor expansion of (2.86), (2.87) we observe that

$$r_j = r - (c_j^x \cos\theta + c_j^y \sin\theta) + O(r^{-1}), \quad r \to \infty \tag{2.89}$$

$$\cos\theta_j = \cos\theta + O(r^{-1}), \quad r \to \infty \tag{2.90}$$

$$\sin\theta_j = \sin\theta + O(r^{-1}), \quad r \to \infty \tag{2.91}$$

Because the angle $\theta_j \in [0, 2\pi)$ is uniquely determined by the pair

$$(\cos\theta_j, \sin\theta_j) \to (\cos\theta, \sin\theta), \quad r \to \infty, \tag{2.92}$$

we conclude that $\theta_j \to \theta$, as $r \to \infty$, and therefore that

$$\cos n(\theta_j - \theta') \sim \cos n(\theta - \theta'), \quad r \to \infty,\ \theta' \in [0, 2\pi). \tag{2.93}$$

The asymptotic behavior of the Hankel functions [1] is given by

$$H_n^{(1)}(kr_j) \sim \sqrt{\frac{2}{k\pi r_j}} e^{i\left(kr_j - \frac{1}{2}n\pi - \frac{1}{4}\pi\right)} = \frac{e^{ikr_j}}{\sqrt{kr_j}} \frac{1-i}{\sqrt{\pi}} (-i)^n, \quad r \to \infty. \tag{2.94}$$

From (2.89) we conclude

$$\sqrt{kr_j} \sim \sqrt{kr} \text{ and } e^{ikr_j} \sim e^{ikr} e^{-ik(c_j^x \cos\theta + c_j^y \sin\theta)}, \quad r \to \infty. \tag{2.95}$$

Each purely outgoing wave field u_j, given by (2.10), therefore has the asymptotic behavior

$$u_j(r_j, \theta_j) \sim \frac{e^{ikr}}{\sqrt{kr}} \frac{1-i}{\pi\sqrt{\pi}} e^{-ik(c_j^x \cos\theta + c_j^y \sin\theta)} \times$$

$$\times {\sum_{n=0}^{\infty}}' \frac{(-i)^n}{H_n^{(1)}(kR_j)} \int_0^{2\pi} u_j(R_j, \theta') \cos n(\theta - \theta')\, d\theta', \quad r \to \infty. \tag{2.96}$$

Since $u = \sum_{j=1}^{J} u_j$, the result follows by summing over j. □

2.6 Numerical examples

We shall now combine the multiple-DtN (2.66), (2.67) and -MDtN (2.68), (2.69) condition with a finite difference scheme. We shall also compare the scattered fields obtained either with the double-DtN approach or with the single-DtN approach in a very large computational domain and demonstrate their high accuracy and convergence properties via numerical examples.

We consider the following two scatterer model problem with two obstacles, where the computational domain $\Omega = \Omega_1 \cup \Omega_2$, the obstacle boundary $\Gamma = \Gamma_1 \cup \Gamma_2$, and the artificial boundary $B = B_1 \cup B_2$:

$$\begin{aligned} \Delta u + k^2 u &= f \quad \text{in } \Omega, && (2.97)\\ u &= g \quad \text{on } \Gamma, && (2.98)\\ \partial_n u &= \boldsymbol{T} u_{\text{out}} \quad \text{on } B, && (2.99)\\ \boldsymbol{P} u_{\text{out}} &= u \quad \text{on } B. && (2.100) \end{aligned}$$

To precisely describe the typical structure of the resulting discrete linear system, we consider a polar equidistant grid along B_1 and B_2. Inside Ω_1 and Ω_2, we discretize the solution with step size h_r in the r-direction and h_θ in the θ-direction. Then we use second order centered finite differences in r- and θ-direction to discretize (2.97). The vectors $u_N^{(1)}$ and $u_N^{(2)}$ denote the values of the numerical solution on the artificial boundary. The discretization of (2.97) involves the values $u_{N+1}^{(1)}$ and $u_{N+1}^{(2)}$ at "ghost" points, which lie outside the computational domain Ω. These unknown values are eliminated by using a second order finite difference discretization of (2.99), (2.100). Next, we let the vectors u_1 and u_2 denote the values of the purely outgoing wave fields on their respective boundary components. Then the discretization of the multiple-DtN condition (2.99), (2.100) is given by

$$\begin{pmatrix} \frac{2}{h_r^2}\boldsymbol{I} & \boldsymbol{0} & \boldsymbol{Q}^{(1)} & \boldsymbol{0} & \boldsymbol{M}^{(1)} & \boldsymbol{T}^{(1)}_{(2)} \\ \boldsymbol{0} & \frac{2}{h_r^2}\boldsymbol{I} & \boldsymbol{0} & \boldsymbol{Q}^{(2)} & \boldsymbol{T}^{(2)}_{(1)} & \boldsymbol{M}^{(2)} \\ \boldsymbol{0} & \boldsymbol{0} & -\boldsymbol{I} & \boldsymbol{0} & \boldsymbol{I} & \boldsymbol{P}^{(1)}_{(2)} \\ \boldsymbol{0} & \boldsymbol{0} & \boldsymbol{0} & -\boldsymbol{I} & \boldsymbol{P}^{(2)}_{(1)} & \boldsymbol{I} \end{pmatrix} \begin{pmatrix} u_{N-1}^{(1)} \\ u_{N-1}^{(2)} \\ u_N^{(1)} \\ u_N^{(2)} \\ u_1 \\ u_2 \end{pmatrix} = \begin{pmatrix} 0 \\ 0 \\ 0 \\ 0 \end{pmatrix}, \quad (2.101)$$

with identity matrices $\boldsymbol{I}$, all-zero matrices $\boldsymbol{0}$ and tridiagonal matrices $\boldsymbol{Q}$. The matrices $\boldsymbol{M}$, $\boldsymbol{T}$ and $\boldsymbol{P}$ are full matrices obtained by discretizing the integral operators with the second order trapezoidal quadrature rule.

A typical sparsity pattern of the entire finite difference matrix, including the discretization of (2.97) in the interior is shown in Fig. 2.2, for the special case of two circular obstacles with an equidistant polar mesh throughout Ω_1 and Ω_2. Here the ordering of the interior and boundary nodes is chosen by starting from the innermost "layers" in both domains and moving outward with increasing index. The 6 small full blocks in the lower right corner correspond to the full block-matrices in (2.101). In all computations below we have used the sparse direct solver provided by Matlab. Further details about the efficient iterative solution of the system of linear equations corresponding to a *single-scattering DtN problem* can be found in [66].

2.6.1 Accuracy and convergence study

To demonstrate the accuracy and convergence of our method, we consider the following test problem: We let an incident plane wave impinge on a circular disk shaped obstacle centered at $(0, -d)$, with radius 0.5 and distance $d = 1.5$ from the origin – see Fig. 2.1 for an illustration. The obstacle is located inside Ω_1 and is bounded by Γ_1. In Ω_2, no physical obstacle is present. The sound-soft boundary condition requires that the total field be zero on Γ_1, while the Jacobi-Anger expansion (see for example [18], p. 67) yields the exact solution for the scattered field everywhere outside Γ_1. Then we prescribe its values on the boundary of a second virtual obstacle, centered at $(0, d)$ with radius 0.75, and compute the numerical solution in the two (disjoint) computational domains Ω_1, Ω_2, bounded by circles B_1 and B_2 with radii $R_1 = 1$ and $R_2 = 1.25$, respectively. We then compare the numerical result with the exact solution for single scattering. We choose $k = 2\pi$ for the wave number and truncate the DtN expansion at $N = 50$. We also compute the exact far-field pattern and compare it with that given by our numerical result. The maximal relative errors for different grids and incidence angles are shown in Table 2.1. We observe second order convergence of our method in every case, as expected, as the mesh size $h \to 0$.

To study the effect of the truncation parameter N on the error we choose $\alpha = \pi/4$ for the incidence angle and compute the solution with varying N, either with the DtN and MDtN condition imposed at B. The relative error is shown in Fig. 2.3. We observe that the modified DtN condition leads to better accuracy, even for small truncation indices N. When $N \geq \max\{kR_1, kR_2\}$, the two solutions computed with DtN and MDtN essentially coincide for this model problem. This behavior of the DtN and MDtN conditions illustrated in Fig. 2.3 is typical, and has been reported previously for single scattering problems [45, 35].

Table 2.1: The maximal relative errors for plane wave scattering from a single obstacle, with the values of the exact solution prescribed on the boundary of the second "obstacle". Incidence angle α, wave number $k = 2\pi$, DtN expansion truncated at $N = 50$, comparison with exact solution. Grids with $N_r \times N_\theta$ cells in r- and θ-direction, respectively.

α	5×60	10×120	20×240	40×480
relative error in the solution				
0	$7.53 \cdot 10^{-2}$	$1.77 \cdot 10^{-2}$	$4.38 \cdot 10^{-3}$	$1.09 \cdot 10^{-3}$
$\pi/4$	$7.85 \cdot 10^{-2}$	$1.84 \cdot 10^{-2}$	$4.54 \cdot 10^{-3}$	$1.13 \cdot 10^{-3}$
$\pi/2$	$9.77 \cdot 10^{-2}$	$2.24 \cdot 10^{-2}$	$5.49 \cdot 10^{-3}$	$1.37 \cdot 10^{-3}$
relative error in the far-field pattern				
0	$4.68 \cdot 10^{-2}$	$1.11 \cdot 10^{-2}$	$2.76 \cdot 10^{-3}$	$6.87 \cdot 10^{-4}$
$\pi/4$	$6.05 \cdot 10^{-2}$	$1.45 \cdot 10^{-2}$	$3.60 \cdot 10^{-3}$	$8.97 \cdot 10^{-4}$
$\pi/2$	$7.69 \cdot 10^{-2}$	$1.85 \cdot 10^{-2}$	$4.57 \cdot 10^{-3}$	$1.14 \cdot 10^{-3}$

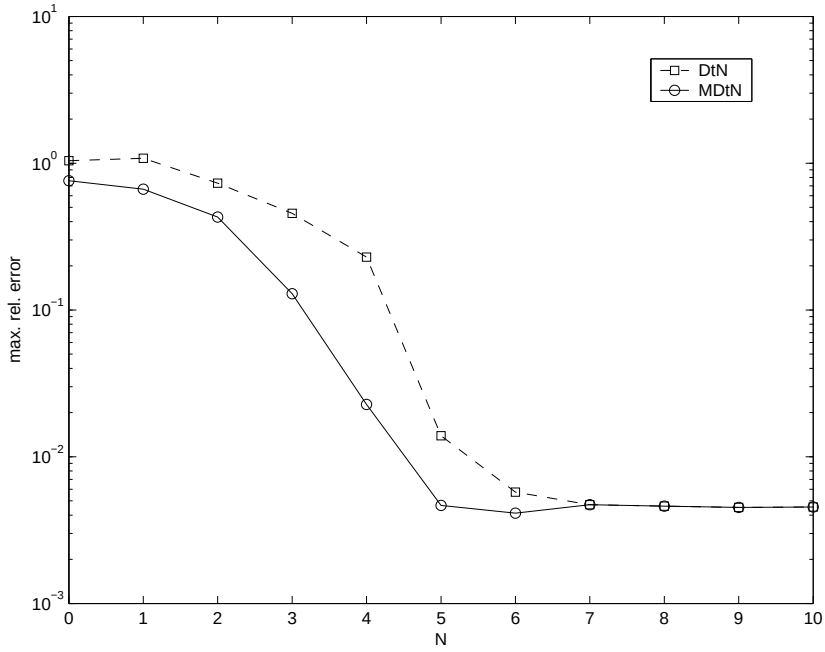

Figure 2.3: The maximal relative error in the solution vs. the truncation index N, for $k = 2\pi$ and incidence angle $\alpha = \pi/4$, on the 20×240 grid. Comparison of DtN (squares) and MDtN (circles).

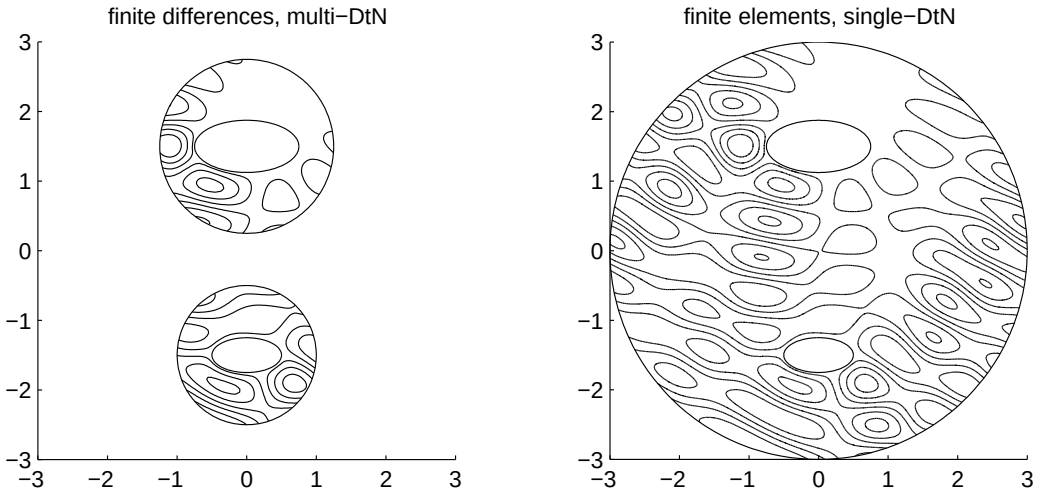

Figure 2.4: Scattering from two ellipses, $k = 2\pi$, $\alpha = 3\pi/8$. Contour lines of the real parts of the total wave fields for two solutions are shown. Left: the numerical solution obtained by a second-order finite difference method combined with the multiple-DtN condition; Right: the numerical solution obtained by a (piecewise linear) finite element method combined with the single-DtN condition.

2.6.2 Comparison with the single-DtN FE approach

Here we consider the scattering of a plane wave with incidence angle $\alpha = 3\pi/8$ on two obstacles with sound-soft elliptic boundaries. The semi-major axes of the ellipses were chosen 0.75 and 0.5, whereas the semi-minor axes are 0.375 and 0.25, respectively. The numerical solution obtained by using our finite difference scheme with the multiple-DtN condition on the artificial boundaries is compared with a numerical solution obtained by using a finite element scheme in a larger domain, which contains both obstacles, with the single-DtN condition imposed at the artificial boundary $r = 3$. The wave number is $k = 2\pi$ and the resolutions are comparable, with about 45 grid points per wavelength. Here the modified DtN map is used and the truncation index is set to $N = 50$. The contour lines of the real part of the total field are shown for both solutions in Fig. 2.4. Note that the size of the computational sub-domains in the multiple-DtN case is independent of the relative distance between them, leading to a much smaller computational domain, in comparison with the single-DtN case.

In Fig. 2.5, the values of the two solutions on the artificial boundary at $r = 3$, which was used for the finite element solution, are shown. The

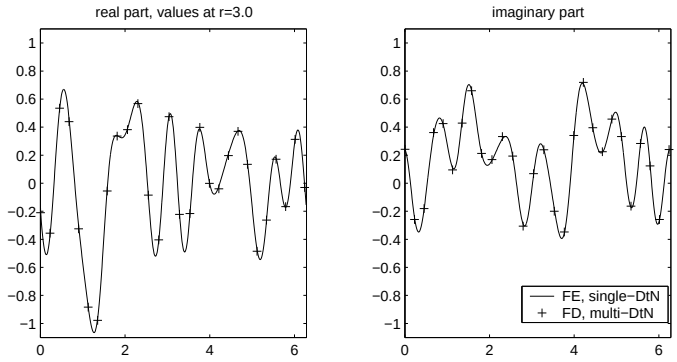

Figure 2.5: Comparison of multiple-DtN with single-DtN. Values of the scattered field on the artificial boundary $r = 3$ used for the finite element solution shown in Fig. 2.4.

multiple-DtN solution is evaluated on that boundary by using the Fourier representation (2.84) for the purely outgoing wave fields.

For a given far-field pattern f, the scattering cross section $\hat{\sigma}$ is defined as

$$\hat{\sigma}(\theta) = 20 \log_{10} |f(\theta)|, \quad \theta \in [0, 2\pi). \tag{2.102}$$

In Fig. 2.6 the scattering cross section for plane wave scattering from two ellipses, obtained by using (2.88), is displayed for the single-DtN and multiple-DtN solutions. The two cross sections coincide.

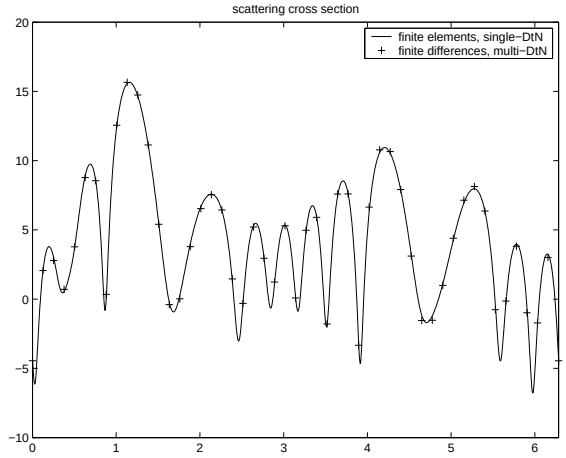

Figure 2.6: Comparison of multiple-DtN with single-DtN. Values of the scattering cross section (2.102) for both numerical solutions.

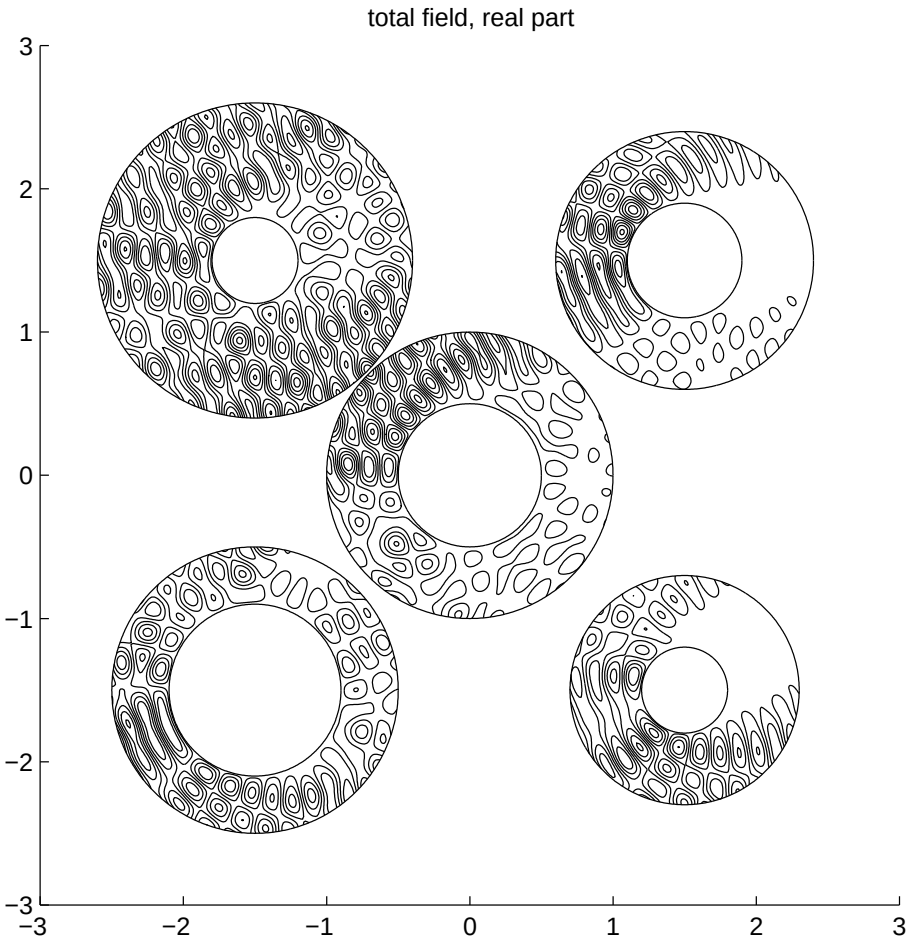

Figure 2.7: The total field for plane wave scattering from five cylinders, $k = 8\pi$, incidence angle $\alpha = \pi/8$.

2.6.3 An example with five obstacles

An important advantage of our multiple-DtN approach is that no further analytical derivation is needed to extend it to higher numbers of scatterers, once the DtN condition is known for two domains. Here we consider the scattering of a plane wave with incidence angle $\alpha = \pi/8$ impinging on five cylindrical obstacles of different sizes with sound-soft boundaries. The wave number is set to $k = 8\pi$ and the grid consists of about 20 points per wavelength. We use the modified DtN map and truncate the infinite series at $N = 50$. The real part of the total field and the scattering cross section (2.102) are shown in Figs. 2.7 & 2.8.

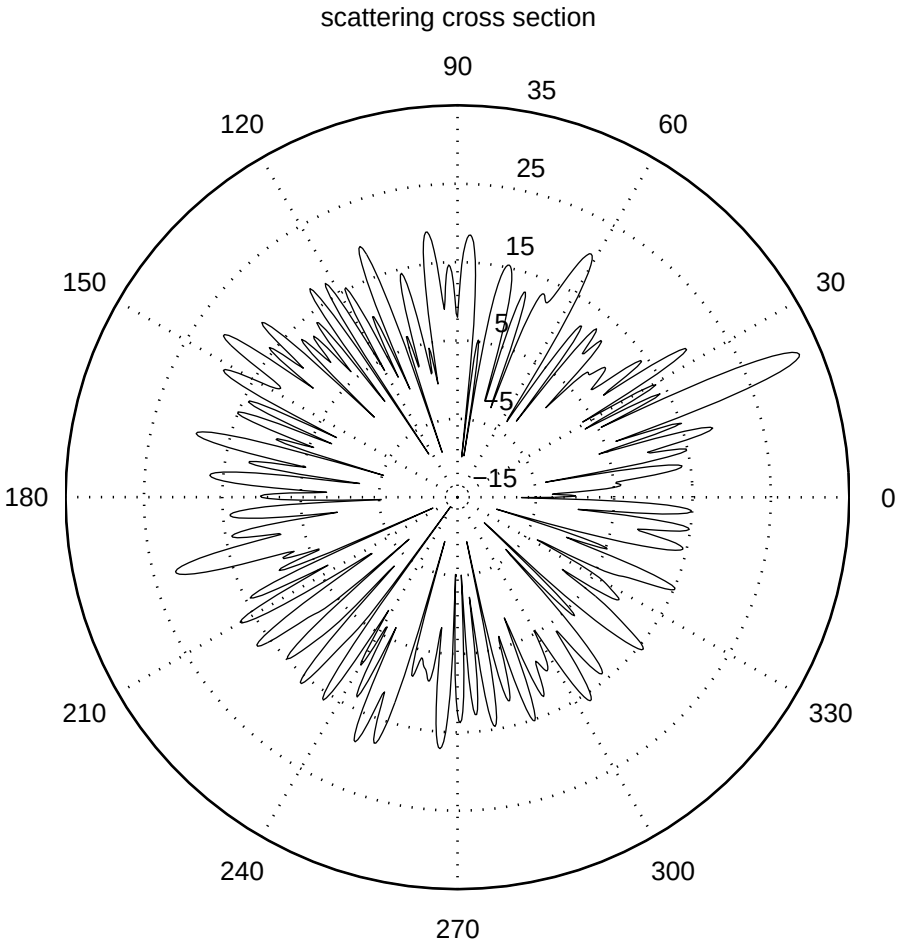

Figure 2.8: The scattering cross section (2.102), obtained by using (2.88), for the five cylinders, $k = 8\pi$, incidence angle $\alpha = \pi/8$.

2.7 Conclusion

We have derived a Dirichlet-to-Neumann (DtN) map for multiple scattering problems, which is based on a decomposition of the scattered field into several purely outgoing wave fields. We have proved that the corresponding DtN boundary condition is exact. When the multiple-DtN boundary condition is used to solve multiple scattering problems, the size of the computational domain is much smaller, in comparison to the use of one single large artificial boundary. In particular, the size of the computational sub-domains in the multiple-DtN case does not depend on the relative distances between the components of the scatterer. Although the artificial boundaries must be of

simple geometric shape, here a circle, the DtN condition is not tied to any coordinate system inside the computational domain; in particular, it remains exact independently of the discretization used inside Ω.

We have presented a variational formulation of a multiple scattering problem with this boundary condition and also derived a formula for the far-field of the solution, which is obtained by exploiting auxiliary values used in the formulation. Accuracy and convergence have been demonstrated on a simple test problem, and a comparison with single-DtN has been made in the situation of two elliptical obstacles.

This approach is based on the decomposition of the scattered field into several purely outgoing wave fields. It can also be used to derive exact non-reflecting boundary conditions for multiple scattering problems for other equations and geometries, such as ellipses, spheres, or even wave guides, both in two and in three space dimensions, for which the DtN map with a single artificial boundary is explicitly known.

For large-scale applications in multiple scattering, it may be useful, or even necessary, to solve the sequence of sub-problems in Ω_1, Ω_2, etc. iteratively, while exchanging boundary values between the disjoint exterior boundary components via the operators M, P, and T. Parallelism can be increased even further by using standard domain decomposition techniques [11, 7] separately within each sub-domain Ω_j. Although the convergence of such a Jacobi or Gauss-Seidel like iterative procedure remains an open question, it could certainly be used as an efficient preconditioner.

In this work we have only treated the time-harmonic case. In the time-dependent case, a similar approach can be used to derive exact non-reflecting boundary conditions for multiple scattering problems, by using a representation formula derived in [40]. The authors are currently investigating the time-dependent case and will report on their results elsewhere in the near future.

Acknowledgements The authors would like to thank Joseph B. Keller for useful comments and suggestions. They also wish to thank Patrick Meury for his finite element code with a single-DtN boundary condition.

Open questions and future research

The following questions regarding non-reflecting boundary conditions for time-harmonic multiple scattering problems remained open. These might be subjects for future research:

- The proof of uniqueness of the solution to the boundary-value problem in Ω, with the NRBC on B, involves an integral over Ω. This is even true for the single-scattering case [45]. It is unsatisfactory that this proof can only be done for media that are isotropic and homogeneous inside Ω. As the NRBC was derived by analyzing the exterior problem (in D) only, it would be interesting to find a proof which does not involve the material properties in Ω explicitly, but which only relies on the assumption of well-posedness of the original problem in Ω_∞.

- The matrix of the linear system after discretization of the boundary-value problem is complex-valued as in the single-scattering case, but it is also non-symmetric. The numerical solution of the linear system would be facilitated, if a symmetric version of the multiple-DtN condition was found.

- The dependence of the condition number of the system matrix on the parameters of the boundary-value problem, such as the wave number or the distance between the artificial boundary components, should be analyzed.

- The computational work could be drastically reduced, if the NRBC did not involve harmonic transformations. A local, approximate non-reflecting boundary condition for multiple scattering problems is thus very desirable.

- In the case of many scatteres, $J \gg 1$, clustering techniques could become useful. As these are also used in the fast multipole method, a better understanding of these techniques is desirable. A link between the fast multipole and the multiple-DtN method should then be established, which allows a better comparison of the two methods.

- It would be interesting to do a stability analysis for multiple scattering NRBC, and to derive conditions for stability of the boundary-value problem in Ω.

- It is not clear (neither in the single-scattering case) whether the DtN condition is good in the high-frequency regime, $|k| \gg 1$, as well. An answer to this question would be nice.

Chapter 3

The time-dependent case

The contents of this chapter have been submitted to J. Comput. Phys.

Abstract An exact non-reflecting boundary condition (NRBC) is derived for the numerical solution of time-dependent multiple scattering problems in three space dimensions, where the scatterer consists of several disjoint components. Because each sub-scatterer can be enclosed by a separate artificial boundary, the computational effort is greatly reduced and becomes independent of the relative distances between the different sub-domains. Furthermore, the storage required does not depend on the simulation time, but only on the geometry. Numerical examples show that the NRBC for multiple scattering is as accurate as the NRBC for single scattering problems [J. Comput. Phys. 127 (1996), 52], while being more efficient due to the reduced size of the computational domain.

3.1 Introduction

For the numerical solution of scattering problems in unbounded domains, a well-known approach is to enclose all obstacles, inhomogeneities and nonlinearities with an artificial boundary B. A boundary condition is then imposed on B, which leads to a numerically solvable initial/boundary-value problem in a bounded domain Ω. The boundary condition should be chosen such that the solution of the problem in Ω coincides with the restriction to Ω of the solution in the original unbounded region.

If the scatterer consists of several obstacles, which are well separated from each other, the use of a single artificial boundary to enclose the entire scattering region, becomes too expensive. Instead it is preferable to enclose every sub-scatterer by a separate artificial boundary B_j. Then we seek an

exact boundary condition on $B = \bigcup B_j$, where each B_j surrounds a single computational sub-domain Ω_j. This boundary condition must not only let outgoing waves leave Ω_j without spurious reflection from B_j, but also propagate the outgoing wave from Ω_j to all other sub-domains Ω_ℓ, which it may reenter subsequently. To derive such an exact boundary condition, an analytic expression for the solution everywhere in the exterior region, and for all times, is needed. We shall make use of a Fourier series representation for our construction.

Exact non-reflecting boundary conditions have been derived for various equations and geometries, but always in the situation of a single computational domain, where the scattered wave is purely outgoing outside Ω [9, 21, 29, 33, 34, 36, 37, 38, 39, 43, 72, 74, 78]. In a situation of multiple disjoint computational domains, however, waves are not purely outgoing outside the computational domain $\Omega = \bigcup \Omega_j$, as they may bounce back and forth between domains. We shall show how to overcome this difficulty and derive an exact non-reflecting boundary condition for multiple scattering. The derivation presented below for the wave equation in three space dimensions readily extends to multiple scattering problems in other geometries and also to different equations. Because this exact boundary condition allows the size of the computational sub-domains, Ω_j, to be chosen independently of the relative distances between them, the computational domain, Ω, can be chosen much smaller than that resulting from the use of a single, large computational domain.

Numerical methods used for time-dependent multiple scattering so far have mainly been based on integral representations. The direct evaluation of these formulae in the multiple scattering context is too expensive, however: In 3D, if N_s grid points are used in each space direction for the discretization of Ω, the computational cost for the non-reflecting boundary condition would behave like $O(N_s^4)$, which is one order of magnitude higher than the cost of a typical finite element or finite difference method used in the interior. The fast plane wave time domain method [22], a generalization of the fast multipole method to the time-dependent case, can be used to rapidly evaluate the integral kernels, with work $O(N_s^2 \log N_s)$. In the single-scattering case, the integral representation approach is also known [29, 74, 78], but there are alternatives as well, such as absorbing boundaries or layers. To our knowledge this work constitutes the first attempt to generalize non-reflecting boundary conditions to multiple scattering. With the separation of radial and temporal variables from angular variables by the spherical harmonics expansion, and with the restriction to spherical artificial boundaries, we will be able to effectively reduce work and storage counts.

In Section 2, we derive the exact non-reflecting boundary condition for two scatterers, and we show how to efficiently evaluate the operators that are involved. We show that the solution to the initial/boundary value problem in Ω, with the DtN condition imposed on B, coincides with the restriction to Ω of the solution in the unbounded region Ω_∞. The formulation is generalized to an arbitrary number of scatterers in Section 3. In Section 4, we examine in detail the computational cost of the multiple scattering non-reflecting boundary condition, and we present an explicit finite difference time-stepping scheme for the solution of a multiple scattering problem. In Section 5, we demonstrate the accuracy and convergence of the numerical scheme. We also compare the multiple scattering approach to the already known single-scattering non-reflecting boundary condition [34, 36, 37], and show that the numerical solutions obtained by these two different methods coincide.

3.2 Two scatterers

We consider acoustic wave scattering from two bounded disjoint scatterers in unbounded three-dimensional space. Each scatterer may contain one or several obstacles, inhomogeneities, and nonlinearity. We let Γ denote the piecewise smooth boundary of all obstacles and impose on Γ a Dirichlet-type boundary condition, for simplicity. In Ω_∞, the unbounded region outside Γ, the scattered field $U = U(\boldsymbol{x}, t)$ then solves the following initial/boundary value problem:

$$\begin{aligned}
\frac{\partial^2 U}{\partial t^2} - \operatorname{div}(\underline{\boldsymbol{A}}\nabla U) &= F \quad \text{in } \Omega_\infty \times I, \qquad I := (0,T),\ T > 0, && (3.1)\\
U &= U_0 \quad \text{in } \Omega_\infty \times \{0\}, && (3.2)\\
\frac{\partial U}{\partial t} &= V_0 \quad \text{in } \Omega_\infty \times \{0\}, && (3.3)\\
U &= G \quad \text{on } \Gamma \times I. && (3.4)
\end{aligned}$$

The material properties described by $\underline{\boldsymbol{A}}$ may vary in space, while both F and G can vary in space and time; F may also be nonlinear.

Next, we assume that both scatterers are *well separated*, that is we assume that we can surround them by two non-intersecting spheres B_1, B_2 centered at c_1, c_2 with radii R_1, R_2, respectively. In the unbounded region D, outside the two spheres, we assume that the medium is homogeneous and isotropic; hence, in D $\underline{\boldsymbol{A}} \equiv c^2\underline{\boldsymbol{I}}$, where $c > 0$ constant and $\underline{\boldsymbol{I}}$ the identity. Moreover, we assume that the source F and the initial values U_0, V_0 vanish in $\overline{D}$. Thus,

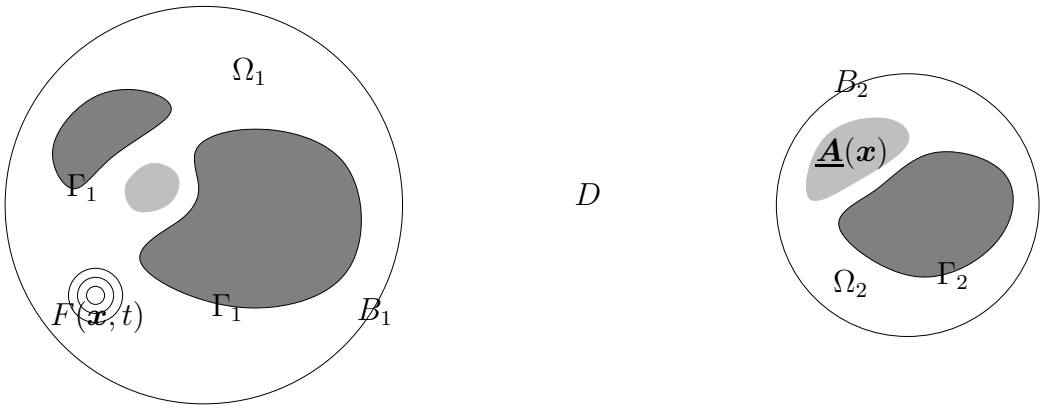

Figure 3.1: A typical configuration with two scatterers is shown. Each scatterer consists of possibly several obstacles bounded by Γ_1 and Γ_2, but may also contain inhomogeneity, anisotropy, nonlinearity and sources. The computational domain $\Omega = \Omega_1 \cup \Omega_2$ is externally bounded by the artificial boundary $B = B_1 \cup B_2$; the unbounded region outside Ω is denoted by D.

in the exterior region the scattered wave U satisfies the homogeneous wave equation with constant wave speed c and homogeneous initial conditions,

$$\frac{1}{c^2}\frac{\partial^2 U}{\partial t^2} - \Delta U = 0 \quad \text{in } D \times I, \qquad c > 0 \text{ constant}, \tag{3.5}$$

$$U = 0 \quad \text{in } D \times \{0\}, \tag{3.6}$$

$$\frac{\partial U}{\partial t} = 0 \quad \text{in } D \times \{0\}. \tag{3.7}$$

Because of the finite speed of propagation and the compact support of the initial data, the scattered field U is purely radiating at large distance.

We wish to compute the scattered wave, U, in the computational domain $\Omega = \Omega_\infty \setminus D$, which consists of the two disjoint components Ω_1 and Ω_2. Hence Ω is internally bounded by $\Gamma = \Gamma_1 \cup \Gamma_2$, and externally by $B = \partial D$, which consists of the two spheres B_1 and B_2 – see Fig. 3.1. To solve the scattering problem (3.1)–(3.4) inside Ω, a boundary condition is needed at the exterior *artificial boundary* $B = B_1 \cup B_2$. This boundary condition must ensure that the solution in Ω, with that boundary condition imposed on B, coincides with the restriction to Ω of the solution in the original unbounded region Ω_∞.

3.2.1 Non-reflecting boundary condition

In contrast to the situation of a single spherical artificial boundary, as considered for example by Hagstrom and Hariharan [43] or Grote and Keller [36], we cannot simply expand u outside B either in a Fourier series or as a superposition of purely outgoing multipole fields. In fact, since part of the scattered field leaving Ω_1 will reenter Ω_2 at later times, and vice versa, u is not purely outgoing in D. Thus, the boundary condition we seek at B must not only let outgoing waves leave Ω_1 without spurious reflection from B_1, but also propagate that wave field to Ω_2, and so forth, without introducing any spurious reflections.

Let D_1 denote the unbounded region outside B_1 and D_2 the unbounded region outside B_2. We now decompose the scattered wave U inside $D = D_1 \cap D_2$ in two purely outgoing waves U_1 and U_2, which solve the following two problems:

$$\frac{1}{c^2}\frac{\partial^2 U_1}{\partial t^2} - \Delta U_1 = 0 \quad \text{in } D_1 \times I, \tag{3.8}$$

$$U_1 = 0 \quad \text{in } D_1 \times \{0\}, \tag{3.9}$$

$$\frac{\partial U_1}{\partial t} = 0 \quad \text{in } D_1 \times \{0\}, \tag{3.10}$$

and

$$\frac{1}{c^2}\frac{\partial^2 U_2}{\partial t^2} - \Delta U_2 = 0 \quad \text{in } D_2 \times I, \tag{3.11}$$

$$U_2 = 0 \quad \text{in } D_2 \times \{0\}, \tag{3.12}$$

$$\frac{\partial U_2}{\partial t} = 0 \quad \text{in } D_2 \times \{0\}. \tag{3.13}$$

Each wave field is only influenced by a single scatterer and completely oblivious to the other. Therefore, U_1 and U_2 are entirely determined by their values on B_1 or B_2, respectively [56]. We now couple U_1 and U_2 with U by matching the values of $U_1 + U_2$ with those of U at $B = B_1 \cup B_2$:

$$U_1 + U_2 = U \quad \text{on } B \times I. \tag{3.14}$$

The two wave fields U and U_1+U_2 both solve the homogeneous wave equation (3.5) in D, together with zero initial conditions (3.6), (3.7). Since U and U_1+U_2 coincide on B, they must coincide everywhere and for all time in the exterior region $\overline{D}$ (up to the boundary) [56], because the initial/boundary value problem in $\overline{D}$ is well-posed. We summarize this result in the following proposition. Moreover, before proceeding with the derivation of the non-reflecting boundary condition, we shall also prove that the decomposition $U = U_1 + U_2$ introduced above always exists and is unique.

Proposition 2. *Let U solve the exterior Dirichlet problem (3.1)–(3.4) and assume that U satisfies (3.5)–(3.7) in the exterior region D. Then,*

$$U \equiv U_1 + U_2 \quad \text{in } \overline{D} \times I, \tag{3.15}$$

where U_1 and U_2 are solutions to the problems (3.8)–(3.10) and (3.11)–(3.13), respectively, together with the matching condition (3.14). The decomposition of U into the two purely outgoing waves U_1 and U_2 is unique.

Proof. By the argument above we have already shown that if $U = U_1 + U_2$ on $B \times I$, where U_1 and U_2 solve (3.8)–(3.13), then $U \equiv U_1 + U_2$ everywhere in $\overline{D} \times I$. We shall now show that U_1 and U_2 exist and, in fact, are unique.
Existence: In the exterior region $D \times I$ we use Kirchhoff's formula (see, for instance, [6]) to write

$$U(\boldsymbol{x}, t) = \frac{1}{4\pi} \int\limits_B \left\{ [U] \frac{\partial}{\partial \boldsymbol{n}} \left(\frac{1}{\rho} \right) - \frac{1}{c\rho} \frac{\partial \rho}{\partial \boldsymbol{n}} \left[\frac{\partial U}{\partial t} \right] - \frac{1}{\rho} \left[\frac{\partial U}{\partial \boldsymbol{n}} \right] \right\} ds, \tag{3.16}$$

for $(\boldsymbol{x}, t) \in D \times I$. Here $\rho := |\boldsymbol{x} - \boldsymbol{y}|$, $\boldsymbol{y} \in B$, and $\boldsymbol{n}$ the unit normal vector pointing into D; throughout this paper $[f] := f(t - \rho/c)$ will denote the retarded values of any time-dependent function f. Let

$$U_j(\boldsymbol{x}, t) = \frac{1}{4\pi} \int\limits_{B_j} \left\{ [U] \frac{\partial}{\partial \boldsymbol{n}} \left(\frac{1}{\rho} \right) - \frac{1}{c\rho} \frac{\partial \rho}{\partial \boldsymbol{n}} \left[\frac{\partial U}{\partial t} \right] - \frac{1}{\rho} \left[\frac{\partial U}{\partial \boldsymbol{n}} \right] \right\} ds, \tag{3.17}$$

$(\boldsymbol{x}, t) \in D_j \times I$, $j = 1, 2$. Because (3.17) is a combination of single and double layer retarded potentials with densities $U|_{B_j}$, the functions U_j each solve the wave equation in $D_j \times I$, $j = 1, 2$ [6]. Clearly, $U_1(x, t) + U_2(x, t) = U(x, t)$, everywhere in $D \times I$. With the jump relations for retarded potentials, the expressions (3.16) and (3.17) can be extended up to the artificial boundaries B and B_1, B_2, respectively. Thus, U_1 and U_2 also satisfy the matching condition (3.14).
Uniqueness: Let $U = V_1 + V_2$ be another decomposition in $\overline{D} \times I$, where V_1 and V_2 solve (3.8)–(3.10) and (3.11)–(3.13), respectively. We shall now show that $V_1 \equiv U_1$ and that $V_2 \equiv U_2$ in $\overline{D} \times I$. To do so, we let $W_1 := U_1 - V_1$ and $W_2 := U_2 - V_2$. Hence, W_1 and W_2 satisfy (3.8)–(3.10) and (3.11)–(3.13), respectively, while their sum $W_1 + W_2 = U_1 + U_2 - (V_1 + V_2) \equiv 0$ in $\overline{D} \times I$.

Now, let $\delta > 0$ denote the distance between B_1 and B_2 and consider the two concentric open balls $G_j \supset B_j$, $j = 1, 2$, each at distance $\delta/2$ – see Fig. 3.2. Because each W_j is zero outside B_j at time $t = 0$, it remains zero outside G_j until the time $t_1 := \delta/(2c)$, due to the finite speed of propagation.

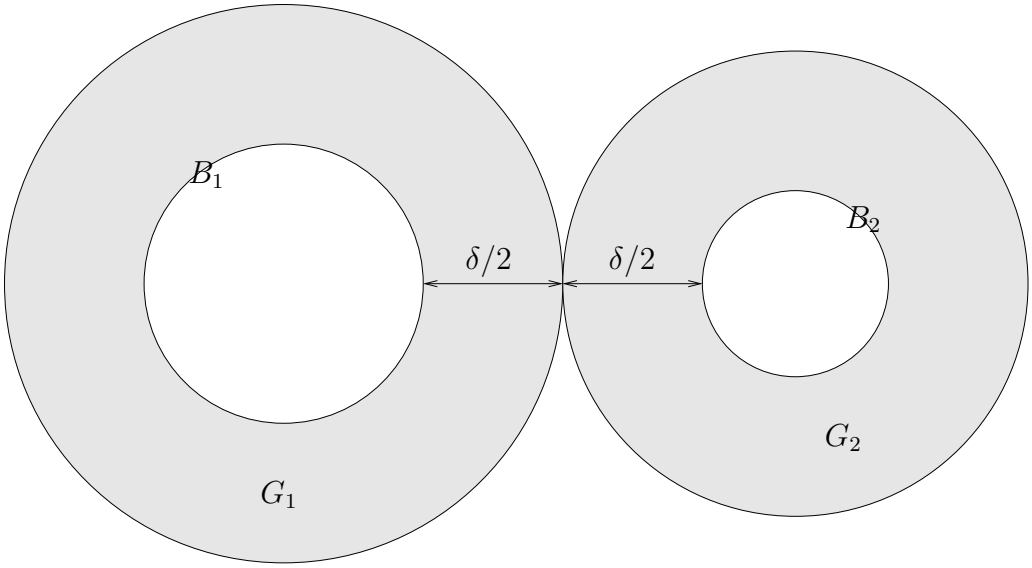

Figure 3.2: The construction used in the proof of Proposition 2: the sphere B_j is contained in the concentric open ball G_j, $j = 1, 2$. The shortest distance between the two artificial boundary components is $\delta > 0$. The shaded regions correspond to $D_1 \cap G_1$ and $D_2 \cap G_2$, respectively.

In particular, W_1 vanishes inside G_2 for $t \leq t_1$. Therefore, $W_2 = -W_1$ must also vanish in $\overline{D}_2 \cap G_2$, and thus everywhere in D_2 up to time t_1. Similarly, $W_1 = 0$ in $D_1 \times [0, t_1]$.

Next, we consider the time interval $[t_1, t_2]$ with $t_2 := t_1 + \delta/(2c)$. Because each W_j is zero outside B_j at time $t = t_1$, it remains zero outside G_j up to time t_2. From the argument above, we conclude that $W_j \equiv 0$ in $D_j \times [0, t_2]$. The same argument may be used repeatedly until the final time T is reached. □

As a consequence of Proposition 2, the decomposition of U in two outgoing wave fields U_1, U_2 is well-defined and we may now use it to determine a non-reflecting boundary condition for U on B. At B_1, for instance, the wave field U at any instant consists of both an outgoing wave U_1 and an incoming wave U_2. Since U_1 is purely outgoing as seen from Ω_1, it satisfies the exact non-reflecting boundary condition [36] at B_1, whereas the field U_2 at B_1 is fully determined by its previous values at B_2. In $\overline{D}_j$, $j = 1, 2$, we introduce the (local) spherical coordinates (r_j, ϕ_j, θ_j), where $r_j \geq R_j$ denotes the radial, $\phi_j \in [0, 2\pi)$ the longitudinal, and $\theta_j \in [0, \pi]$ the azimuthal

variable, respectively. Then,

$$\mathcal{B}_1 U := \left(\frac{1}{c}\frac{\partial}{\partial t} + \frac{\partial}{\partial r_1}\right)(r_1 U) = M_1 U_1 + T_{12} U_2 \quad \text{on } B_1 \times I, \tag{3.18}$$

$$\mathcal{B}_2 U := \left(\frac{1}{c}\frac{\partial}{\partial t} + \frac{\partial}{\partial r_2}\right)(r_2 U) = M_2 U_2 + T_{21} U_1 \quad \text{on } B_2 \times I, \tag{3.19}$$

$$U_1 + P_{12} U_2 = U \quad \text{on } B_1 \times I, \tag{3.20}$$

$$P_{21} U_1 + U_2 = U \quad \text{on } B_2 \times I. \tag{3.21}$$

Here, the operator M corresponds to the (well-known) exact non-reflecting boundary condition in the single scattering case:

$$(\mathcal{B}_j U_j)(R_j, \phi_j, \theta_j, t) = (M_j U_j)(\phi_j, \theta_j, t), \quad j = 1, 2. \tag{3.22}$$

The *transfer operator,* T, and the *propagation operator,* P, are defined as

$$(T_{12} U_2)(\phi_1, \theta_1, t) := (\mathcal{B}_1 U_2)(R_1, \phi_1, \theta_1, t), \tag{3.23}$$

$$(T_{21} U_1)(\phi_2, \theta_2, t) := (\mathcal{B}_2 U_1)(R_2, \phi_2, \theta_2, t), \tag{3.24}$$

$$(P_{12} U_2)(\phi_1, \theta_1, t) := U_2(R_1, \phi_1, \theta_1, t), \tag{3.25}$$

$$(P_{21} U_1)(\phi_2, \theta_2, t) := U_1(R_2, \phi_2, \theta_2, t). \tag{3.26}$$

To utilize (3.22)–(3.26) in computation, we shall need explicit formulas to efficiently evaluate M, P, and T. In particular, we shall need the means to evaluate an outgoing wave and its partial derivatives anywhere in D, given its (past) values on B.

Clearly, the direct evaluation of M, P, or T via Kirchhoff type integrals, such as (3.16), is possible, yet it would require a two-dimensional space-time integral over B for *every* point on B. The resulting computational work would be one order of magnitude higher than that required in the interior, and thus too high a price to pay. Instead, we shall use a special expansion in local spherical coordinates, which then permits the efficient evaluation of all required quantities.

3.2.2 Wilcox expansion and efficient evaluation of M

By combining Fourier series with a progressive wave expansion by Wilcox, we shall now derive an analytic representation for any outgoing wave field U_j in terms of its values at B_j, which holds everywhere outside of B_j. Since the same expression will be used for every individual field U_j, we shall omit the index of the corresponding domain component for the rest of this section. Based on that representation formula, we shall then derive an explicit

expression for M in (3.22), which incidentally coincides with the exact non-reflecting boundary condition proposed in [36, 37].

Let $U = U(r, \phi, \theta, t)$ be a purely outgoing wave field, which satisfies the homogeneous wave equation with constant coefficients and zero initial conditions (3.5)–(3.7) in the region D, outside the sphere B of radius $R > 0$ centered at the origin. We shall now derive an expression for U that holds everywhere in D, which only involves the values of U on the boundary B. That expression will be more efficient than the direct evaluation via Kirchhoff's formula (3.16).

By calculating the inverse Laplace transform of the well-known expansion by Wilcox ([84], eqns. (4) and (5)), we readily obtain the *progressive wave expansion*

$$U(r, \phi, \theta, t) = \frac{1}{r} \sum_{k=0}^{\infty} \frac{f^k(\phi, \theta, t - r/c)}{r^k}, \quad r > R, \tag{3.27}$$

which was also used by Hagstrom and Hariharan in [43]. Here the functions f^k, $k \geq 1$, are determined by f^0 via the recursion formula

$$\frac{1}{c} \frac{\partial f^k}{\partial t} = -\frac{\Delta_S + k(k-1)}{2k} f^{k-1}, \quad k \geq 1, \tag{3.28}$$

with $f^k(\phi, \theta, t) = 0$ for $t \leq 0$, while Δ_S denotes the Laplace-Beltrami operator on the unit sphere.

Let Y_{nm} denote the spherical harmonics normalized over the unit sphere, given by

$$Y_{nm}(\phi, \theta) = \sqrt{\frac{(2n+1)(n-|m|)!}{4\pi(n+|m|)!}} P_n^{|m|}(\cos\theta) e^{im\phi}, \quad 0 \leq |m| \leq n, \tag{3.29}$$

where $P_n^{|m|}$ denote the associated Legendre functions [51]. We now expand f^k in Fourier series, which yields

$$f^k(\phi, \theta, t) = \sum_{n=0}^{\infty} \sum_{m=-n}^{n} f_{nm}^k(t) Y_{nm}(\phi, \theta), \quad k \geq 0. \tag{3.30}$$

Because the spherical harmonics are eigenfunctions of Δ_S and satisfy

$$\Delta_S Y_{nm} = -n(n+1) Y_{nm}, \tag{3.31}$$

we obtain from (3.28) the recursion

$$\frac{1}{c} \frac{d}{dt} f_{nm}^k = \frac{(n+k)(n-k+1)}{2k} f_{nm}^{k-1}, \quad k \geq 1, \tag{3.32}$$

with $f_{nm}^k(t) = 0$ for $t \leq 0$, $k \geq 0$. From (3.32), we also observe that

$$f_{nm}^k \equiv 0, \quad k > n. \tag{3.33}$$

Next, we combine (3.27), (3.30), and (3.33) to obtain the Fourier series representation

$$U(r, \phi, \theta, t) = \sum_{n=0}^{\infty} \sum_{m=-n}^{n} U_{nm}(r, t) Y_{nm}(\phi, \theta) \quad r > R, \tag{3.34}$$

with Fourier coefficients

$$U_{nm}(r, t) = \frac{1}{r} \sum_{k=0}^{n} \frac{f_{nm}^k(t - r/c)}{r^k}. \tag{3.35}$$

Hence, the wave field U is a superposition of infinitely many purely outgoing one-dimensional waves, f_{nm}^k. For $1 \leq k \leq n$, the functions f_{nm}^k are entirely determined by f_{nm}^0 through the recursion (3.32), whereas f_{nm}^0 is determined by the boundary values of U. Indeed, evaluating (3.35) at $r = R$ and solving for f_{nm}^0 yields

$$f_{nm}^0(t - R/c) = R U_{nm}(R, t) - \sum_{k=1}^{n} \frac{f_{nm}^k(t - R/c)}{R^k}. \tag{3.36}$$

Then, we introduce (3.36), with t replaced by $t - (r - R)/c$, into (3.35) and thus obtain

$$\begin{aligned} r U_{nm}(r, t) &= f_{nm}^0 \left(t - \frac{r - R}{c} - \frac{R}{c} \right) + \sum_{k=1}^{n} \left(\frac{R}{r} \right)^k \frac{f_{nm}^k \left(t - \frac{r-R}{c} - \frac{R}{c} \right)}{R^k} \\ &\overset{(3.36)}{=} R U_{nm} \left(R, t - \frac{r - R}{c} \right) - \sum_{k=1}^{n} \frac{f_{nm}^k \left(t - \frac{r-R}{c} - \frac{R}{c} \right)}{R^k} + \\ &\quad + \sum_{k=1}^{n} \left(\frac{R}{r} \right)^k \frac{f_{nm}^k \left(t - \frac{r-R}{c} - \frac{R}{c} \right)}{R^k} \\ &= R \left[U_{nm}(R, \cdot) \right] - \sum_{k=1}^{n} \left(1 - \left(\frac{R}{r} \right)^k \right) \left[\psi_{nm}^k \right]. \end{aligned} \tag{3.37}$$

Here $[f] := f(t - (r - R)/c)$ again denotes the retarded values of any function f; the functions ψ_{nm}^k are defined by

$$\psi_{nm}^k(t) := \frac{f_{nm}^k(t - R/c)}{R^k}, \quad k = 1, \ldots, n. \tag{3.38}$$

By introducing (3.38) into (3.32) and using (3.33), we we find that the vector-valued functions $\boldsymbol{\psi}_{nm} := \{\psi_{nm}^k\}_{k=1}^n$ satisfy a system of *ordinary differential equations*:

$$\begin{aligned} \frac{1}{c}\boldsymbol{\psi}'_{nm}(t) &= \frac{1}{R}\underline{\boldsymbol{A}}_n\boldsymbol{\psi}_{nm}(t) + \frac{n(n+1)}{2}U_{nm}(R,t)\boldsymbol{e}_n, \quad t>0, \quad (3.39)\\ \boldsymbol{\psi}_{nm}(0) &= \mathbf{0}. \quad (3.40) \end{aligned}$$

Here the matrices $\underline{\boldsymbol{A}}_n$ are given by

$$(\underline{\boldsymbol{A}}_n)_{ij} = \begin{cases} -n(n+1)/2, & i=1 \\ (n+i)(n-i+1)/(2i), & i=j+1 \\ 0, & \text{otherwise} \end{cases}, \quad (3.41)$$

and the vectors $\boldsymbol{e}_n$ by

$$(\boldsymbol{e}_n)_i = \delta_{i1}, \quad (3.42)$$

for $i,j = 1,\ldots,n$.

The Fourier coefficients U_{nm} in (3.39) are computed by integration of U over the sphere $r=R$:

$$U_{nm}(R,t) = \int_0^{2\pi}\int_0^{\pi} U(R,\phi,\theta,t)\overline{Y_{nm}(\phi,\theta)}\sin\theta\, d\theta\, d\phi. \quad (3.43)$$

The Fourier expansion (3.34), together with (3.37), (3.39), and (3.43) can now be used to evaluate U in the exterior and for all time, given the boundary values U at B [40]:

$$\begin{aligned} U(r,\phi,\theta,t) &= \frac{R}{r}\sum_{n=0}^{\infty}\sum_{m=-n}^{n}\left[U_{nm}(R,\cdot)\right]Y_{nm}(\phi,\theta) + \\ &\quad -\frac{1}{r}\sum_{n=1}^{\infty}\sum_{m=-n}^{n}\sum_{k=1}^{n}\left(1-\left(\frac{R}{r}\right)^k\right)\left[\psi_{nm}^k\right]Y_{nm}(\phi,\theta), \quad (3.44) \end{aligned}$$

for $r \geq R$. Although the functions $\boldsymbol{\psi}_{nm}$ are unknown a priori, they can be computed concurrently with U by solving (3.39). Thus (3.44) yields an explicit analytical representation of U everywhere outside B in terms of (past) values of U at B and of the auxiliary functions $\boldsymbol{\psi}_{nm}$. In contrast to the Kirchhoff formula (3.16), space and time are no longer coupled through an integral. Instead, for any fixed point in D, past values of $U_{nm}(R,\cdot)$ and $\boldsymbol{\psi}_{nm}$ are needed only from a single instant in time. This feature will be instrumental in the derivation below.

From (3.35) an explicit formula for the operator M in (3.22) now immediately follows. Since the operator $(c^{-1}\partial_t + \partial_r)$ annihilates the first term in (3.35), we find that

$$\left(\frac{1}{c}\frac{\partial}{\partial t} + \frac{\partial}{\partial r}\right)(rU_{nm})(r,t) = -\frac{1}{r}\sum_{k=1}^{n} k\,\frac{f_{nm}^k(t-r/c)}{r^k}. \tag{3.45}$$

By evaluating (3.45) at $r = R$ and using (3.38), we then obtain

$$\left(\frac{1}{c}\frac{\partial}{\partial t} + \frac{\partial}{\partial r}\right)(rU_{nm})(R,t) = -\frac{1}{R}\boldsymbol{d}_n \cdot \boldsymbol{\psi}_{nm}(t), \tag{3.46}$$

with $\boldsymbol{d}_n = (1, 2, \ldots, n)^\top$. Multiplication of (3.46) with Y_{nm} and summation over n and m finally leads to an explicit formula for the operator M:

$$(MU)(\phi,\theta,t) = -\frac{1}{R}\sum_{n=1}^{\infty}\sum_{m=-n}^{n} \boldsymbol{d}_n \cdot \boldsymbol{\psi}_{nm}(t) Y_{nm}(\phi,\theta). \tag{3.47}$$

This operator coincides with the right-hand side in the non-reflecting boundary condition derived by Grote and Keller in [34, 36, 37]. Other partial derivatives of U can also be computed by differentiation of (3.44). For instance, for each Fourier coefficient

$$\frac{1}{c}\frac{\partial U_{nm}}{\partial t}(r,t) = \frac{R}{cr}\left[\frac{\partial U_{nm}}{\partial t}(R,\cdot)\right] - \frac{1}{cr}\sum_{k=1}^{n}\left(1-\left(\frac{R}{r}\right)^k\right)\left[\frac{d\psi_{nm}^k}{dt}\right] \tag{3.48}$$

$$\begin{aligned}\frac{\partial U_{nm}}{\partial r}(r,t) = {} & -\frac{R}{r^2}\left[U_{nm}(R,\cdot)\right] - \frac{R}{cr}\left[\frac{\partial U_{nm}}{\partial t}(R,\cdot)\right] + \\ & + \frac{1}{r^2}\sum_{k=1}^{n}\left(1-(k+1)\left(\frac{R}{r}\right)^k\right)\left[\psi_{nm}^k\right] + \\ & + \frac{1}{cr}\sum_{k=1}^{n}\left(1-\left(\frac{R}{r}\right)^k\right)\left[\frac{d\psi_{nm}^k}{dt}\right].\end{aligned} \tag{3.49}$$

From (3.48) and (3.49), together with appropriate coordinate transformations, we shall now derive explicit formulas for the transfer and propagation operators P and T defined in (3.23)–(3.26).

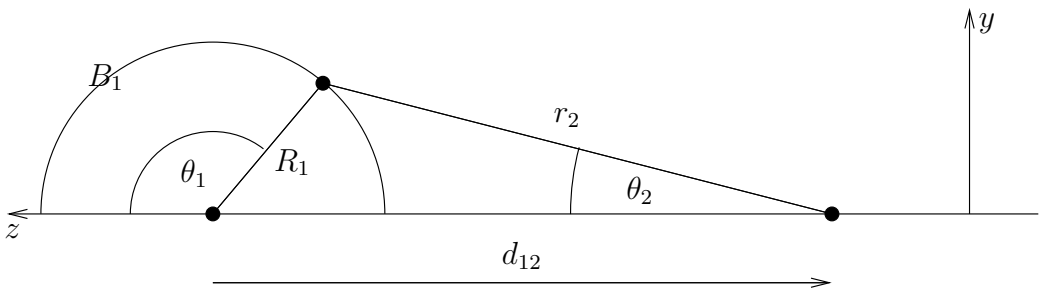

Figure 3.3: Local spherical coordinates (r_1, θ_1) and (r_2, θ_2) in the yz-plane.

3.2.3 Efficient evaluation of P and T

Outside the sphere B_j, $j = 1, 2$, we introduce local spherical coordinates (r_j, ϕ_j, θ_j) and choose the two coordinate systems by aligning their common z-axis, and having the two planes $\phi_1 = 0$ and $\phi_2 = 0$ coincide – see Fig. 3.3. Let d_{12} denote the distance between the two origins. Then, the coordinates of any point on B_1 in the (r_2, ϕ_2, θ_2) coordinate system are given by

$$r_2 = \sqrt{R_1^2 - 2R_1 d_{12} \cos\theta_1 + d_{12}^2}, \tag{3.50}$$

$$\phi_2 = \phi_1, \tag{3.51}$$

$$\cos\theta_2 = \frac{R_1 \cos\theta_1 - d_{12}}{r_2}, \quad \sin\theta_2 = \frac{R_1 \sin\theta_1}{r_2}. \tag{3.52}$$

The normal derivative on B_1 is given in (r_2, ϕ_2, θ_2)-coordinates by

$$\frac{\partial}{\partial r_1} = \frac{1}{r_2}\left((R_1 - d_{12}\cos\theta_1)\frac{\partial}{\partial r_2} - \frac{d_{12}\sin\theta_1}{r_2}\frac{\partial}{\partial \theta_2}\right). \tag{3.53}$$

From (3.50)–(3.53) we can now derive the explicit expressions for P and T, by using (3.34), (3.44), (3.48) and (3.49). For the transfer operator T, we obtain

$$(T_{12}U_2)(\phi_1,\theta_1,t) =$$

$$\begin{aligned}
&= \frac{R_2}{r_2}\left(1-\frac{R_1}{r_2}\alpha_{12}\right)\sum_{n=0}^{\infty}\sum_{m=-n}^{n}\left[U_{2,nm}(R_2,\cdot)\right]Y_{nm}(\phi_2,\theta_2)+\\
&\quad -\frac{R_2}{r_2}\frac{R_1}{r_2}\beta_{12}\sum_{n=0}^{\infty}\sum_{m=-n}^{n}\left[U_{2,nm}(R_2,\cdot)\right]\frac{\partial Y_{nm}}{\partial\theta_2}(\phi_2,\theta_2)+\\
&\quad +\frac{R_2}{r_2}\frac{R_1}{c}\left(1-\alpha_{12}\right)\sum_{n=0}^{\infty}\sum_{m=-n}^{n}\left[\frac{\partial U_{2,nm}}{\partial t}(R_2,\cdot)\right]Y_{nm}(\phi_2,\theta_2)+\\
&\quad -\frac{1}{r_2}\left(1-\frac{R_1}{r_2}\alpha_{12}\right)\sum_{n=1}^{\infty}\sum_{m=-n}^{n}\sum_{k=1}^{n}\left(1-\left(\frac{R_2}{r_2}\right)^k\right)\left[\psi^k_{2,nm}\right]Y_{nm}(\phi_2,\theta_2)+\\
&\quad +\frac{1}{r_2}\frac{R_1}{r_2}\beta_{12}\sum_{n=1}^{\infty}\sum_{m=-n}^{n}\sum_{k=1}^{n}\left(1-\left(\frac{R_2}{r_2}\right)^k\right)\left[\psi^k_{2,nm}\right]\frac{\partial Y_{nm}}{\partial\theta_2}(\phi_2,\theta_2)+\\
&\quad -\frac{1}{r_2}\frac{R_1}{c}\left(1-\alpha_{12}\right)\sum_{n=1}^{\infty}\sum_{m=-n}^{n}\sum_{k=1}^{n}\left(1-\left(\frac{R_2}{r_2}\right)^k\right)\left[\frac{d\psi^k_{2,nm}}{dt}\right]Y_{nm}(\phi_2,\theta_2)+\\
&\quad -\frac{1}{r_2}\frac{R_1}{r_2}\alpha_{12}\sum_{n=1}^{\infty}\sum_{m=-n}^{n}\sum_{k=1}^{n}k\left(\frac{R_2}{r_2}\right)^k\left[\psi^k_{2,nm}\right]Y_{nm}(\phi_2,\theta_2),
\end{aligned}\tag{3.54}$$

with

$$\alpha_{12}(\theta_1) := \frac{R_1 - d_{12}\cos\theta_1}{r_2},\quad \beta_{12}(\theta_1) := \frac{d_{12}\sin\theta_1}{r_2},\quad \alpha_{12}^2+\beta_{12}^2 = 1. \tag{3.55}$$

For the propagation operator, P, we obtain

$$(P_{12}U_2)(\phi_1,\theta_1,t) =$$

$$\begin{aligned}
&= \frac{R_2}{r_2}\sum_{n=0}^{\infty}\sum_{m=-n}^{n}\left[U_{2,nm}(R_2,\cdot)\right]Y_{nm}(\phi_2,\theta_2)+\\
&\quad -\frac{1}{r_2}\sum_{n=1}^{\infty}\sum_{m=-n}^{n}\left[\sum_{k=1}^{n}\psi^k_{2,nm}\right]Y_{nm}(\phi_2,\theta_2)+\\
&\quad +\frac{1}{r_2}\sum_{n=1}^{\infty}\sum_{m=-n}^{n}\sum_{k=1}^{n}\left(\frac{R_2}{r_2}\right)^k\left[\psi^k_{2,nm}\right]Y_{nm}(\phi_2,\theta_2).
\end{aligned}\tag{3.56}$$

Expressions (3.54) and (3.56) involve retarded values $[f] := f(t-(r_2-R_2)/c)$ and the coordinate transformations given by (3.50)–(3.52). Explicit formulas for P_{21} and T_{21} are obtained in a similar way by exchanging the indices 1 and

2 in (3.54), (3.56). Since $R_2/r_2 < 1$, the higher powers $(R_2/r_2)^k$ in (3.54) become vanishingly small with increasing k. This observation will be crucial in reducing both the computational effort and the storage required by the non-reflecting boundary condition – see Section 3.4.1.

3.2.4 Well-posedness

Having derived explicit formulas for the operators M, P, T needed for the non-reflecting boundary condition (3.18)–(3.21), we now state the full initial/boundary value problem for U inside the computational domain $\Omega = \Omega_1 \cup \Omega_2$:

$$\frac{1}{c^2}\frac{\partial^2 U}{\partial t^2} - \Delta U = F \quad \text{in } \Omega \times I, \qquad I = (0,T), \tag{3.57}$$

$$U = U_0 \quad \text{in } \Omega \times \{0\}, \tag{3.58}$$

$$\frac{\partial U}{\partial t} = V_0 \quad \text{in } \Omega \times \{0\}, \tag{3.59}$$

$$U = G \quad \text{on } \Gamma \times I, \tag{3.60}$$

$$\mathcal{B}_1 U := \left(\frac{1}{c}\frac{\partial}{\partial t} + \frac{\partial}{\partial r_1}\right)(r_1 U) = M_1 U_1 + T_{12} U_2 \quad \text{on } B_1 \times I, \tag{3.61}$$

$$\mathcal{B}_2 U := \left(\frac{1}{c}\frac{\partial}{\partial t} + \frac{\partial}{\partial r_2}\right)(r_2 U) = M_2 U_2 + T_{21} U_1 \quad \text{on } B_2 \times I, \tag{3.62}$$

$$U_1 + P_{12} U_2 = U \quad \text{on } B_1 \times I, \tag{3.63}$$

$$P_{21} U_1 + U_2 = U \quad \text{on } B_2 \times I. \tag{3.64}$$

We shall now show that this boundary value problem has a unique solution, which coincides with the solution to the original problem (3.1)–(3.4).

Theorem 3. *Let U be the unique (classical) solution to the exterior Dirichlet problem (3.1)–(3.4) and assume that U satisfies (3.5)–(3.7) in the exterior region, $D \times I$. The two-scatterer boundary value problem (3.57)–(3.64) has a unique solution in Ω, which coincides with the restriction of U to Ω.*

Proof. Existence: We shall show that $U|_{\Omega \times I}$ is a solution to (3.57)–(3.64). Since U satisfies (3.1)–(3.4), it trivially satisfies (3.57)–(3.60). To show that $U|_{\Omega \times I}$ satisfies the non-reflecting boundary condition (3.61)–(3.64) on $B \times I$, we consider in $\overline{D} \times I$ the unique decomposition $U \equiv U_1 + U_2$ provided by Proposition 1. Since $U_1 + U_2$ satisfies by construction the non-reflecting boundary condition (3.61)–(3.64) on $B \times I$, so does the restriction of U to $\Omega \times I$. Therefore, $U|_{\Omega \times I}$ is a solution of the boundary value problem (3.57)–(3.64).

Uniqueness: We shall show that U can be extended from Ω into D as a C^2 solution. Then, by uniqueness of the solution in $\Omega_\infty \times I$, U will also be unique in $\Omega \times I$. Let $\tilde{U}$ be the unique solution of the exterior boundary value problem

$$\tilde{U} = U \quad \text{in } \Omega \times I, \tag{3.65}$$
$$\tilde{U} = 0,\ \partial_t \tilde{U} = 0 \quad \text{in } D \times \{0\}, \tag{3.66}$$
$$\tilde{U} = U \quad \text{on } B \times I, \tag{3.67}$$
$$c^{-2}\partial_{tt}\tilde{U} - \Delta \tilde{U} = 0 \quad \text{in } D \times I. \tag{3.68}$$

Because $\tilde{U}$ is continuous on $B \times I$, all time and tangential derivatives of $\tilde{U}$ are also continuous there. It remains to show that its normal derivative is also continuous across B. With Proposition 1 applied to $\tilde{U}$, we obtain $\tilde{U} = \tilde{U}_1 + \tilde{U}_2$ in $D \times I$, where $\tilde{U}_j = U_j$ in $D_j \times I$, $j = 1, 2$. From (3.61), (3.62), we infer that $\mathcal{B}_j \tilde{U} = \mathcal{B}_j U$ on $B_j \times I$, and thus, by continuity of time and tangential derivatives of $\tilde{U}$, we have $\partial_{r_j} \tilde{U} = \partial_{r_j} U$ on $B_j \times I$, $j = 1, 2$. Therefore, the normal derivative of $\tilde{U}$, together with all its time and tangential derivatives, is continuous across B, which implies that $\tilde{U}$ is a genuine C^2 solution of the initial/boundary value problem in $\Omega_\infty \times I$. Hence, it is unique and so is its restriction U to $\Omega \times I$. □

3.3 Multiple scattering problems

The derivation of the non-reflecting boundary condition presented in Section 3.2 for two scatterers is easily generalized to the case of several scatterers. We consider a situation with J scatterers, and surround each scatterer by a sphere B_j of radius R_j, $j = 1, \ldots, J$. Again, we denote by $B = \bigcup_{j=1}^{J} B_j$ the entire artificial boundary and by D_j the unbounded region outside the j-th sphere. Hence the computational domain $\Omega = \bigcup_{j=1}^{J} \Omega_j$, where Ω_j denotes the finite computational region inside B_j, whereas $D = \bigcap_{j=1}^{J} D_j$ denotes the unbounded exterior region.

In D, we now split the scattered wave into J purely outgoing waves $U_1, \ldots, U_J$, which solve the problems

$$\frac{1}{c^2}\frac{\partial^2 U_j}{\partial t^2} - \Delta U_j = 0 \quad \text{in } D_j \times I, \tag{3.69}$$
$$U_j = 0 \quad \text{in } D_j \times \{0\}, \tag{3.70}$$
$$\frac{\partial U_j}{\partial t} = 0 \quad \text{in } D_j \times \{0\}, \tag{3.71}$$

for $j = 1, \ldots, J$. Thus, every U_j is entirely determined by its values on $B_j \times I$; it is given by (3.44). The matching condition is now given by

$$\sum_{j=1}^{J} U_j = U \quad \text{on } B. \tag{3.72}$$

In analogy to Proposition 1, one can show that

$$U \equiv \sum_{j=1}^{J} U_j \quad \text{in } \overline{D} \times I \tag{3.73}$$

and that this decomposition is unique. Therefore, we immediately find the non-reflecting boundary condition for a multiple scattering problem with J scatterers:

$$\mathcal{B}_j U := \left(\frac{1}{c}\frac{\partial}{\partial t} + \frac{\partial}{\partial r_j} \right)(r_j U) \;=\; M_j U_j + \sum_{\substack{\ell=1 \\ \ell \neq j}}^{J} T_{j\ell} U_\ell \quad \text{on } B_j \times I, \tag{3.74}$$

$$U_j + \sum_{\substack{\ell=1 \\ \ell \neq j}}^{J} P_{j\ell} U_\ell \;=\; U \quad \text{on } B_j \times I, \tag{3.75}$$

for $j = 1, \ldots, J$. Here M, T, and P are defined as follows:

$$M_j : U_j|_{B_j} \mapsto \mathcal{B}_j U_j|_{B_j}\,,\; T_{j\ell} : U_\ell|_{B_\ell} \mapsto \mathcal{B}_j U_\ell|_{B_j}\,,\; P_{j\ell} : U_\ell|_{B_\ell} \mapsto U_\ell|_{B_j}\,. \tag{3.76}$$

No additional analytical derivation due to coordinate transformation, etc. are needed once the situation of two scatterers has been resolved. Hence, M_j is given by

$$(M_j U_j)(\phi_j, \theta_j, t) = -\frac{1}{R_j} \sum_{n=1}^{\infty} \sum_{m=-n}^{n} \boldsymbol{d}_n \cdot \boldsymbol{\psi}_{j,nm}(t) Y_{nm}(\phi_j, \theta_j), \tag{3.77}$$

while the operators T and P are again given by (3.54), (3.56), with '1' replaced by 'j' and '2' replaced by 'ℓ', or vice versa. Each $\boldsymbol{\psi}_{j,nm}$ solves (3.39), (3.40), where coefficients U_{nm} of U at B are replaced by thos of U_j at B_j. For $J = 1$, (3.74) and (3.75) reduce to the non-reflecting boundary condition for single scattering [34, 36, 37], whereas for $J = 2$ they correspond to (3.61)–(3.64).

To further simplify the notation, we define the (symbolic) vectors

$$\mathcal{B}U|_B \;=\; \left(\mathcal{B}_1 U|_{B_1}\,, \mathcal{B}_2 U|_{B_2}\,, \ldots, \mathcal{B}_J U|_{B_J}\right)^\top, \tag{3.78}$$

$$U|_B \;=\; \left(U|_{B_1}, U|_{B_2}, \ldots, U|_{B_J}\right)^\top, \tag{3.79}$$

$$U_{\text{out}}|_B \;=\; \left(U_1|_{B_1}\,, U_2|_{B_2}\,, \ldots, U_J|_{B_J}\right)^\top \tag{3.80}$$

and the operator matrices

$$\boldsymbol{T} = \{T_{j\ell}\}_{j,\ell=1}^{J}, \quad \boldsymbol{P} = \{P_{j\ell}\}_{j,\ell=1}^{J}. \tag{3.81}$$

With these notations we can now state the full initial/boundary value problem in $\Omega = \bigcup \Omega_j$ with the non-reflecting boundary condition (3.74), (3.75) in compact notation as

$$\begin{aligned}
\frac{1}{c^2}\frac{\partial^2 U}{\partial t^2} - \Delta U &= F \quad \text{in } \Omega \times I, \qquad I = (0,T), && (3.82)\\
U &= U_0 \quad \text{in } \Omega \times \{0\}, && (3.83)\\
\frac{\partial U}{\partial t} &= V_0 \quad \text{in } \Omega \times \{0\}, && (3.84)\\
U &= G \quad \text{on } \Gamma \times I, && (3.85)\\
\mathcal{B}U &= \boldsymbol{T}U_{\text{out}} \quad \text{on } B \times I, && (3.86)\\
\boldsymbol{P}U_{\text{out}} &= U \quad \text{on } B \times I. && (3.87)
\end{aligned}$$

3.4 Efficient implementation and discretization

We consider the multiple scattering problem (3.82)–(3.85) and let N_s be the typical number of grid points in Ω_j in any space direction. Then, the work per time step W_Ω for any standard finite difference or finite element scheme in the interior will be proportional to N_s^3, and so will be the storage required, S_Ω. We shall now show how to efficiently evaluate the terms appearing in (3.86), (3.87) so that the additional computational work, W_B, and storage, S_B, due to the non-reflecting boundary condition, scale like N_s^3 as well. Then, we shall discuss in detail a standard implementation of (3.82)–(3.87) and exhibit the full algorithm.

3.4.1 Work and storage

In practice, the Fourier series (3.44) used in the non-reflecting boundary condition (3.86), (3.87) is truncated at some finite number, N_B. Let U_{N_B} denote the corresponding approximation,

$$U_{N_B}(r,\phi,\theta,t) :=$$

$$\begin{aligned} &= \frac{R}{r}\sum_{n=0}^{N_B}\sum_{m=-n}^{n}\left[U_{nm}(R,\cdot)\right]Y_{nm}(\phi,\theta) + \\ &\quad -\frac{1}{r}\sum_{n=1}^{N_B}\sum_{m=-n}^{n}\sum_{k=1}^{n}\left(1-\left(\frac{R}{r}\right)^k\right)\left[\psi_{nm}^k\right]Y_{nm}(\phi,\theta). \end{aligned} \tag{3.88}$$

Then, the error $\|U-U_{N_B}\|_2$ is bounded from above by $N_B^{-(k+1)}$ if $U \in C^k$, due to spectral accuracy. Because the discretization error in the interior typically decays only like N_s^{-p} for a p-th order method, we can always choose N_B much smaller than N_s for reasonably smooth solutions.

We now consider the computational cost due to the solution of the ordinary differential equations (3.39). If implicit time discretization is used, we need to solve for every (n,m), $n \le N_B$, an $n \times n$ linear system at each time step. Clearly, the LU decomposition of the matrices $\underline{\boldsymbol{I}} - c\Delta t/(2R)\underline{\boldsymbol{A}}_n$ (see also Section 3.4.2) needs to be computed only once. Thus the work per time step scales like N_B^4; it can be reduced to N_B^3 by using either the compression techniques of [3, 57, 72], or predictor-corrector time integrators. The storage required for the solution of (3.39), (3.40) also scales like N_B^3, because the matrices $\underline{\boldsymbol{A}}_n$ only depend on n.

Next, we consider the cost due to the computation of the Fourier coefficients U_{nm} in (3.88). Because the ϕ-dependence of the spherical harmonics (3.29) depends only on m, we evaluate the integral

$$U_{nm}(r,t) = c_{nm}\int_0^{\pi}\underbrace{\int_0^{2\pi} U(R,\phi,\theta,t)e^{-im\phi}\,d\phi}\,P_n^{|m|}(\cos\theta)\sin\theta\,d\theta, \tag{3.89}$$

first over ϕ, for every $m = -N_B,\ldots,N_B$ and for all grid values of θ. Then, we evaluate the remaining *one-dimensional* integrals over θ for all n and m, which requires $O(N_B N_s^2 + N_B^2 N_s)$ operations and storage.

For the evaluation of MU in (3.47) (after interchanging the two sums) $(MU)(\phi,\theta,t) =$

$$-\frac{1}{R}\sum_{m=-N_B}^{N_B}\underbrace{\sum_{n=\max\{|m|,1\}}^{N_B}\underbrace{\boldsymbol{d}_n\cdot\boldsymbol{\psi}_{nm}(t)}\,c_{nm}P_n^{|m|}(\cos\theta)}\,e^{im\phi}, \tag{3.90}$$

we first evaluate the inner bracket, then the outer bracket, and finally the whole expression. This requires $O(N_B^3+N_B^2N_s+N_BN_s^2)$ work (per time step) and $O(N_B^2N_s + N_BN_s^2)$ total storage.

To reduce the work and storage due to the propagation and transfer operators, we shall further approximate (3.88) by neglecting vanishingly small terms in the triple sum. Thus, for some $K_B \leq N_B$ we define

$$
\begin{aligned}
U_{N_B,K_B}(r,\phi,\theta,t) :=& \\
&= \frac{R}{r}\sum_{n=0}^{N_B}\sum_{m=-n}^{n}\left[U_{nm}(R,\cdot)\right]Y_{nm}(\phi,\theta) + \\
&\quad -\frac{1}{r}\sum_{n=1}^{N_B}\sum_{m=-n}^{n}\left[\sum_{k=1}^{n}\psi_{nm}^{k}\right]Y_{nm}(\phi,\theta) + \\
&\quad +\frac{1}{r}\sum_{n=1}^{N_B}\sum_{m=-n}^{n}\sum_{k=1}^{\min\{n,K_B\}}\left(\frac{R}{r}\right)^{k}\left[\psi_{nm}^{k}\right]Y_{nm}(\phi,\theta). \qquad (3.91)
\end{aligned}
$$

Recall that the square brackets denote time retarded values. The error of this second approximation behaves like $(R/r)^{-(K_B+2)}$. Since R/r is strictly smaller than 1, the error decays exponentially fast and we can choose K_B much smaller than N_B and independently of the mesh size.

The propagation operator $P_{j\ell}$ applied to U_ℓ is evaluated on B_j for instance,

$$
(P_{j\ell}U_\ell)(\phi_j,\theta_j,t) = \sum_{m=-N_{B_\ell}}^{N_{B_\ell}}\underbrace{\sum_{n=|m|}^{N_{B_\ell}}\underbrace{U_{\ell,nm}(r_\ell,t)}c_{nm}P_n^{|m|}(\cos\theta_\ell)}\,e^{im\phi_\ell}, \qquad (3.92)
$$

where each Fourier coefficient $U_{\ell,nm}$ in (3.91), given by
$r_\ell U_{\ell,nm}(r_\ell,t) \simeq$

$$
R_\ell\left[U_{\ell,nm}(R_\ell,\cdot)\right] - \left[\sum_{k=1}^{n}\psi_{\ell,nm}^{k}\right] + \sum_{k=1}^{\min\{n,K_{B_\ell}\}}\left(\frac{R_\ell}{r_\ell}\right)^{k}\left[\psi_{\ell,nm}^{k}\right]. \qquad (3.93)
$$

The quality of the approximation (3.93) has been examined in [40]. Because $\phi_\ell = \phi_j$, the distance $r_\ell(\theta_j)$ from the center of B_ℓ to $(R_j,\theta_j) \in B_j$ depends only on θ_j. Indeed, the relation between the j- and ℓ-coordinates on the artificial boundary component B_j is given by

$$
\begin{aligned}
r_\ell\sin\theta_\ell &= R_j\sin\theta_j, && (3.94)\\
r_\ell\sin\theta_\ell &= R_j\sin\theta_j, && (3.95)\\
r_\ell\cos\theta_\ell &= R_j\cos\theta_j - d_{j\ell}, && (3.96)
\end{aligned}
$$

As a consequence of this observation, the outer bracket in (3.92) is independent of ϕ_j and thus needs to be evaluated only for every n, m, and θ_j. Therefore, the work involved in (3.92) is $O(N_{B_\ell}^2 K_{B_\ell} N_s + N_{B_\ell} N_s^2)$ operations per time step.

The storage of the retarded values of $U_{\ell,nm}(R_\ell, \cdot)$, $\psi_{\ell,nm}^k$ and $\sum_{k=1}^n \psi_{\ell,nm}^k$ is essentially given by $O(m_\ell N_{B_\ell}^2 + m_\ell N_{B_\ell}^2 K_{B_\ell} + N_{B_\ell}^2 N_s + N_{B_\ell} N_s^2)$, where m_ℓ denotes the number number of time steps a wave needs to propagate from B_ℓ to the farthest point on any other sphere B_j, $j \neq \ell$. It is given by

$$m_\ell = \left\lceil \frac{\max_{j\neq\ell}(d_{\ell j} + R_j) - R_\ell}{c\Delta t} \right\rceil, \quad \ell = 1, \ldots, J, \tag{3.97}$$

and hence depends linearly on the problem size.

The transfer operator $T_{j\ell}$ applied to U_ℓ and evaluated on B_j is given by

$$\begin{aligned} (T_{j\ell} U_\ell)(\phi_j, \theta_j, t) &= \left(\frac{1}{c}\frac{\partial}{\partial t} + \frac{\partial}{\partial r_j}\right)(r_j U_\ell)(R_j, \phi_j, \theta_j, t) && (3.98)\\ &= R_j \left(\frac{1}{c}\frac{\partial}{\partial t} + \frac{\partial}{\partial r_j} + \frac{1}{R_j}\right)(U_\ell)(R_j, \phi_j, \theta_j, t), && (3.99) \end{aligned}$$

where the radial partial derivative $\partial/\partial r_j$ in ℓ-coordinates is

$$\frac{\partial}{\partial r_j} = \frac{1}{r_\ell}\left((R_j - d_{j\ell}\cos\theta_j)\frac{\partial}{\partial r_\ell} - \frac{d_{j\ell}\sin\theta_j}{r_\ell}\frac{\partial}{\partial \theta_\ell}\right). \tag{3.100}$$

Thus, we obtain the explicit formula

$$\begin{aligned} &(T_{j\ell} U_\ell)(\phi_j, \theta_j, t) = \\ &= \sum_{n=0}^{N_{B_\ell}} \sum_{m=-n}^{n} R_j \left(\frac{1}{c}\frac{\partial}{\partial t} + \frac{R_j - d_{j\ell}\cos\theta_j}{r_\ell}\frac{\partial}{\partial r_\ell}\right)(U_{\ell,nm})(r_\ell, t) Y_{nm}(\phi_\ell, \theta_\ell) + \\ &\quad - \sum_{n=0}^{N_{B_\ell}} \sum_{m=-n}^{n} U_{\ell,nm}(r_\ell, t) R_j \frac{d_{j\ell}\sin\theta_j}{r_\ell^2}\frac{\partial Y_{nm}}{\partial \theta_\ell}(\phi_\ell, \theta_\ell) + \\ &\quad + \sum_{n=0}^{N_{B_\ell}} \sum_{m=-n}^{n} U_{\ell,nm}(r_\ell, t) Y_{nm}(\phi_\ell, \theta_\ell), \end{aligned} \tag{3.101}$$

where the Fourier coefficients are again approximated by (3.93). By definition of the retarded values for a time-dependent function f, we have

$$[f] = [f](r_\ell, t) = f\left(t - \frac{r_\ell - R_\ell}{c}\right), \tag{3.102}$$

$$\frac{1}{c}\frac{\partial [f]}{\partial t} = -\frac{\partial [f]}{\partial r_\ell} = \frac{1}{c}[f']. \tag{3.103}$$

The partial derivatives of $U_{\ell,nm}$ are obtained via finite differences applied to the retarded time derivatives of $U_{\ell,nm}(R_\ell,\cdot)$, $\psi^k_{\ell,nm}$ and $\sum_{k=1}^n \psi^k_{\ell,nm}$. Hence, the work and storage requirements are of the same order as for the propagation operator, namely $O(N^2_{B_\ell} K_{B_\ell} N_s + N_{B_\ell} N_s^2)$ for the work per time step and $O(m_\ell N^2_{B_\ell} + m_\ell N^2_{B_\ell} K_{B_\ell} + N^2_{B_\ell} N_s + N_{B_\ell} N_s^2)$ for the total storage.

Gathering the above work and storage estimates we find that the total work and storage required for the non-reflecting boundary condition (3.86), (3.87) scales like

$$W_{B_\ell} = O(N_{B_\ell} N_s^2 + N^2_{B_\ell} K_{B_\ell} N_s + N^4_{B_\ell} + N^3_{B_\ell}), \tag{3.104}$$

$$S_{B_\ell} = O(N_{B_\ell} N_s^2 + N^2_{B_\ell} N_s + m_\ell N^2_{B_\ell} K_{B_\ell} + N^3_{B_\ell}), \tag{3.105}$$

for the ℓ-th artificial boundary component, $\ell = 1,\ldots,J$. Because K_{B_ℓ} is independent of the mesh size, and hence independent of N_s, while N_{B_ℓ} scales at worst like N_s, the total work per time step is $W_B = O(N_s^3)$. The total storage required for a scheme with N_t time steps per unit time is $S_B = O(N_s^3 + N_t N_s^2)$.

3.4.2 Finite Difference discretization

We shall now show how to discretize the multiple scattering problem (3.82)–(3.87) with a standard second order finite difference scheme. In each subdomain Ω_j, we choose local spherical coordinates (r_j,ϕ_j,θ_j). For simplicity, we assume a regular equidistant grid along each artificial boundary B_j, and denote by N_r the corresponding radial grid point index. The time interval I is discretized at equidistant points t_m with step size Δt. We denote by U_i^k the values of the numerical solution on layer i at time step m, and discretize (3.82) by second order central finite differences in space and time, omitting the subdomain index j. At B, $i = N_r$, and (3.82) reduces to

$$0 = \frac{U^{m+1}_{N_r} - 2U^m_{N_r} + U^{m-1}_{N_r}}{c^2\Delta t^2} - \frac{1}{R^2}\left(\Delta_S U\right)^m_{N_r} + \\ - \frac{\left(R+\frac{\Delta r}{2}\right)^2 U^m_{N_r+1} - 2\left(R^2+\frac{\Delta r^2}{4}\right)U^m_{N_r} + \left(R-\frac{\Delta r}{2}\right)^2 U^m_{N_r-1}}{R^2\Delta r^2}, \tag{3.106}$$

with the Laplace-Beltrami operator Δ_S, defined by

$$\Delta_S = \frac{1}{\sin\theta}\frac{\partial}{\partial\theta}\left(\sin\theta\frac{\partial}{\partial\theta}\right) + \frac{1}{\sin^2\theta}\frac{\partial^2}{\partial\phi^2}. \tag{3.107}$$

The values $(\Delta_S U)^m_i$ are computed by a second order central difference discretization in the angular variables ϕ and θ. The values on the "ghost layer"

$i = N_r + 1$ that appear in (3.106) are eliminated by the second order discretization of the non-reflecting boundary condition (3.86) and of the matching condition (3.87),

$$R\frac{U_{N_r}^{m+1} - U_{N_r}^{m-1}}{2c\Delta t} + \frac{(R+\Delta r)U_{N_r+1}^m - (R-\Delta r)U_{N_r-1}^m}{2\Delta r} = (TU_{\text{out}})^m, \quad (3.108)$$

$$(PU_{\text{out}})^m = U_{N_r}^m. \quad (3.109)$$

Here, $R = R_j$ denotes the radius of the artificial boundary $B = B_j$, $(TU_{\text{out}})^m$ denotes the values on the right-hand side of (3.86) at the time step m, $(PU_{\text{out}})^m$ denotes the values on the left-hand side of (3.87) at the time step m, and $c > 0$ denotes the wave speed, assumed constant in the exterior region.

The ordinary differential equations (3.39) is discretized with the unconditionally stable implicit trapezoidal rule

$$\left(\underline{\boldsymbol{I}} - \frac{c\Delta t}{2R}\underline{\boldsymbol{A}}_n\right)\boldsymbol{\psi}_n^m = \left(\underline{\boldsymbol{I}} + \frac{c\Delta t}{2R}\underline{\boldsymbol{A}}_n\right)\boldsymbol{\psi}_n^{m-1} + \frac{c\Delta t}{2}\frac{n(n+1)}{2}\left(U_n^m + U_n^{m-1}\right)\boldsymbol{e}_n. \quad (3.110)$$

Finally, we thus obtain the following explicit numerical scheme for the solution of (3.82)–(3.87).

Algorithm

- initialize U^0 and U^1 in $\overline{\Omega}$
- initialize the Fourier coefficients of U_{out}^0 and $\boldsymbol{\psi}^0$
- at each time step $m \geq 1$, given U^m, U^{m-1}, and U_{out}^{m-1}, $\boldsymbol{\psi}^{m-1}$:
  - compute U_{out}^m by (3.109), with (3.92), (3.93)
  - compute the Fourier coefficients of U_{out}^m by (3.89)
  - advance to $\boldsymbol{\psi}^m$ by (3.110)
  - advance to U^{m+1} inside Ω
  - compute $(TU_{\text{out}})^m$ by (3.101), (3.93)
  - compute $U_{N_r}^{m+1}$ by (3.108), (3.106)

3.5 Numerical results

3.5.1 Accuracy and convergence study

We have implemented the explicit time-stepping scheme described in the previous section for the situation of solutions to the wave equation that are symmetric with respect to rotations around the z-axis. To check the convergence of our method, we consider a test problem with an exact solution, given in (r_2, θ_2)-coordinates by

$$U(r_2, \theta_2, t) = \frac{g(r' - ct)}{r'}, \quad r' = \left| \begin{pmatrix} r_2 \sin\theta_2 \\ r_2 \cos\theta_2 \end{pmatrix} - \begin{pmatrix} 0 \\ d \end{pmatrix} \right|, \tag{3.111}$$

with a parameter $d \in [0, a_2)$. The wave profile $g = g(x)$ is chosen twice continuously differentiable, such that $U = 0$ in $\overline{D} \times \{0\}$. The function U then corresponds to a spherically symmetric wave originating from the off-centered point $\boldsymbol{c}_2 + (0, d)$. The exact values of U are prescribed on the boundaries of the "obstacles", $r_j = a_j$, $j = 1, 2$, at each time step. The exact values of U and of $\partial_t U$ are prescribed everywhere in $\overline{\Omega} \times \{0\}$. If the boundary condition on the artificial boundaries at $r_j = R_j$, $j = 1, 2$, is exact, the numerical solution in $\Omega \times I$ must converge to the exact solution in $\Omega \times I$, as the mesh size $h \to 0$ and the time step $\Delta t \to 0$. We choose $\boldsymbol{c}_1 = (0, 1)$, $\boldsymbol{c}_2 = (0, -1)$, $a_1 = 0.5$, $a_2 = 0.6$, $R_1 = 1$, $R_2 = 0.9$, and the parameter $d = 0.4$. We run our time-stepping scheme up to $T = 8$ and compute the absolute L^2-error of the numerical solution with respect to the exact solution, $E^h(t) := \|U_{\text{ex}}(\cdot, \cdot, t) - U_{\text{num}}(\cdot, \cdot, t)\|_{L^2(\Omega)}$ by numerical integration, at each time step. In Figure 3.4, the L^2-error $\|E^h(t)\|_{L^2(0,T)}$ is plotted vs. the mesh size h for various truncation indices for the non-reflecting boundary condition, N_B. We observe second order convergence of the method, if N_B is chosen large enough.

3.5.2 Comparison with the single-scattering NRBC

We consider the scattering of an acoustic wave from two obstacles with sound-soft spherical boundaries. The radii of the spheres were chosen 0.5 and 0.6. The numerical solution obtained by using our finite difference scheme with the non-reflecting boundary condition for multiple scattering problems on the artificial spherical boundaries with radii 1 and 0.9, respectively, is compared with a numerical solution obtained by using a finite element scheme in a much larger domain, $R = 2$, which contains both obstacles; here the non-reflecting boundary condition for single scattering problems is imposed at the artificial spherical boundary. The numerical solution at time $t = 1$ from both methods

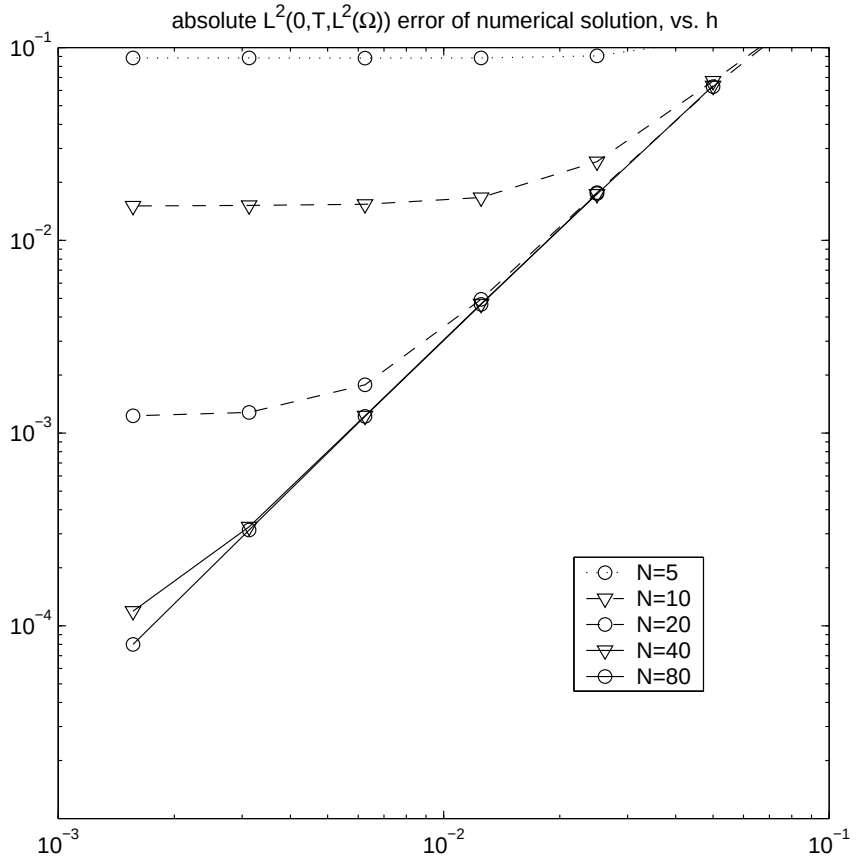

Figure 3.4: L^2-errors vs. mesh size for various values of N_B.

is shown in Fig. 3.5. The two solutions obtained by the multiple and single non-reflecting boundary condition, respectively, coincide well.

3.5.3 Multiple scattering of an incident plane wave packet

We consider an incident plane wave packet $U^i(\boldsymbol{x}, t) = f(z - t)$ scattered by two sound-soft spheres. The profile of the wave packet is shown in Fig. 3.6. The numerical solution with the multiple scattering non-reflecting boundary condition at the two artificial boundary components is shown at selected points in time in Fig. 3.7. We illustrate the influence of the truncation index N_B on the quality of the non-reflecting boundary condition in Fig. 3.8. Here, we show the numerical solution at three selected points in space over time. The upper two pictures are from a point above the north pole of the lower

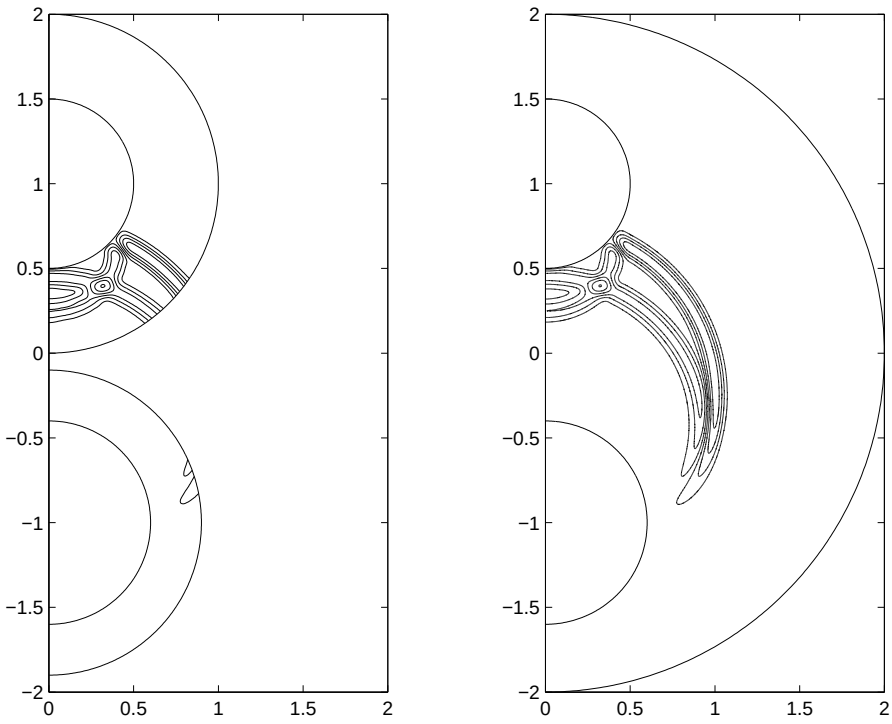

Figure 3.5: Scattering from two sound-soft spheres. Acoustic wave generated by an inhomogeneous initial velocity field. Contour lines of the scattered wave at time $t = 1$ for two solutions are shown. Left: the numerical solution obtained by a second-order finite difference method combined with the non-reflecting boundary condition for multiple scattering problems; right: the numerical solution obtained by a (piecewise linear) finite element method combined with the non-reflecting boundary condition for single scattering problems.

obstacle, in the lower subdomain. For $N_B = 0$, spurious reflection occurs from the artificial boundary surrounding this subdomain. For $N_B = 40$, however, the plane wave passes the artificial boundary components of the lower and of the upper subdomain, and is reflected at the upper obstacle. The reflected wave passes the two artificial boundary components again, and enters the lower subdomain. This ist the correct behavior of the solution, and it is not reproduced with $N_B = 0$. The two pictures in the middle show the solution at a point on the right of the lower obstacle. The incident wave passes through this point early. After some time, the reflected wave from the upper obstacle passes through. With $N_B = 0$, this reflected wave is not well reproduced and hardly visible. The lower two pictures show the solution at a point on

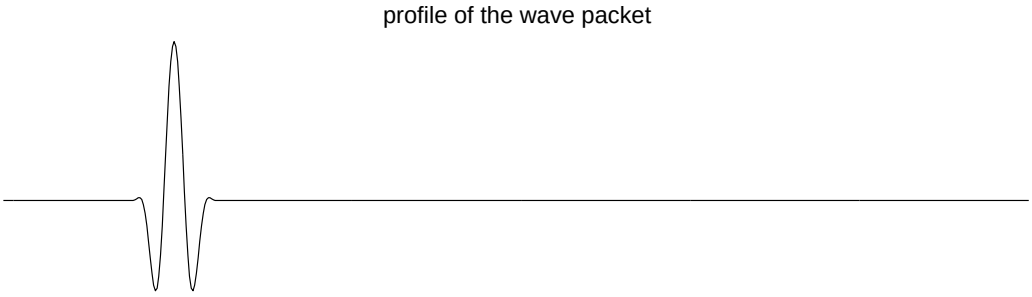

Figure 3.6: Incident plane wave scattering: The profile of the wave packet.

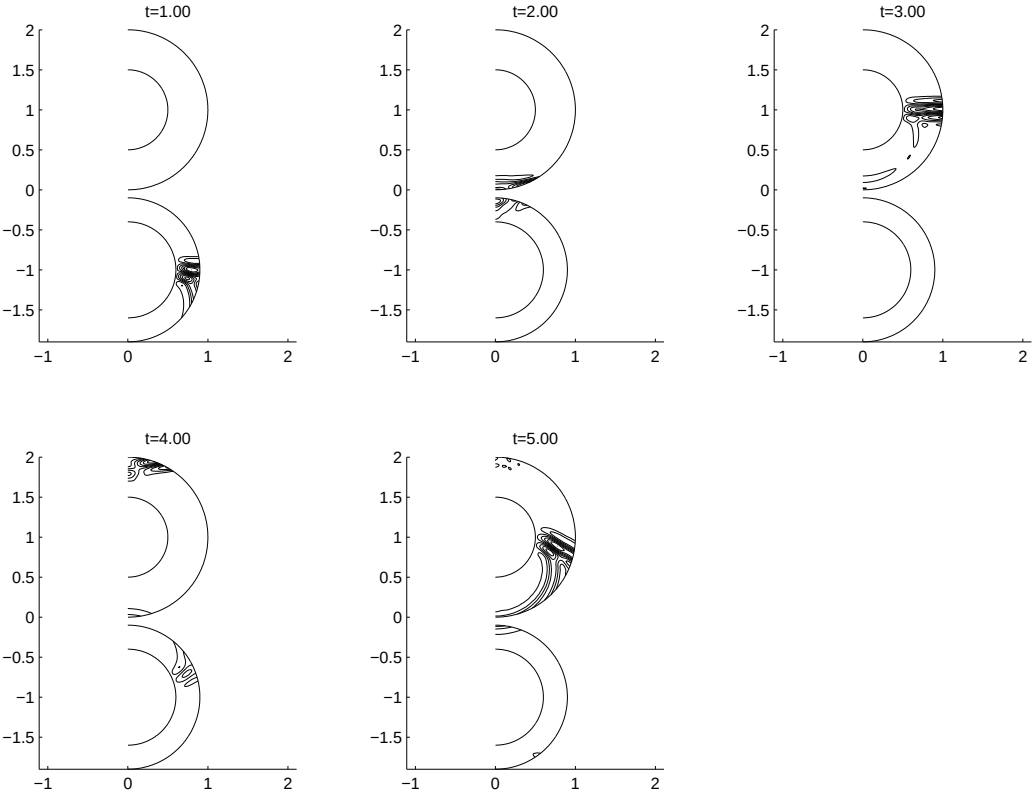

Figure 3.7: Incident plane wave scattering: The total wave at selected points in time.

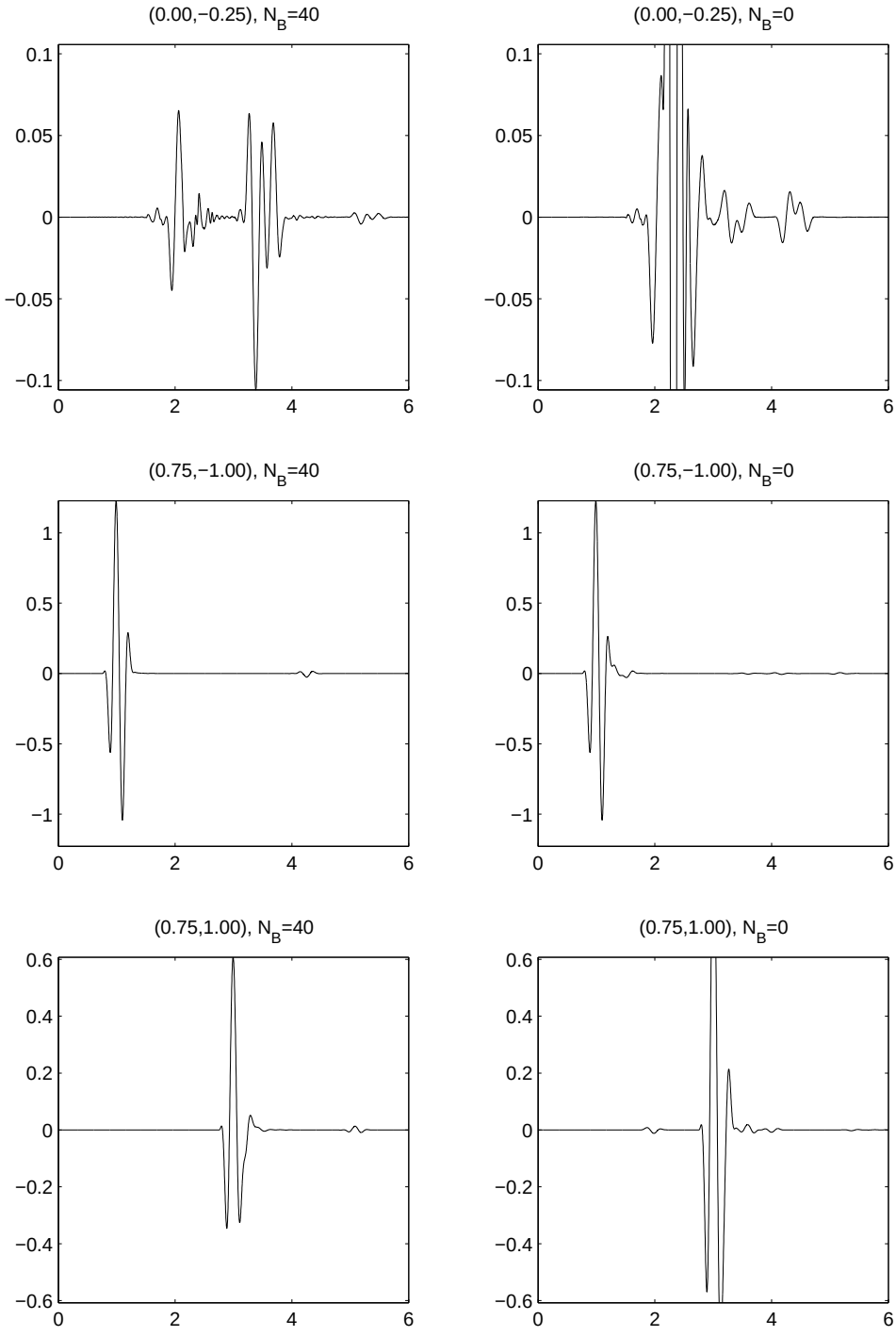

Figure 3.8: Incident plane wave scattering: The total wave at selected points in space, for different values of N_B.

the right of the upper obstacle. The incident wave passes this point, and the reflected wave from the lower obstacle follows. For $N_B = 0$, this reflection is again not well reproduced. Furthermore, for $N_B = 0$, a spurious wave arrives even before the incident wave packet! Because the boundary operators are global, a spurious wave is generated when the incident wave hits the upper artificial boundary component. With $N_B = 40$, there are enough Fourier modes present to eliminate this spurious wave.

3.6 Conclusion

We have derived a non-reflecting boundary condition for multiple scattering problems, which is based on a decomposition of the scattered wave into several purely outgoing waves. We have proved that this boundary condition is exact. When it is used to solve multiple scattering problems, the size of the computational domain is much smaller, in comparison to the use of one single large artificial boundary. In particular, the size of the computational sub-domains in the multiple scattering case does not depend on the relative distances between the components of the scatterer. Although the artificial boundaries must be of simple geometric shape, here a sphere, the boundary condition is not tied to any coordinate system inside the computational domain; in particular, it remains exact independently of the discretization used inside Ω.

We have presented the finite difference discretization of a multiple scattering problem with this boundary condition and demonstrated accuracy and convergence on a simple test problem. A comparison with the single scattering non-reflecting boundary condition has been made in the situation of two obstacles.

This approach is based on the decomposition of the scattered wave into several purely outgoing waves. It can also be used to derive exact non-reflecting boundary conditions for multiple scattering problems for other equations and geometries, such as ellipsoids or wave guides, for which the non-reflecting boundary condition with a single artificial boundary is explicitly known.

The computational cost for the multiple scattering non-reflecting boundary condition is of the same order as the cost for the method in the interior, and past values only need to be stored for a fixed number of time steps, which depends on the geometry of the problem. The storage can be further reduced by compressing the time history of the past values. This will be subject of future work.

Open questions and future research

The following questions regarding non-reflecting boundary conditions for time-dependent multiple scattering problems remained open. These might be subjects for future research:

- As mentioned before in the conclusion, the storage could be reduced if the retarded values of the Fourier coefficients of U_{out} and of $\boldsymbol{\psi}$ were compressed. It would thus be interesting to find out more about the behavior of these functions over time, in order to determine a good compression algorithm. For that purpose, the ordinary differential equation for $\boldsymbol{\psi}$ should be analyzed. Early experiments showed that a simple coarsening is not a good way for compressing the retarded values.

- A spatially local, approximate boundary condition, which does not involve harmonic transformations, is highly desirable. Together with compression of the retarded values, and with clustering techniques in the case of many scatterers, a very efficient method for wave propagation problems in unbounded domains could be obtained. In this context, it is also desirable to have a good comparison with the fast plane wave time domain method.

- It would be interesting to do a stability analysis for multiple scattering NRBC, and to derive conditions for stability of the initial/boundary-value problem in $\Omega \times I$.

Bibliography

[1] M. Abramowitz, I. A. Stegun: *Handbook of mathematical functions* (Dover Publications, Inc., New York, 1992)

[2] U.E. Aladl, A.S. Deakin, H. Rasmussen: *Nonreflecting boundary condition for the wave equation.* J. Comput. Appl. Math. **138**, pp. 309–323, 2002

[3] B. Alpert, L. Greengard, T. Hagstrom: *Rapid Evaluation of Nonreflecting Boundary Kernels for Time-Domain Wave Propagation.* SIAM J. Numer. Anal. **37** (4), pp. 1138–1164, 2000

[4] B. Alpert, L. Greengard, T. Hagstrom: *Nonreflecting boundary condition for the time-dependent wave equation* J. Comput. Phys. **180** (1), pp. 270–296, 2002

[5] F. M. Arscott, A. Darai: *Curvilinear coordinate systems in which the Helmholtz equation separates.* IMA J. Appl. Math. **27**, pp. 33–70, 1981

[6] B.B. Baker, E.T. Copson: *The Mathematical Theory of Huygens' Principle* (Oxford University Press, 1939)

[7] M. Balabane: *A domain decomposition algorithm for the Helmholtz equation. 1 – The dissipating case.* Asymptot. Anal., in press

[8] A. Bayliss, M. Gunzburger, E. Turkel: *Boundary conditions for the numerical solution of elliptic equations in exterior regions.* SIAM J. Appl. Math. **42** (2), pp. 430–451, 1982

[9] A. Bayliss, E. Turkel: *Radiation Boundary Conditions for Wave-Like Equations.* Comm. Pure Appl. Math. **33** (6), pp. 707–725, 1980

[10] E. Bécache, S. Fauqueux, P. Joly: *Stability of perfectly matched layers, group velocities and anisotropic waves.* J. Comput. Phys. **188** (2), pp. 399–433, 2003

[11] J.-D. Benamou, B. Després: *A Domain Decomposition Method for the Helmholtz Equation and Related Optimal Control Problems.* J. Comput. Phys. **136** (1), pp. 68–82, 1997

[12] J.P. Bérenger: *A Perfectly Matched Layer for the Absorption of Electromagnetic Waves.* J. Comput. Phys. **114** (2), pp. 185–200, 1994

[13] J.E. Burke, V. Twersky: *On scattering of waves by many bodies.* J. Res. Nat. Bur. Standards **68D**, pp. 500–510, 1964

[14] D.S. Burnett, R.L. Holford: *Prolate and oblate spheroidal acoustic infinite elements.* Comput. Methods Appl. Mech. Engrg. **158** (1–2), pp. 117–141, 1998

[15] A.J. Burton, G.F. Miller: *The application of integral equation methods to the numerical solution of some exterior boundary-value problems.* Proc. Roy. Soc. London. Ser. A **323** (1553), pp. 201–210, 1971

[16] F. Collino, P.B. Monk: *Optimizing the perfectly matched layer.* Comput. Methods Appl. Mech. Engrg. **164** (1–2), pp. 157–171, 1998

[17] D. Colton, R. Kress: *Integral Equation Methods in Scattering Theory* (John Wiley & Sons, Inc., New York, 1983)

[18] D. Colton, R. Kress: *Inverse Acoustic and Electromagnetic Scattering Theory* (Springer-Verlag, Berlin, 1998)

[19] A.S. Deakin, H. Rasmussen: *Nonreflecting boundary condition for the Helmholtz equation.* Comput. Math. Appl. **41** (3–4), pp. 307–318, 2001

[20] L. Demkowicz, F. Ihlenburg: *Analysis of a coupled finite-infinite element method for exterior Helmholtz problems.* Numer. Math. **88** (1), pp. 43–73, 2001

[21] B. Engquist, A. Majda: *Absorbing Boundary Conditions for the Numerical Simulation of Waves.* Math. Comp. **31** (139), pp. 629–651, 1977

[22] A.A. Ergin, B. Shanker, E. Michielssen: *Fast Evaluation of Three-Dimensional Transient Wave Fields Using Diagonal Translation Operators.* J. Comput. Phys. **146** (1), pp. 157–180, 1998

[23] E. Fuchs: *On discrete polynomial least-squares approximation in moving time windows.* Internat. Ser. Numer. Math. **131**, pp. 93–107, 1999

[24] G. K. Gächter, M.J. Grote: *Dirichlet-to-Neumann Map for Three-Dimensional Elastic Waves.* Wave Motion **37** (3), pp. 293–311, 2003

[25] K. Gerdes: *A summary of Infinite Element formulations for exterior Helmholtz problems.* Comput. Methods Appl. Mech. Engrg. **164** (1–2), pp. 95–105, 1998

[26] D. Givoli: *Numerical Methods for Problems in Infinite Domains* (Elsevier Scientific Publishing Co., Amsterdam, 1992)

[27] D. Givoli: *Recent Advances in the DtN FE Method.* Arch. Comput. Methods Engrg. **6** (2), pp. 71–116, 1999

[28] D. Givoli: *High-order local non-reflecting boundary conditions: a review* Wave Motion **39** (4), pp. 319–326, 2004

[29] D. Givoli, D. Cohen: *Nonreflecting Boundary Conditions Based on Kirchhoff-Type Formulae.* J. Comput. Phys. **117** (1), pp. 102–113, 1995

[30] D. Givoli, J.B. Keller: *Nonreflecting boundary conditions for elastic waves.* Wave Motion **12** (3), pp. 261–279, 1990

[31] D. Givoli, I. Patlashenko: *An optimal high-order non-reflecting finite element scheme for wave scattering problems.* Internat. J. Numer. Methods Engrg. **53** (10), pp. 2389–2411, 2002

[32] L. Greengard, V. Rokhlin: *A Fast Algorithm for Particle Simulations.* J. Comput. Phys. **73** (2), pp. 325–348, 1987

[33] M.J. Grote: *Nonreflecting Boundary Conditions for Elastodynamic Scattering.* J. Comput. Phys. **161** (1), pp. 331–353, 2000

[34] M.J. Grote: *Nonreflecting Boundary Conditions.* In Absorbing Boundaries and Layers, Domain Decomposition Methods, Eds. L. Tourrette, L. Halpern, Nova Sci. Publ., pp. 242–276, 2001

[35] M.J. Grote, J.B. Keller: *On Nonreflecting Boundary Conditions.* J. Comput. Phys. **122** (2), pp. 231–243, 1995

[36] M.J. Grote, J.B. Keller: *Exact Nonreflecting Boundary Conditions for the Time Dependent Wave Equation.* SIAM J. Appl. Math. **55** (2), pp. 280–297, 1995

[37] M.J. Grote, J.B. Keller: *Nonreflecting Boundary Conditions for Time-Dependent Scattering.* J. Comput. Phys. **127** (1), pp. 52–65, 1996

[38] M.J. Grote, J.B. Keller: *Nonreflecting Boundary Conditions for Maxwell's Equations.* J. Comput. Phys. **139** (2), pp. 327–342, 1998

[39] M.J. Grote, J.B. Keller: *Exact Nonreflecting Boundary Conditions for Elastic Waves.* SIAM J. Appl. Math. **60** (3), pp. 803–819, 2000

[40] M.J. Grote, C. Kirsch: *Far-field evaluation via nonreflecting boundary conditions.* In Hyperbolic problems: theory, numerics, applications, pp. 195–204, Springer, Berlin, 2003

[41] M.J. Grote, C. Kirsch: *Dirichlet-to-Neumann boundary conditions for multiple scattering problems.* J. Comput. Phys **201** (2), pp. 630–650, 2004

[42] T. Hagstrom: *Radiation boundary conditions for the numerical simulation of waves.* Acta Numer. **8**, pp. 47–106, 1999

[43] T. Hagstrom, S.I. Hariharan: *A formulation of asymptotic and exact boundary conditions using local operators.* Appl. Numer. Math. **27** (4), pp. 403–416, 1998

[44] I. Harari, T.J.R. Hughes: *A cost comparison of boundary element and finite element methods for problems of time-harmonic acoustics.*. Comput. Methods Appl. Mech. Engrg. **97** (1), pp. 77–102, 1992

[45] I. Harari, T.J.R. Hughes: *Analysis of continuous formulations underlying the computation of time-harmonic acoustics in exterior domains.* Comput. Methods Appl. Mech. Engrg. **97** (1), pp. 103–124, 1992

[46] I. Harari, I. Patlashenko, D. Givoli: *Dirichlet-to-Neumann maps for unbounded wave guides.* J. Comput. Phys. **143** (1), pp. 200-223, 1998

[47] I. Harari, Z. Shohet: *On non-reflecting boundary conditions in unbounded elastic solids.* Comput. Methods Appl. Mech. Engrg. **163** (1–4), pp. 123–139, 1998

[48] I. Harari, M. Slavutin, E. Turkel: *Analytical and numerical studies of a finite element PML for the Helmholtz equation.* J. Comput. Acoust. **8** (1), pp. 121-137, 2000

[49] C. Hazard, M. Lenoir: *On the solution of time-harmonic scattering problems for Maxwell's equations.* SIAM J. Math. Anal. **27** (6), pp. 1597–1630, 1996

[50] R. Hiptmair: *Coupling of finite elements and boundary elements in electromagnetic scattering.* SIAM J. Numer. Anal. **41** (3), pp. 919–944, 2003

[51] E.W. Hobson: *The theory of spherical and ellipsoidal harmonics* (Cambridge University Press, 1931)

[52] F. Ihlenburg: *Finite element analysis of acoustic scattering* (Springer-Verlag, New York, 1998)

[53] K. Jänich: *Funktionentheorie*, Springer, 1993

[54] J.B. Keller, D. Givoli: *Exact non-reflecting boundary conditions.* J. Comput. Phys. **82** (1), pp. 172–192, 1989

[55] R.E. Kleinman, G.F. Roach: *Boundary Integral Equations for the Three-Dimensional Helmholtz Equation.* SIAM Review **16** (2), pp. 214–236, 1974

[56] A.E.H. Love: *Wave-motions with Discontinuities at Wave-fronts.* Proc. London Math. Soc. II. **1**, pp. 37–62, 1904

[57] C. Lubich, A. Schädle: *Fast convolution for nonreflecting boundary conditions.* SIAM J. Sci. Comput. **24** (1), pp. 161–182, 2002

[58] W.J. Mansur, C.A. Brebbia: *Formulation of the boundary element method for transient problems governed by the scalar wave equation.* Appl. Math. Modelling **6**, pp. 307–311, 1982

[59] P.A. Martin: *Integral-equation methods for multiple-scattering problems. I. Acoustics.* Quart. J. Mech. Appl. Math. **38** (1), pp. 105–118, 1985

[60] P.A. Martin: *Multiple Scattering: an Invitation.* In Mathematical and numerical aspects of wave propagation, pp. 3–16, SIAM, Philadelphia, PA, 1995

[61] P.A. Martin: *Multiple scattering and modified Green's functions.* J. Math. Anal. Appl. **275**, pp. 642–656, 2002

[62] P.A. Martin, F.J. Rizzo: *Partitioning, boundary integral equations, and exact Green's functions.* Internat. J. Numer. Methods Engrg. **38** (20), pp. 3483–3495, 1995

[63] M.J. Mohlenkamp: *A fast transform for spherical harmonics.* J. Fourier Anal. Appl. **5**, pp. 159–184, 1999

[64] C. Müller: *Spherical Harmonics*, Springer 1966

[65] J.-C. Nédélec: *Acoustic and electromagnetic equations: integral representations for harmonic problems* (Springer-Verlag, New York, 2001)

[66] A.A. Oberai, M. Malhotra, P. M. Pinsky: *On the implementation of the Dirichlet-to-Neumann radiation condition for iterative solution of the Helmholtz equation.* Appl. Numer. Math. **27** (4), pp. 443–464, 1998

[67] B. Peterson, S. Ström: *Matrix formulation of acoustic scattering from an arbitrary number of scatterers.* J. Acoust. Soc. Amer. **56** (3), pp. 771–780, 1974

[68] P. G. Petropoulos: *Reflectionless sponge layers as absorbing boundary conditions for the numerical solution of Maxwell equations in rectangular, cylindrical, and spherical coordinates.* SIAM J. Appl. Math. **60** (3), pp. 1037–1058, 2000

[69] F. Rellich: *Über das asymptotische Verhalten der Lösungen von* $\Delta u + \lambda u = 0$ *in unendlichen Gebieten.* Jber. Deutsch. Math. Verein. **53**, pp. 57–65, 1943

[70] Y. Saad, M.H. Schultz: *GMRES: a generalized minimal residual algorithm for solving nonsymmetric linear systems.* SIAM J. Sci. Statist. Comput. **7** (3), pp. 856–869, 1986

[71] J.J. Shirron, I. Babuška: *A comparison of approximate boundary conditions and infinite element methods for exterior Helmholtz problems.* Comput. Methods Appl. Mech. Engrg. **164** (1–2), pp. 121–139, 1998

[72] I.L. Sofronov: *Conditions for complete transparency on a sphere for a three-dimensional wave equation.* Russian Acad. Sci. Dokl. Math. **46** (2), pp. 397–401, 1993

[73] A. Sommerfeld: *Die Greensche Funktion der Schwingungsgleichung.* Jber. Deutschen Math. Verein. **21**, pp. 309–353, 1912

[74] Z.-H. Teng: *Exact boundary condition for time-dependent wave equation based on boundary integral.* J. Comput. Phys. **190** (2), pp. 398–418, 2003

[75] L.L. Thompson, R. Huan: *Implementation of exact non-reflecting boundary conditions in the finite element method for the time-dependent wave equation.* Comput. Methods Appl. Mech. Engrg. **187**, pp. 137–159, 2000

[76] L.L. Thompson, R. Huan: *Computation of far field solutions based on exact nonreflecting boundary conditions for the time-dependent wave equation.* Comput. Methods Appl. Mech. Engrg. **190**, pp. 1551–1557, 2000

[77] L.L. Thompson, R. Huan, C. Ianculescu: *Finite element formulation of exact Dirichelt-to-Neumann radiation conditions on elliptic and spheroidal boundaries.* In Proc. Internat. Mech. Engrg. Congress and Exposition, 1999

[78] L. Ting, M.J. Miksis: *Exact boundary conditions for scattering problems.* J. Acoust. Soc. Amer. **80** (6), pp. 1825–1827, 1986

[79] S.V. Tsynkov: *Numerical solution of problems on unbounded domains. A review.* Appl. Numer. Math. **27** (4), pp. 465–532, 1998

[80] E. Turkel, A. Yefet: *Absorbing PML boundary layers for wave-like equations.* Appl. Numer. Math. **27** (4), pp. 533–557, 1998

[81] V. Twersky: *On multiple scattering of waves.* J. Res. Nat. Bur. Standards **64D**, pp. 715–730, 1960

[82] S.S. Vinogradov, P.D. Smith, E.D. Vinogradova: *Canonical Problems in Scattering and Potential Theory*, Chapman & Hall/CRC, 2002

[83] D.V. Widder: *The Laplace Transform*, Princeton University Press, 1946

[84] C.H. Wilcox: *A Generalization of Theorems of Rellich and Atkinson.* Proc. Amer. Math. Soc. **7**, pp. 271–276, 1956

[85] F. Záviška: *Über die Beugung elektromagnetischer Wellen an parallelen, unendlich langen Kreiszylindern.* Ann. Phys. **4** (40), pp. 1023–1056, 1913